TECHNICAL REPORT T-78-31

AN INVESTIGATION OF THE AERODYNAMIC STABILIZING EFFECTIVENESS OF SEVERAL SPLIT FLARE AFTERBODY CONFIGURATIONS IN THE PRESENCE OF AN UNDEREXPANDED JET PLUME AT TRANSONIC MACH NUMBERS

James R. Burt
Aeroballistics Directorate
Technology Laboratory

U.S. ARMY MISSILE RESEARCH AND DEVELOPMENT COMMAND

9 January 1978

Approved for public release; distribution unlimited

Redstone Arsenal, Alabama 35809

DMI FORM 1000, 1 APR 77

SECURITY CLASSIFICATION OF THIS PAGE (When Data Entered)

REPORT DOCUMENTATION PAGE		READ INSTRUCTIONS BEFORE COMPLETING FORM
1. REPORT NUMBER UNCLASSIFIED	2. GOVT ACCESSION NO.	3. RECIPIENT'S CATALOG NUMBER (9)
4. TITLE (and Subtitle) (6) An Investigation of the Aerodynamic Stabilizing Effectiveness of Several Split Flare Afterbody Configurations in the Presence of an Underexpanded Jet Plume at Transonic Mach Numbers.		5. TYPE OF REPORT & PERIOD COVERED Technical Report
		6. PERFORMING ORG. REPORT NUMBER (14) RTR-026-2
7. AUTHOR(s) (10) James R. Burt		8. CONTRACT OR GRANT NUMBER(s) (15) DAAK40-77-C-0008
9. PERFORMING ORGANIZATION NAME AND ADDRESS Commander, US Army Missile Research and Development Command ATTN: DRDMI-TD Redstone Arsenal, Alabama 35809		10. PROGRAM ELEMENT, PROJECT, TASK AREA & WORK UNIT NUMBERS
11. CONTROLLING OFFICE NAME AND ADDRESS Commander, US Army Missile Research and Development Command ATTN: DRDMI-TI Redstone Arsenal, Alabama 35809		12. REPORT DATE (11) 9 Jan 78
		13. NUMBER OF PAGES 87
14. MONITORING AGENCY NAME & ADDRESS (if different from Controlling Office) (12) 83p.		15. SECURITY CLASS. (of this report) Unclassified
		15a. DECLASSIFICATION/DOWNGRADING SCHEDULE

16. DISTRIBUTION STATEMENT (of this Report)

Approved for public release, distribution unlimited.

(18) DRDMI-T

17. DISTRIBUTION STATEMENT (of the abstract entered in Block 20, if different from Report)

(19) 78-31

18. SUPPLEMENTARY NOTES

This report was prepared from data plotted by REMTECH, Inc., Huntsville, AL. All data presented are in a data base maintained by REMTECH and are available in tabular or magnetic tape form.

19. KEY WORDS (Continue on reverse side if necessary and identify by block number)

Thrust Effects
Longitudinal Stability
Plume Effects
Base Pressure
Plume
Boundary Layer Separation

20. ABSTRACT (Continue on reverse side if necessary and identify by block number)

A study of the stabilizing effectiveness of several folding, split flare afterbodies in the presence of an underexpanded jet plume is presented. Mach number was varied from 0.7 to 1.4 and angle of attack from -4° to 6°. It is shown that the split flare afterbody can be an effective stabilizing device for tube launched missiles.

deg

DD FORM 1 JAN 73 1473 EDITION OF 1 NOV 65 IS OBSOLETE

UNCLASSIFIED

SECURITY CLASSIFICATION OF THIS PAGE (When Data Entered)

408 564

1B

TABLE OF CONTENTS

I. INTRODUCTION

A common requirement for tube launched missiles is that the aerodynamic stabilizing surfaces be approximately the same diameter as the missile body when in the tube. Several devices have been designed and tested which satisfy this requirement. Among these are: wraparound fins, folding fin configurations, and trailing ring-tails. All of these devices have disadvantages in certain flight conditions. Wraparound fins generally have large induced roll moments which vary with Mach number. Folding fins usually have a high aspect ratio and, therefore, lose much of their stabilizing effectiveness at high supersonic Mach numbers. The effectiveness of trailing ring-tails is greatly reduced by an underexpanded rocket plume; and therefore, they are not suitable for a high acceleration rocket with a motor burning after tube exit.

An alternate to the above stabilizing devices is a split flare which would be folded into a cylindrical shape while in the launch tube and expanded into a partial or split flare upon tube exit. Intuitively, this configuration would have two advantages over the other stabilizing devices suitable for a tube launched, high acceleration, supersonic rocket. Solid flares are more effective than fins as stabilizing devices at high supersonic Mach numbers; therefore, a split flare may also be more effective. Also, a solid flare is an effective device for inhibiting the onset of the adverse effects of an underexpanded rocket plume on rocket static stability; therefore, a split flare may also be effective as a thrust effects inhibitor.

Wind tunnel data were obtained for seven model configurations consisting of solid flares, split flares, and a cylindrical afterbody in the presence of a normal jet plume simulator.

Mach number was varied from 0.7 to 1.4, and the angle of attack range was -4° to 6°. The effect of roll angle on split flare effectiveness was investigated.

II. EXPERIMENTAL PROGRAM

A. Test Facility.

The AEDC-PWT Aerodynamic Wind Tunnel (1T) is a continuous flow, nonreturn facility, with Mach number capability from 0.2 to 1.5. The tunnel total pressure is essentially nonvariant at approximately 2850 psfa with ± 5 percent variation. The total temperature variation can be controlled from 80 to 120 degrees F. The test section is one foot square and 37.5 inches long with 6 percent porosity with all four perforated walls installed.

During the visualization phase the sidewalls were replaced with solid transparent walls.

A more detailed description of the 1T facility may be found in the AEDC Test Facility Handbook (reference 1).

B. Model

The model was a sting mounted body of revolution having a diameter of 1.1 inches, Figure 1. It had a 3-caliber, tangent ogive nose and a total length of 10.4 calibers (11.44 in.). A cylindrical afterbody, two solid flare afterbodies, and four split flare afterbodies were tested. All afterbodies were the same length (1.725 in.) with two base diameters used for the solid and split flare configurations (1.705 in. and 2.071 in.). The split flare afterbodies had either 6 or 12 petals, and one of the 6-petal configurations had partially filled slots or skirts. The model assembly is shown in Figure 2, and the afterbodies tested are shown in Figure 3. The plume simulator was located 0.73 in. behind the model base. Effective plume shape was controlled by regulating nitrogen flow through 12 holes, 5/64 in. diameter, equally spaced around the circumference of the simulator. The simulator had a total sonic jet orifice area of 6% of the model cross-sectional area and was 0.815 in. in diameter. Detailed descriptions of the plume simulator and all model parts are contained in MIRADCOM drawings TDK-13900 series.

Model	Nomenclature
C	Cylindrical afterbody
FD1	Small diameter solid flare afterbody
FD2	Large diameter solid flare afterbody
F6D2	Large diameter, 6-petal, split flare afterbody
F6D2S	Large diameter, 6-petal, split flare afterbody, skirt
F12D1	Small diameter, 12-petal, split flare afterbody
F12D2	Large diameter, 12-petal, split flare afterbody

III. TEST PROCEDURE

All configurations were tested at Mach numbers of 0.7, 1.05, 1.25, and 1.4. Data for a single run were obtained by varying angle of attack from -4° to 6° while holding Mach number and plume simulator chamber pressure constant. The plume simulator nitrogen supply was adjusted to give the preselected chamber pressure that gave the desired radial thrust coefficient (CRT) for the tunnel test section conditions. Nominal test conditions are given in Table 1, and the values for chamber pressure at specified values of CRT along with the expression for computation is contained in Table II. Zero roll position for the split flare configurations was with a petal flat up. Most of the runs were made at zero roll angle, but the effect of roll on stability was investigated with the F6D2 configuration.

Shadowgraphs and oil flow photographs were taken at selected test points.

IV. DATA

All balance force coefficients are referenced to the cross-sectional area of the body, 0.95033 sq. in. The moment reference center is located at model station 5.83 inches aft of the nose (5.1 calibers forward of the body base). The moment coefficients are referenced to the body cross-sectional area times the body diameter (1.1 in.). The sign convention is the standard body axis system, positive nose up and right (climbing right turn). The two base pressures were averaged and ratioed to the free stream ambient pressure. Corrections to angle-of-attack were made for sting and balance deflections caused by aerodynamic loads and model weight.

The 2σ data uncertainties, calculated from the balance calibration, are shown in Table III.

V. DISCUSSION AND RESULTS

There are two primary geometry differences between the split flares and solid flares, and the effects of these differences are qualitatively easy but quantitatively difficult to predict. First, the split flares have less surface area than solid flares of the same length and diameter. Intuitively, the effect of this difference would be reduced stabilizing effectiveness for the split flare, but not a reduction equal to the surface area ratio, because of petal-to-petal interference.

Second, the split flare probably would not inhibit the onset of afterbody flow separation due to an underexpanded jet plume as well as the geometrically similar solid flare because of the high base pressure feeding up through the splits in the afterbody. In this study the effects of base diameter, number of petals, and a partial fill in skirt on split flare stabilizing effectiveness as compared to solid flares are investigated.

The basic longitudinal stability coefficients for all configurations tested are shown in Figure 4. Typical variation of base pressure with CRT is shown in Figure 5. The data in this figure was taken at Mach number 1.25 and zero angle of attack. A comparison of the plateau base pressure of the afterbodies tested gives an indication of their effectiveness in inhibiting flow separation, with a high plateau pressure indicating a good flow separation inhibitor.

As expected, the large diameter, solid flare, FD2, has the highest base pressure plateau and the cylindrical afterbody yields the lowest base pressure plateau. The data shows that the 6-petal configuration is more effective than the 12-petal configuration and that the skirt added to the 6-petal configuration causes little change in base pressure plateau.

Normal force coefficient and pitching moment coefficient versus angle of attack slopes at small angles of attack are shown as a function of CRT in Figure 6. Clearly, the large diameter, solid flare, FD2, is the most effective stabilizing afterbody tested. The 6-petal, large diameter split flare and the addition of the fill-in-skirt to the large diameter split flare increases its stabilizing effectiveness very little. Total axial force coefficients for all configurations tested are shown in Figure 7.

SUMMARY AND CONCLUSIONS

This report is a study of the aerodynamic stabilizing effectiveness of several split flare afterbodies suitable for use in tube launched, free rocket design. The split flares were compared to solid flares with the same base diameter and length in a transonic wind tunnel test. Mach number was varied from 0.7 to 1.4 and angle of attack from -4^{o} to 6^{o}.

The following conclusions were drawn from this study:

1) The solid flares are more effective aerodynamic stabilizing devices than the split flares of the same base diameter and length.

2) The 6-petal split flare is a more effective aerodynamic stabilizing device than the 12-petal split flare.

3) The addition of partial fill-in-skirts to the 6-petal split flare design only caused a slight increase in aerodynamic stabilizing effectiveness.

REFERENCE

1. "Test Facilities Handbook" (Tenth Edition), Propulsion Wind Tunnel Facility, Vol. 4, Arnold Engineering Development Center, May 1974.

NOMENCLATURE

SYMBOL	PLOT SYMBOL	DEFINITION
C_A		total measured axial force coefficient
C_m	C_{LM}	pitching moment coefficient
C_N	C_N	normal force coefficient
C_{m_α}	$C_{M_{ALPHA}}$	pitching moment slope at zero angle of attack
C_{N_α}	$C_{N_{ALPHA}}$	normal force slope at zero angle of attack
CRT	CRT	radial thrust coefficient
FA		axial force
FN		normal force
FY		side force
ℓ_{ref}	LREF	reference length, in.
M_ℓ		rolling moment
M_m		pitching moment
M_n		yawing moment
M_∞	MACH	tunnel test section Mach number
P_b/P_∞		base to tunnel static pressure ratio
P_t		tunnel stagnation pressure, psfa

NOMENCLATURE (Continued)

SYMBOL	PLOT SYMBOL	DEFINITION
q_{∞}		tunnel test section dynamic pressure, psf
R_N		Reynolds number, per foot
S_{ref}	SREF	reference area used to reduce data to coefficient form, in.
X_{mrp}	XMRP	moment reference point on X axis
α	ALPHA	angle of attack, degrees
ϕ	PHI	angle of roll, degrees

TABLE 1. NOMINAL TEST CONDITIONS.

M_∞	P_t (psfa)	q_∞ (psf)	$R_N \times 10^{-6}$ (per ft.)
0.7	2850	705	4.426
1.05	↓	1090	5.237
1.25	↓	1204	4.999
1.4	↓	1229	4.916

TABLE 2. NOMINAL PLUME SIMULATOR CHAMBER PRESSURE.

MACH	CRT											
	2.5	4.0	5.0	6.1	7.0	9.1	10.2	11.2	14.2	16.6	18.6	25.5
0.7				395			661				1190	1630
1.05	255			615				1120		1630		
1.25	280		557			1005			1580			
1.40	280	460			800			1265				

$$CRT = A_{nj}\ (0.5283 \times P_c\ (1.4 \times M_j^2\ + 1) - P_s/144\ /\ (A_{ref} \times q/144)$$

where

A_{nj} = Total exit area, 12 orifices

A_{nj}/A_{ref} = 0.06

M_j = Sonic jet (M=1.0)

q = Free stream dynamic pressure, psf

P_c = Chamber pressure in simulator, psi

P_s = Tunnel static pressure, psf

P_t = 2850 psf -- tunnel total pressure

TABLE 3. DATA UNCERTAINTY.

2σ uncertainties calculated from the balance calibration

	Type of Loading			
	FN	FY	FA	Mℓ
ΔFN	0.06	0.02	0.06	0.12
ΔFY	0.02	0.03	0.08	0.04
ΔFA	0.03	0.10	0.06	0.05
ΔMℓ	0.02	0.02	0.01	0.04
ΔMm	0.04	0.05	0.08	0.15
ΔMn	0.04	0.08	0.09	0.09

TABLE 4. DATA SET SUMMARY.

TEST AEDC TM-359

Config	Mach No.	α	φ	CRT 0	2.5	4.0	5.0	6.1	7.0	9.1	10.2	11.2	14.2	16.6	18.6	25.5
C	0.70	A	0	3				10			9				8	7
C	1.05	A	0	11	12			18				16		25		
C	1.25	A	0	22	21		20			19			26			
C	1.40	A	0	27	31	30			29			28				
FD1	0.70	A	0	55				59			58				57	56
FD1	1.05	A	0	53	60			50				49		48		
FD1	1.25	A	0	42	41		40			39			45			
FD1	1.40	A	0	34	38	37			36			35				
FD2	0.70	A	0	64				70			71				72	63
FD2	1.05	A	0	65	69			68				67		66		
FD2	1.25	A	0	75	79		78			77			76			
FD2	1.40	A	0	80	84	83			82			81				
F6D2S	0.70	A	0	104				108			107				106	105
F6D2S	1.05	A	0	103	113			112				111		101		
F6D2S	1.25	A	0	97	96		95			94			93			
F6D2S	1.40	A	0	92	91	90			88			87				
F12D1	0.70	A	0	117				125			124				123	116
F12D1	1.05	A	0	118	122			121				120		119		
F12D1	1.25	A	0	133	132		131			126			129			
F12D1	1.40	A	0	134	138	137			136			135				
F12D2	0.70	A	0	160				164			163				162	151
F12D2	1.05	A	0	155	152			153				154		159		
F12D2	1.25	A	0	147	151		156			149			148			
F12D2	1.40	A	0	145	144	143			142			141				
F6D2	0.70	A	0	167				171			170				169	168
F6D2	1.05	A	0	175	174			173				172		173		
F6D2	1.25	A	0	184	183		182			161			180			
F6D2	1.40	A	0	185	189	188			187			186				
F6D2	0.70	A	30	206				210			209				208	207
F6D2	1.05	A	30	205	213			212				211		204		
F6D2	1.25	A	30	197	198		199			200			203			
F6D2	1.40	A	30	192	196	195			194			193				
F6D2	0.70	A	180	215				218								
F6D2	1.05	A	180	219				220								

A = -4, -2, -1, -0.25, 0, 0.25, 0.5, 1.0, 2.0, 4.0, & 6.0

TEST RUN NUMBERS

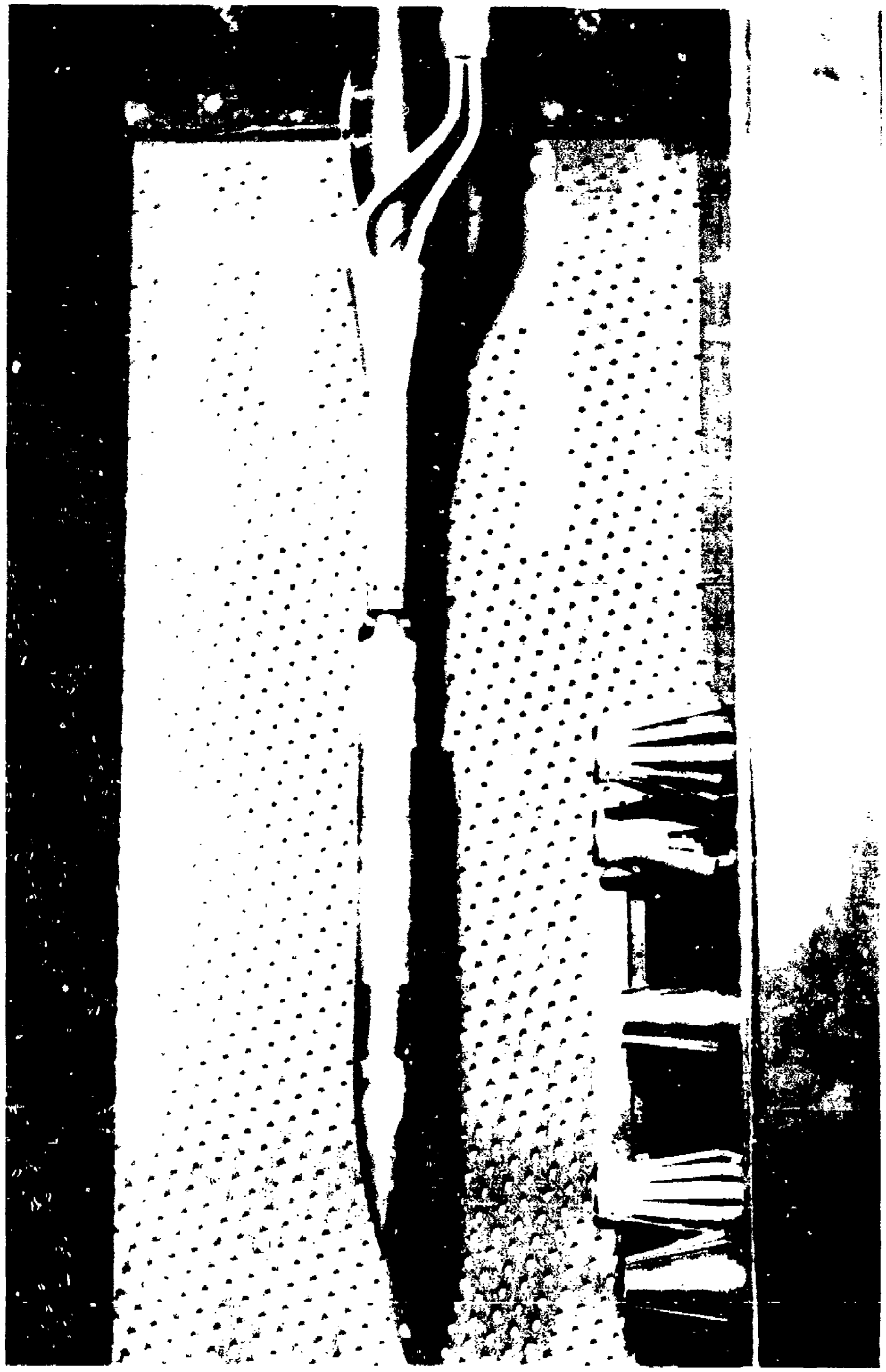

Figure 1. Model installation photograph.

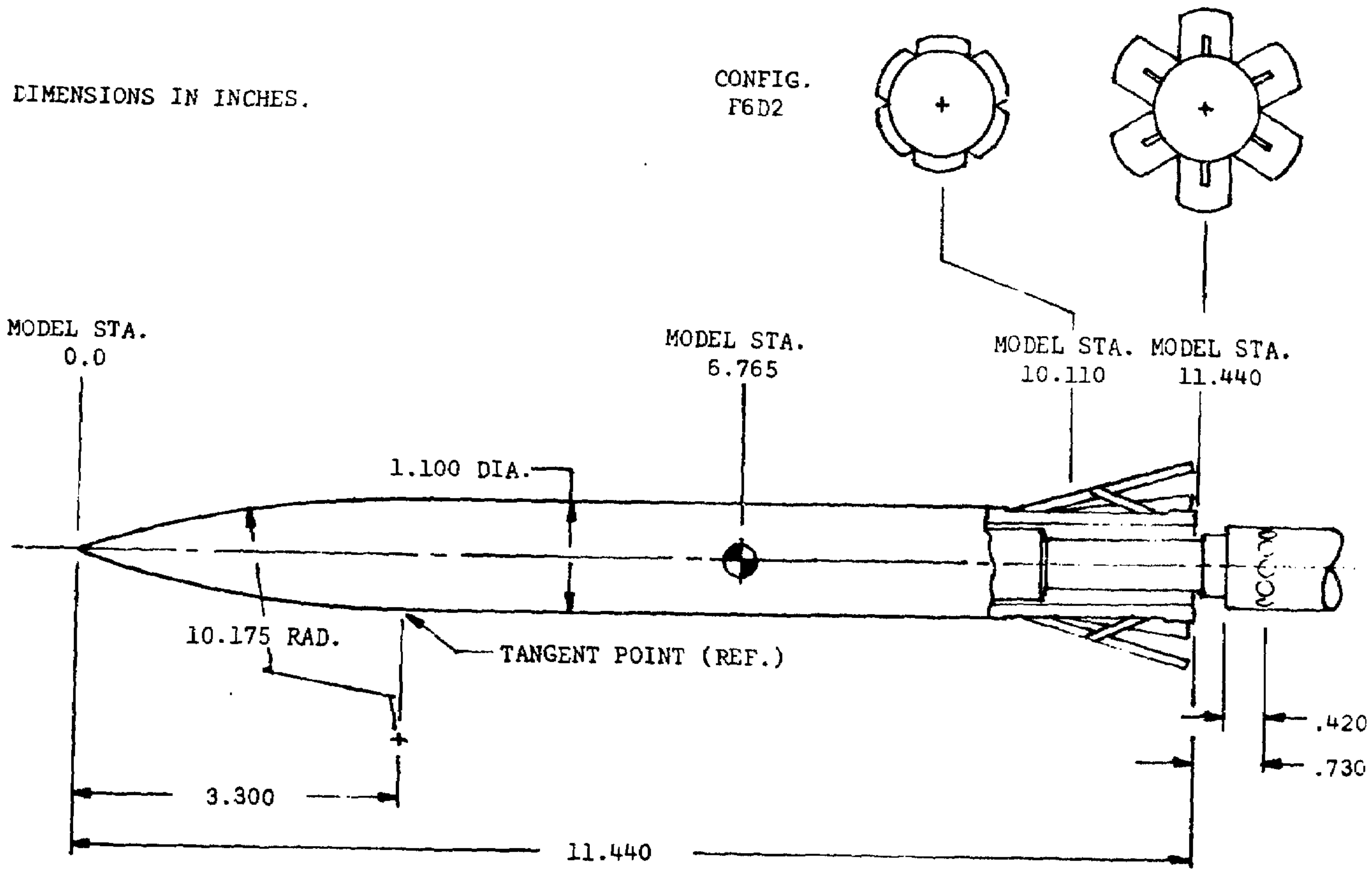

Figure 2. Model assembly.

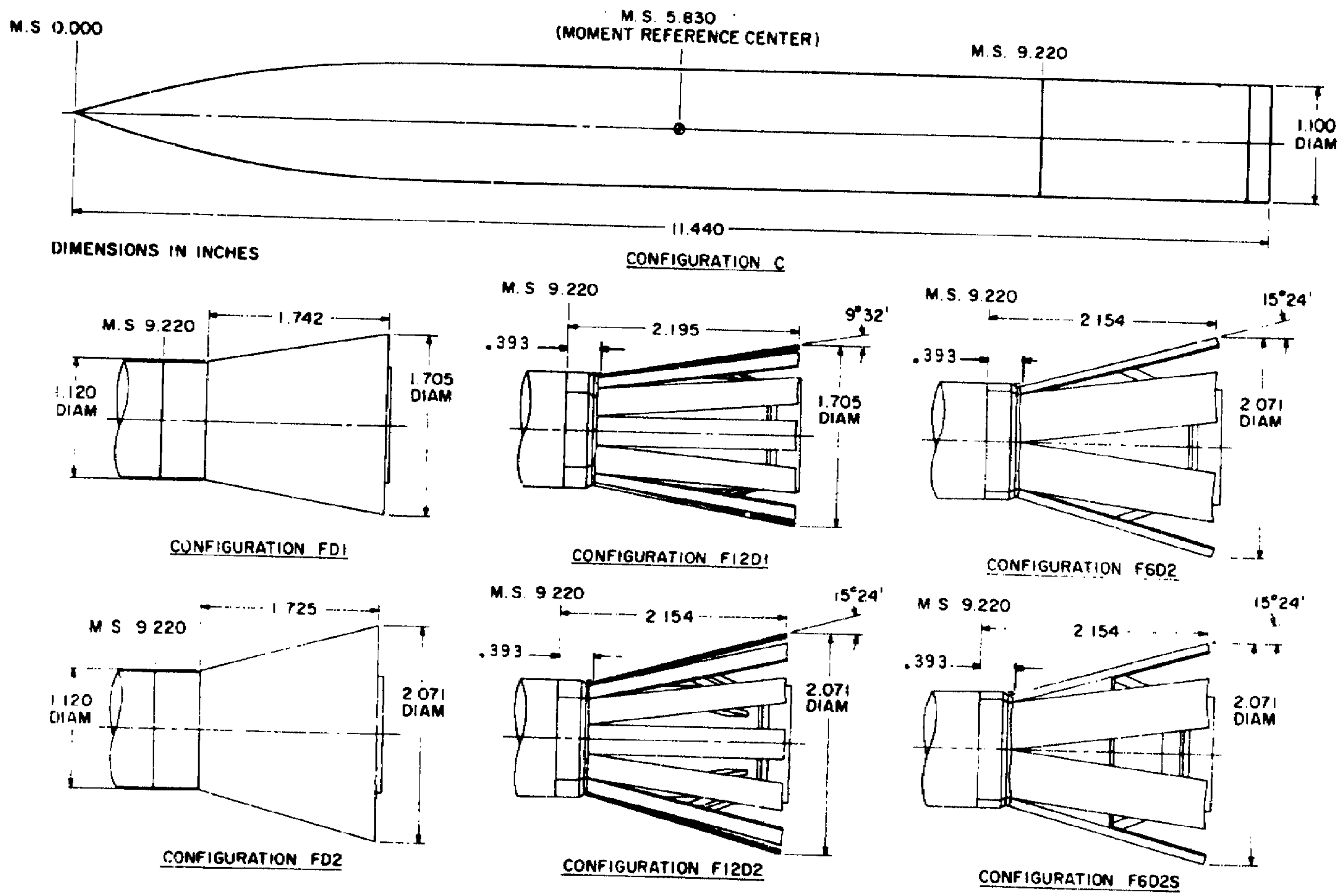

REFERENCE AREA (S): 0.950 in.^{2} REFERENCE LENGTH: 1.100 in.

Figure 3. Model details and identificat:

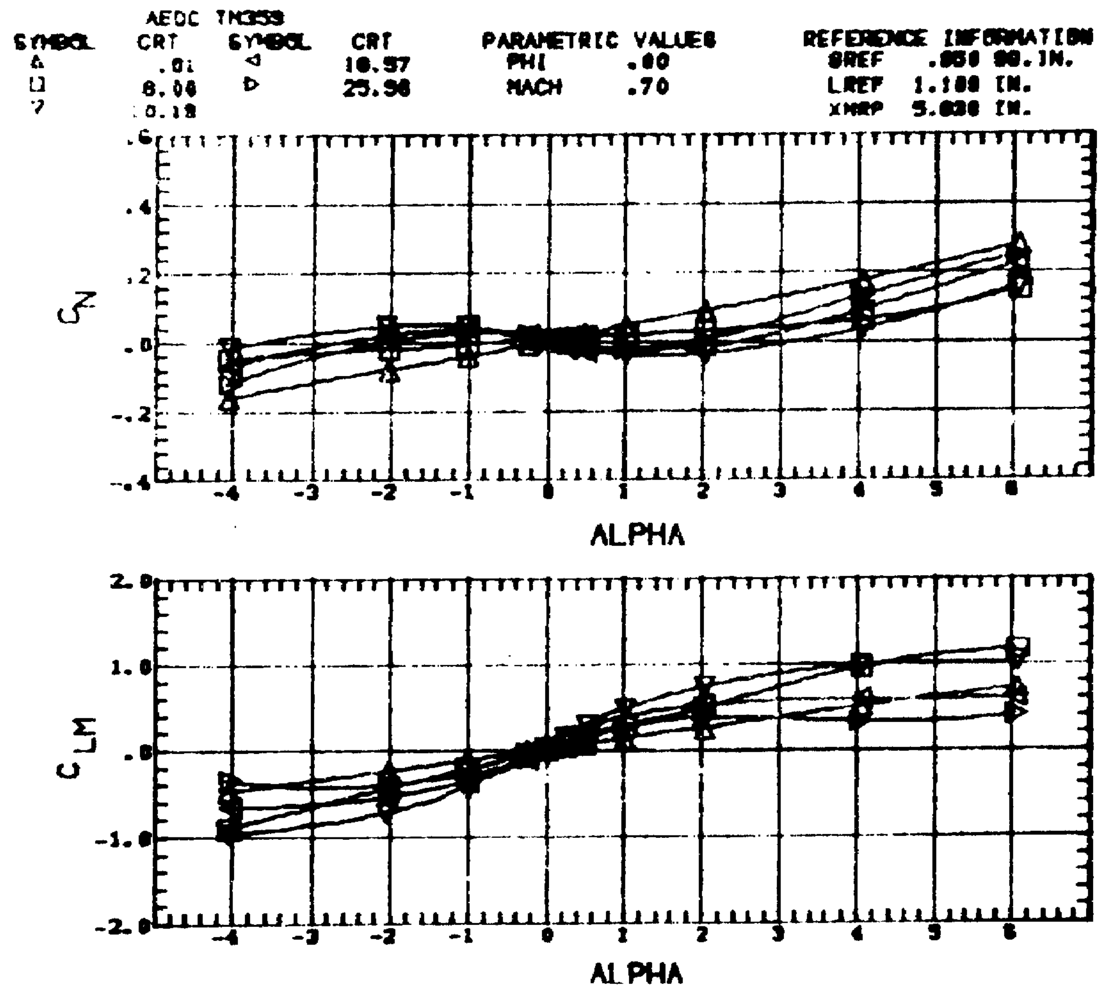

Figure 4. Thrust effects on stability coefficients. C

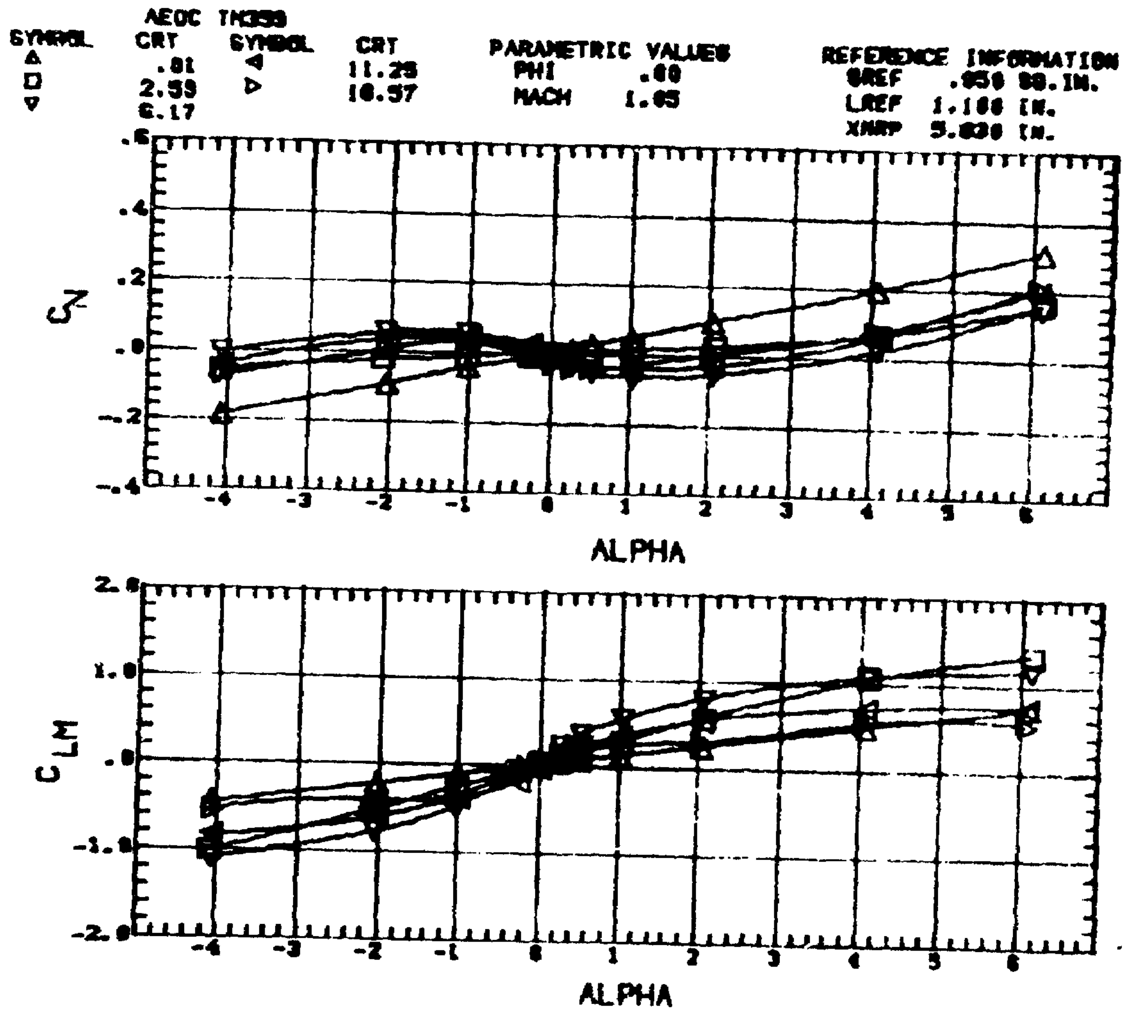

Figure 4. Continued. C

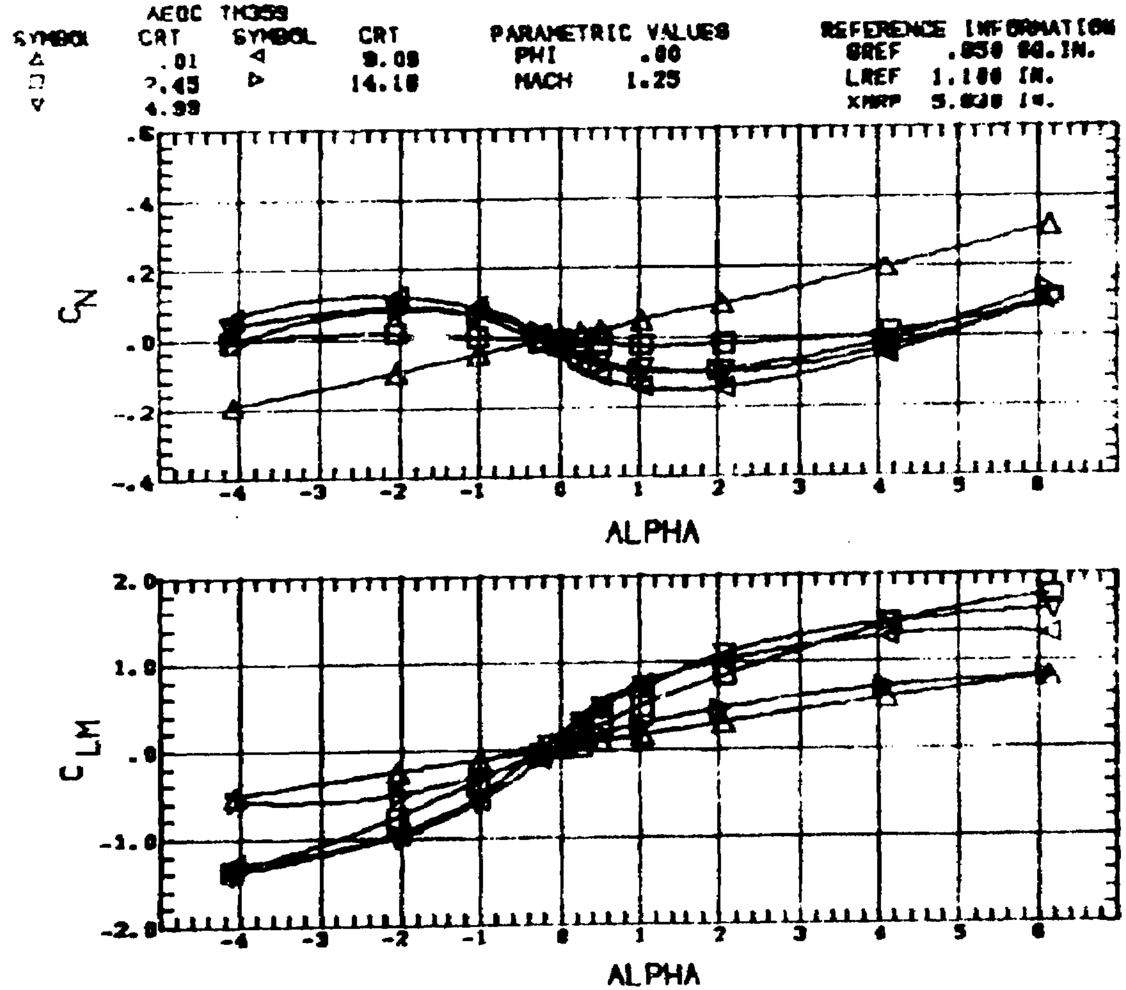

Figure 4. Continued. C

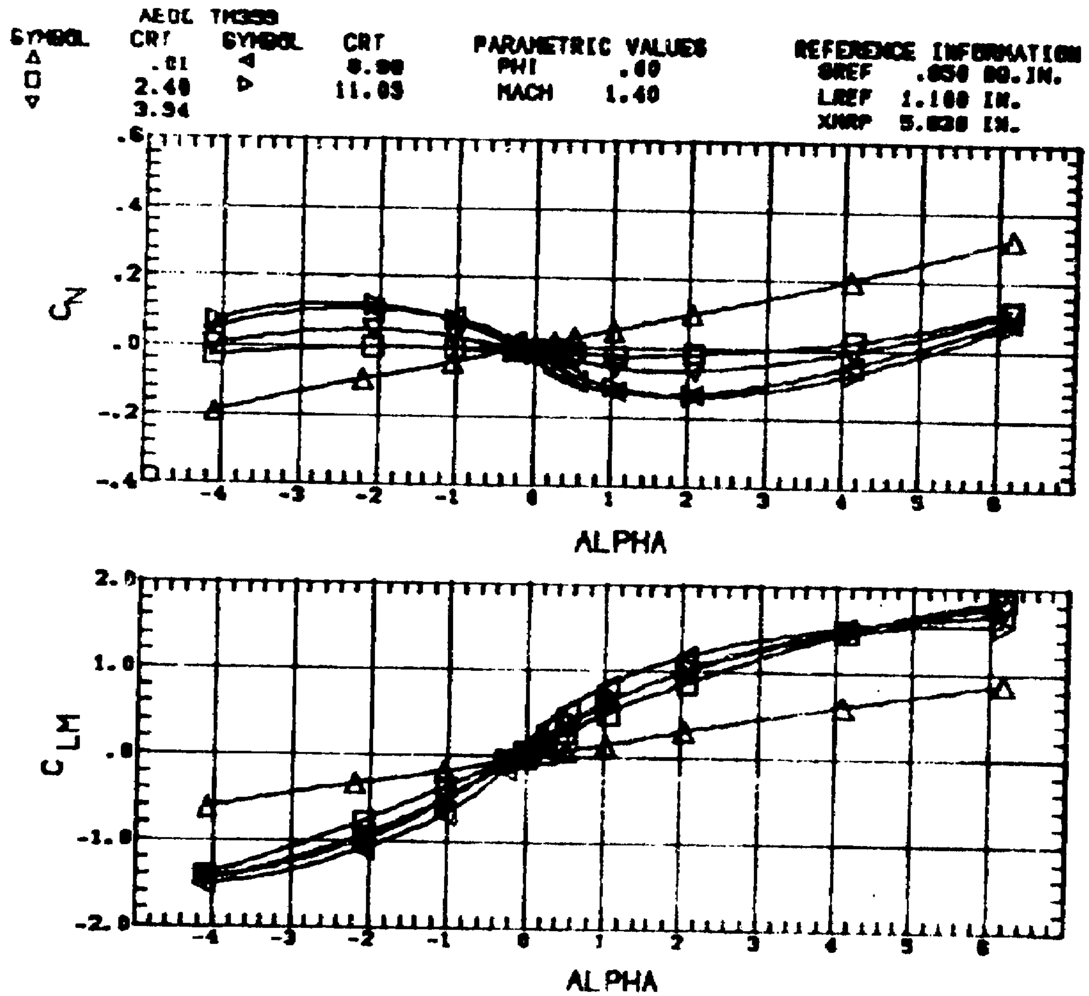

Figure 4. Continued. C

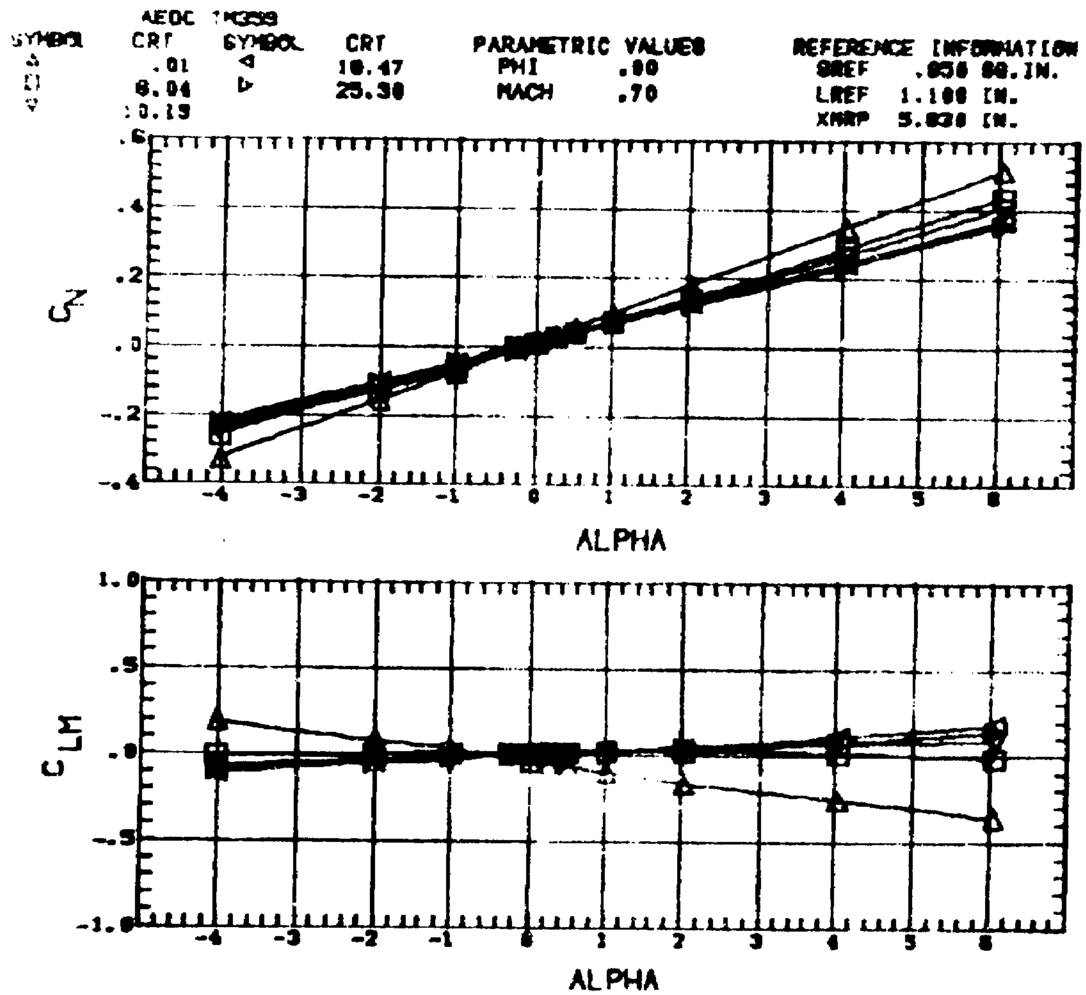

Figure 4. Continued. FD1

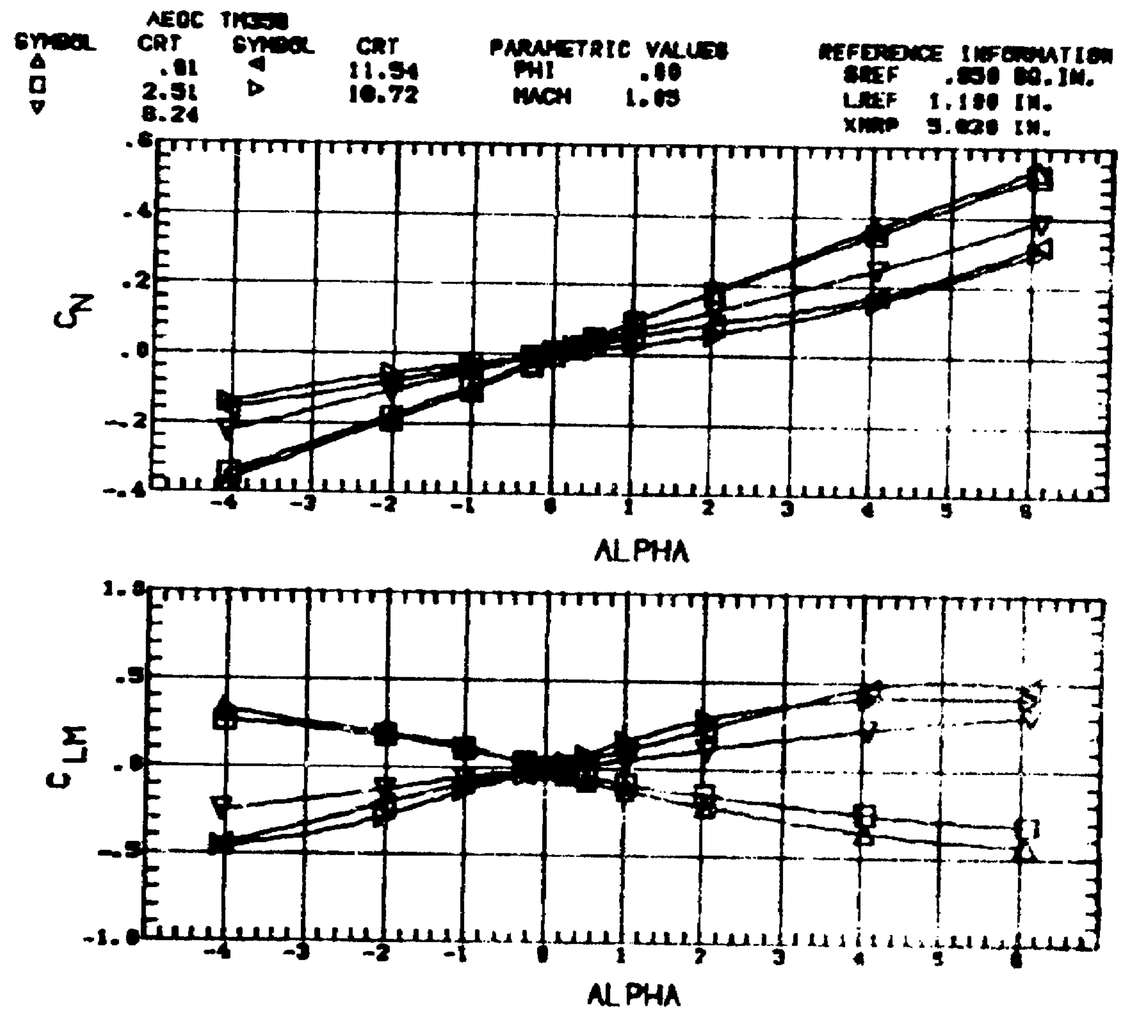

Figure 4. Continued. FD1

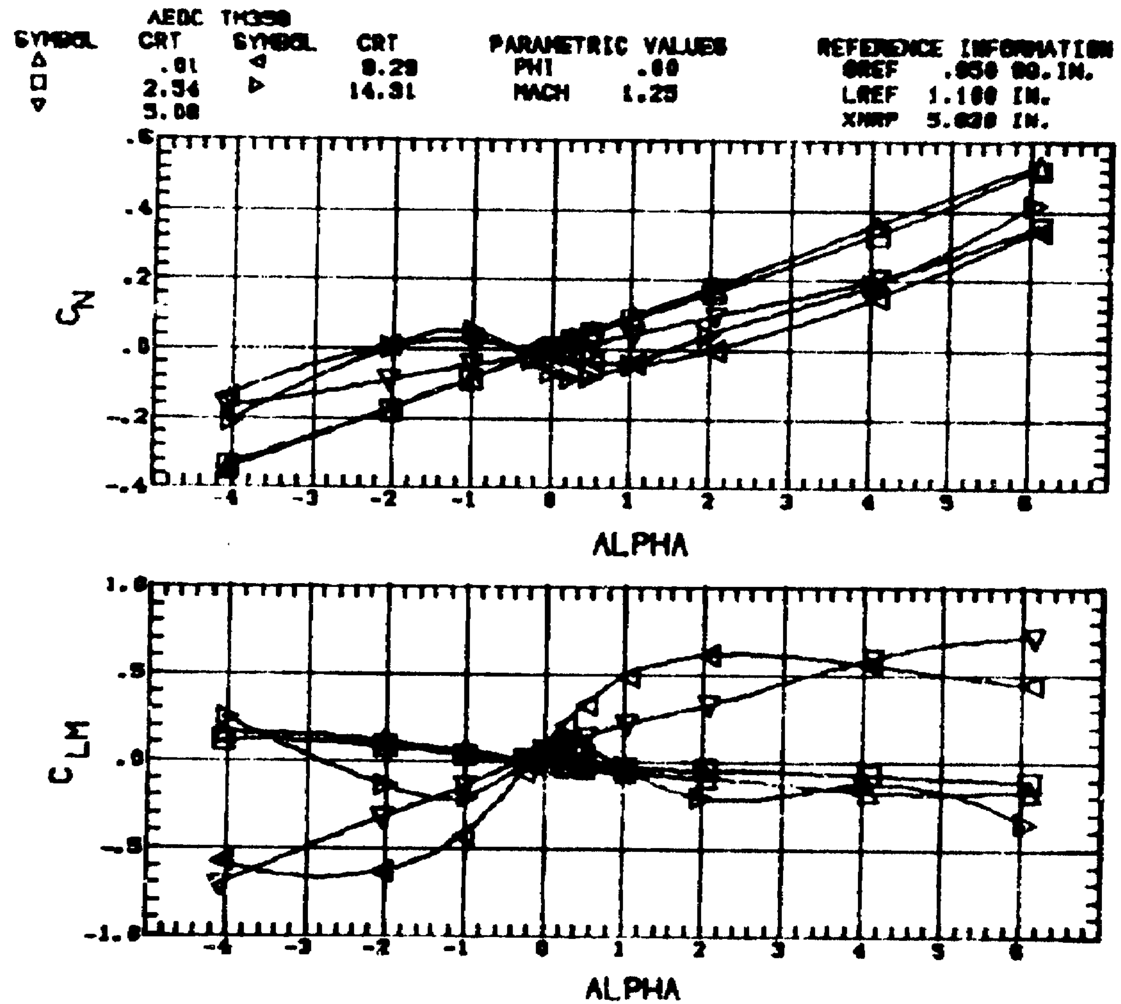

Figure 4. Continued. FD1

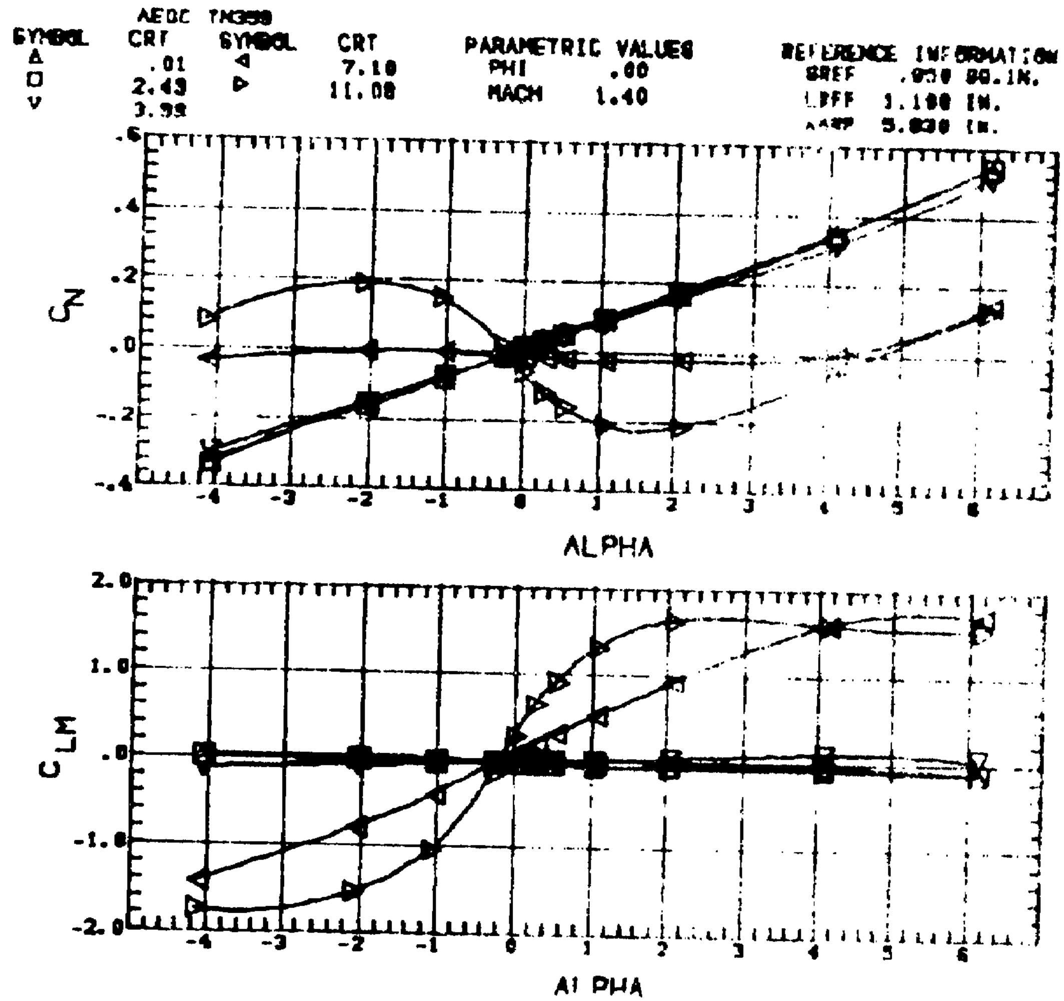

Figure 4. Continued. FD1

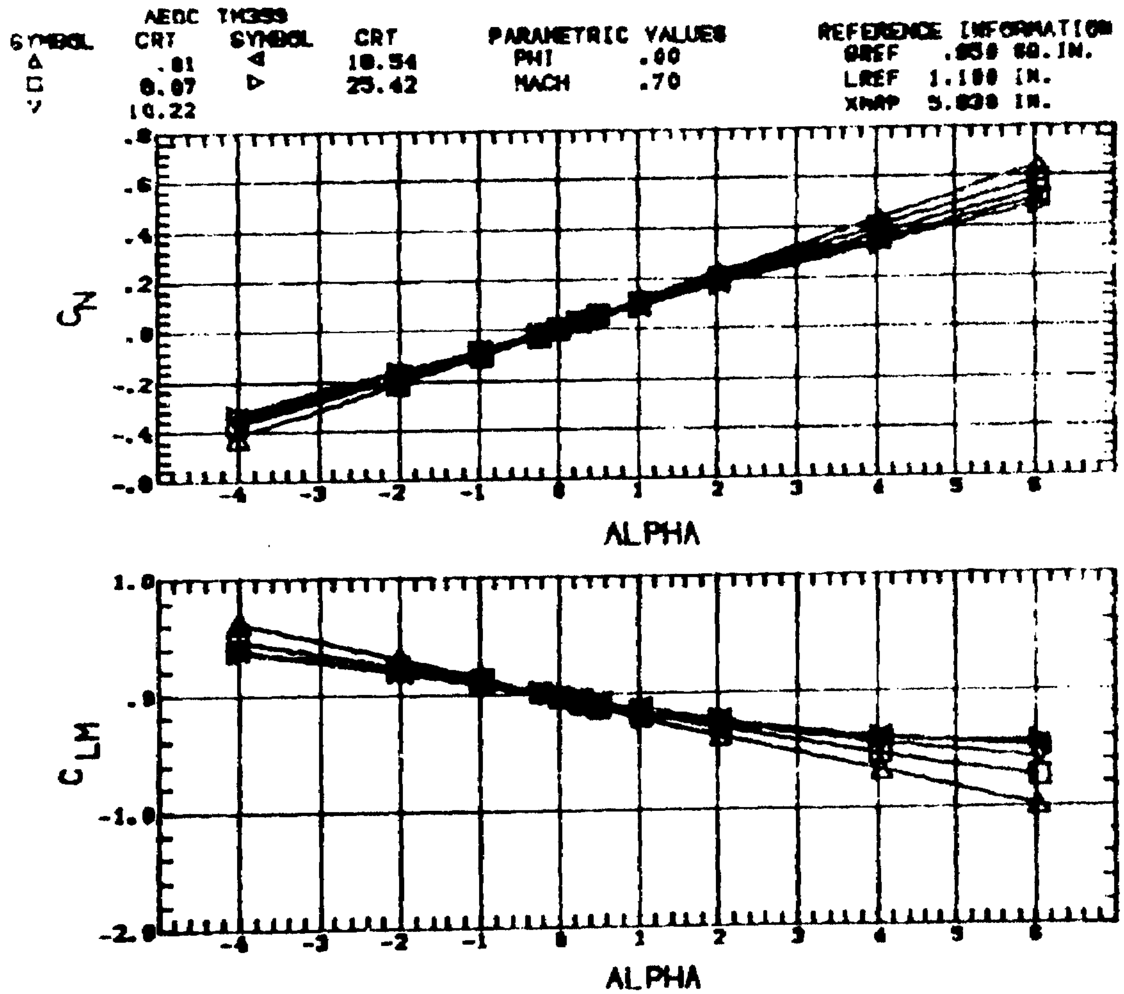

Figure 4. Continued. FD2

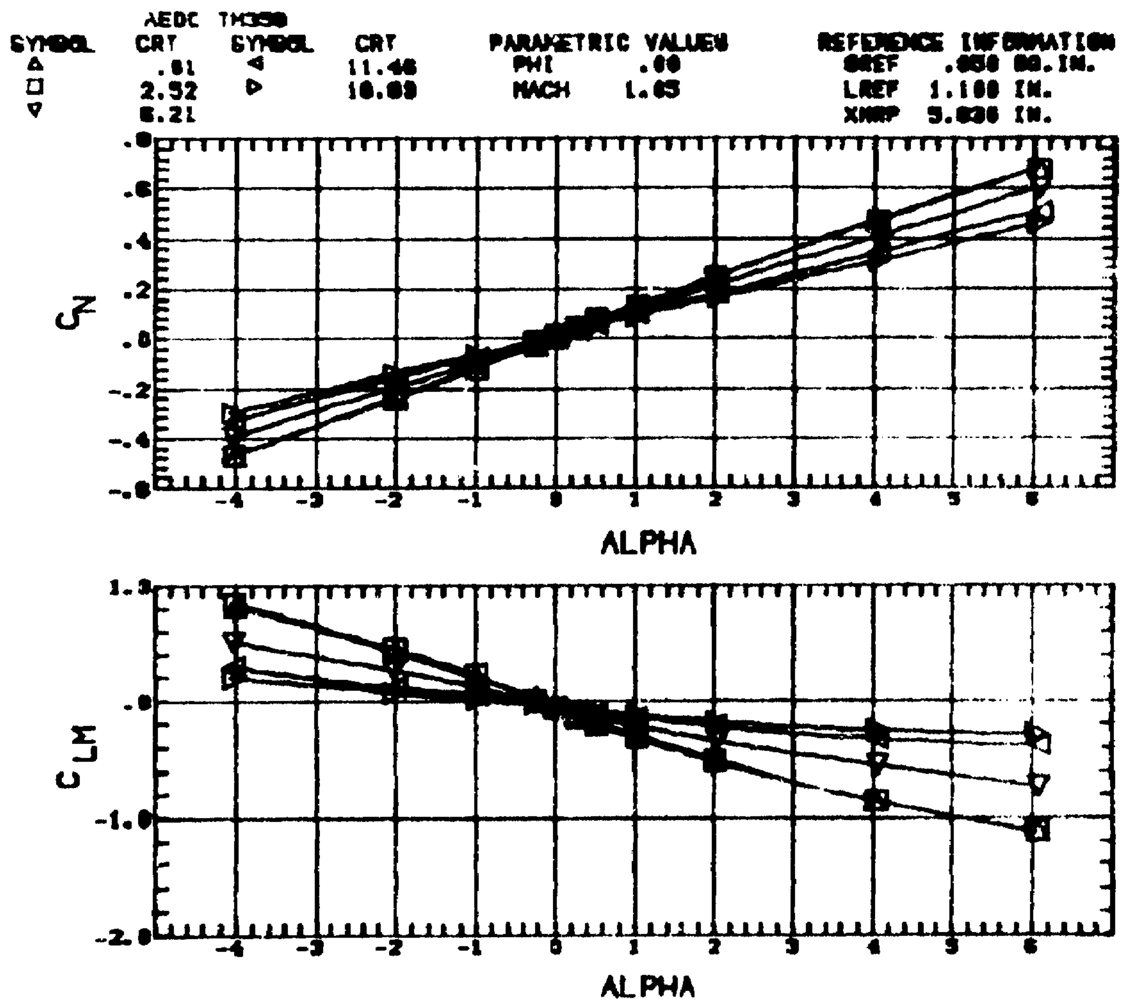

Figure 4. Continued. FD2

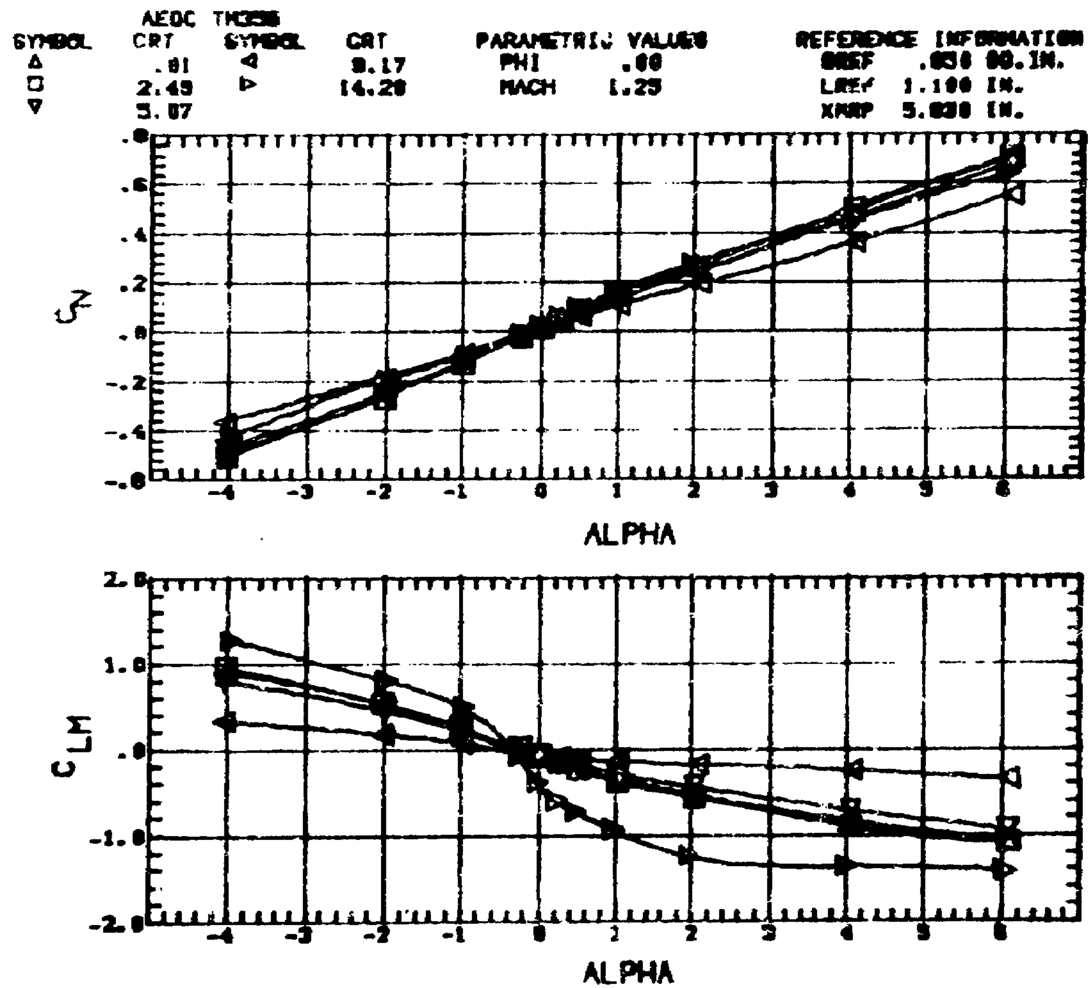

Figure 4. Continued. FD2

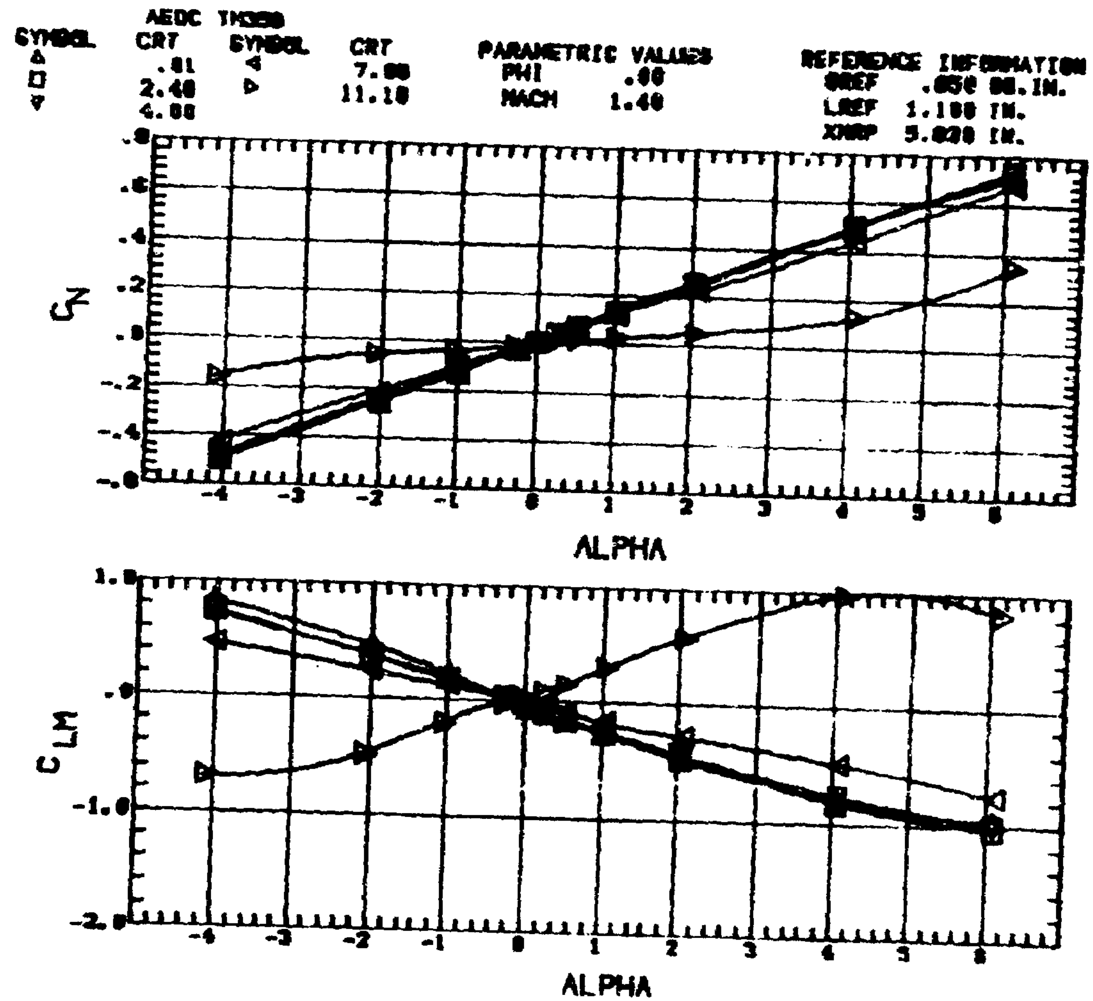

Figure 4. Continued. FD2

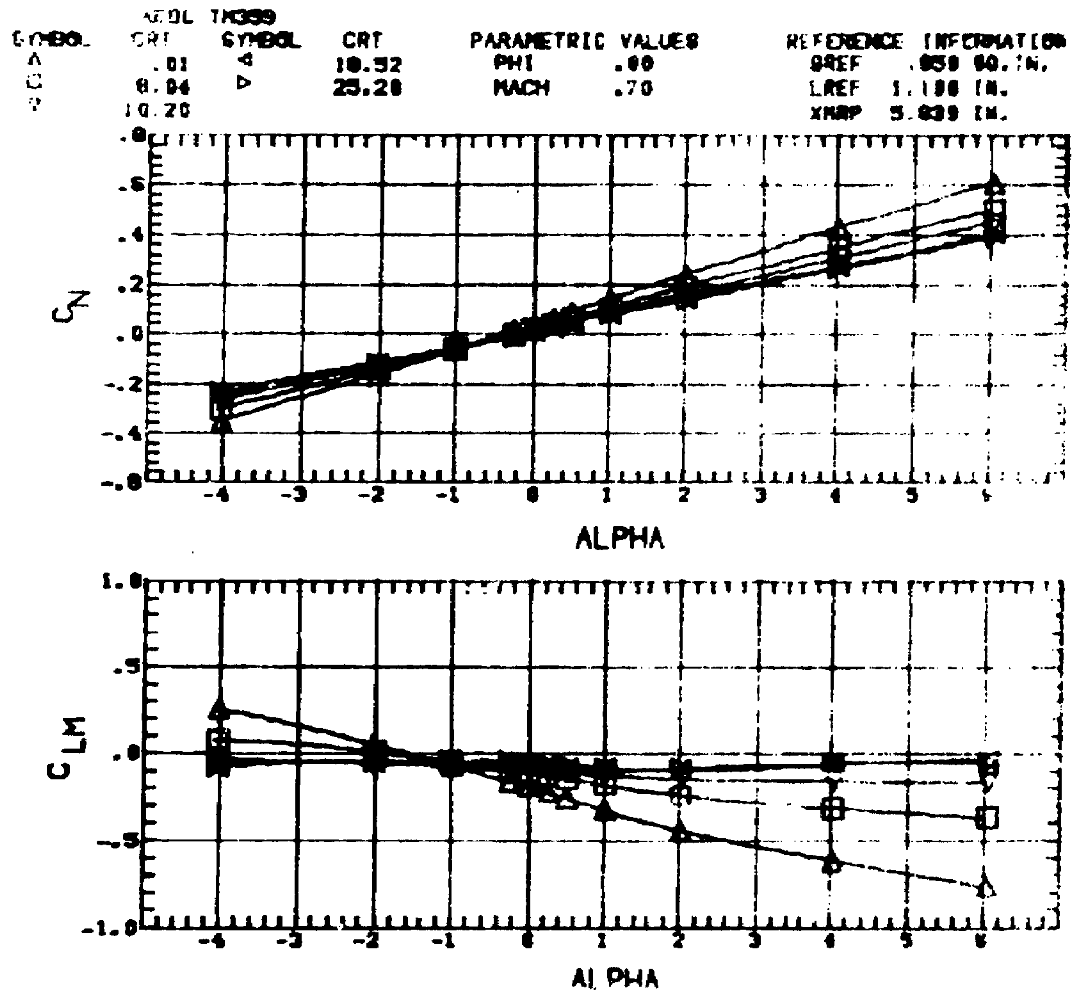

Figure 4. Continued. F6D2S

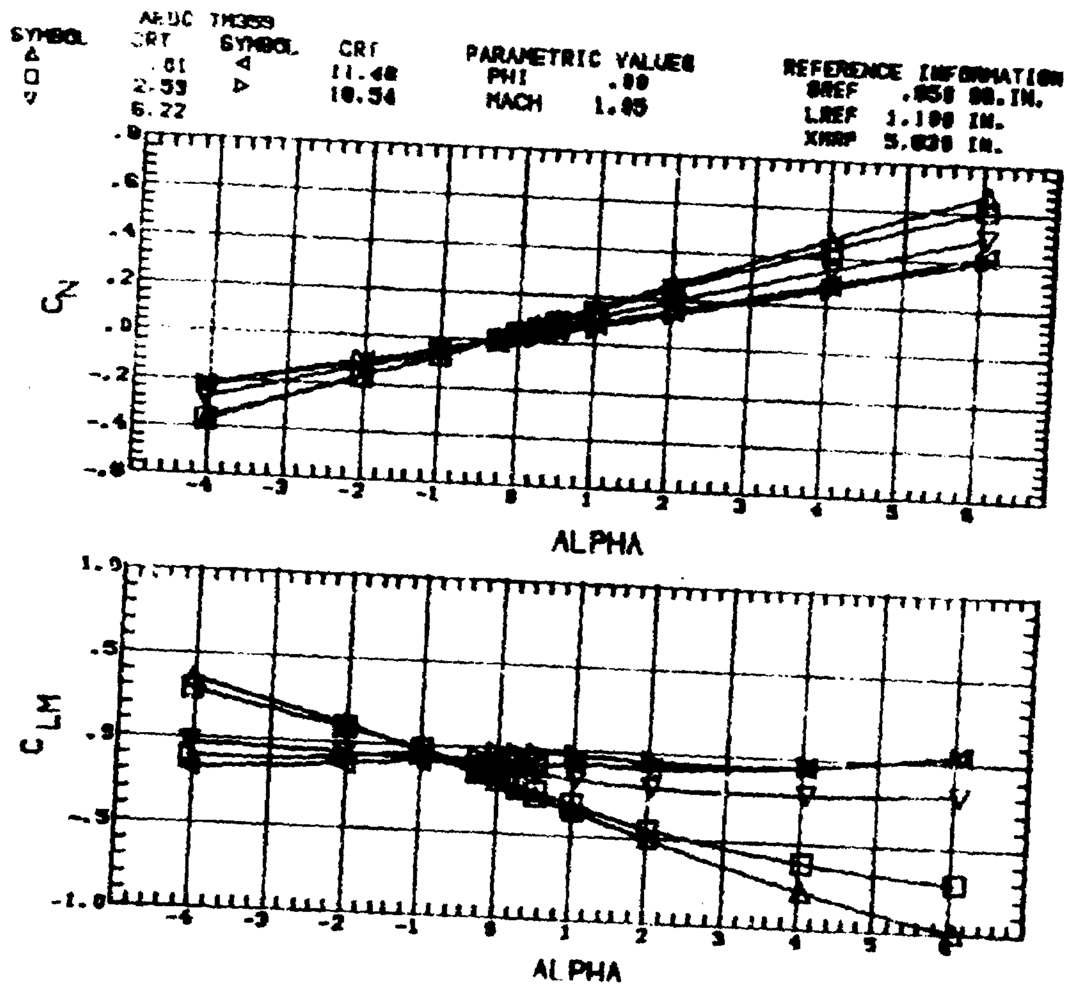

Figure 4. Continued. F6D2S

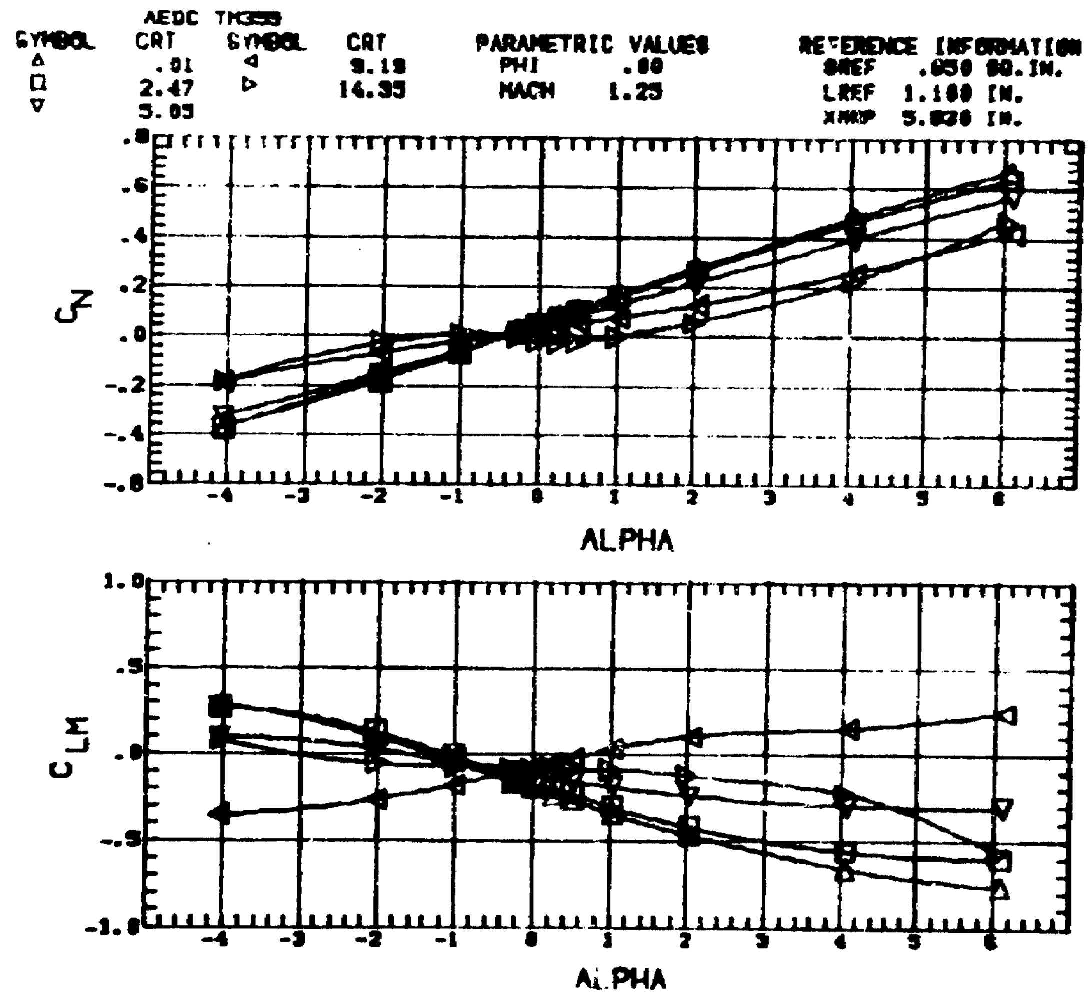

Figure 4. Continued. F6D2S

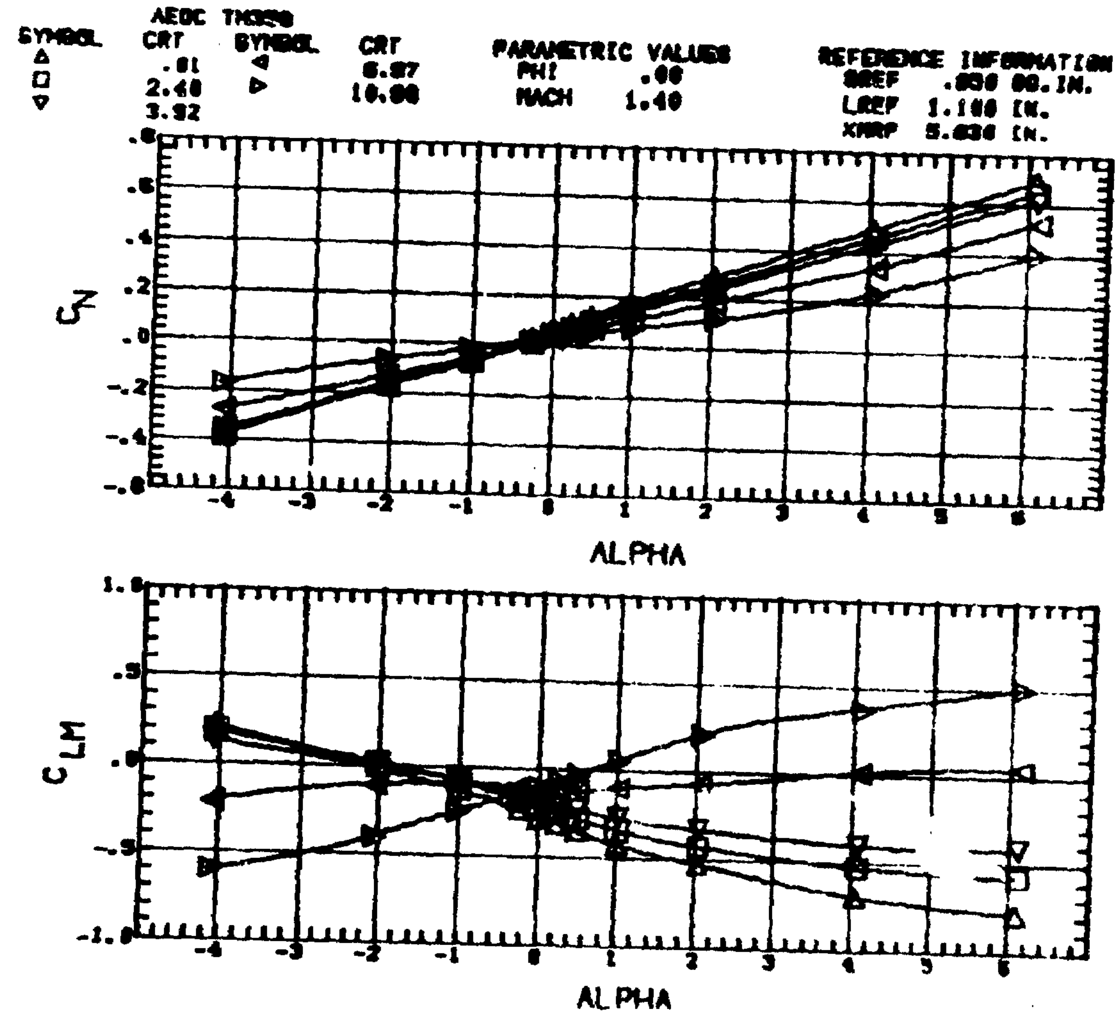

Figure 4. Continued. F6D2S

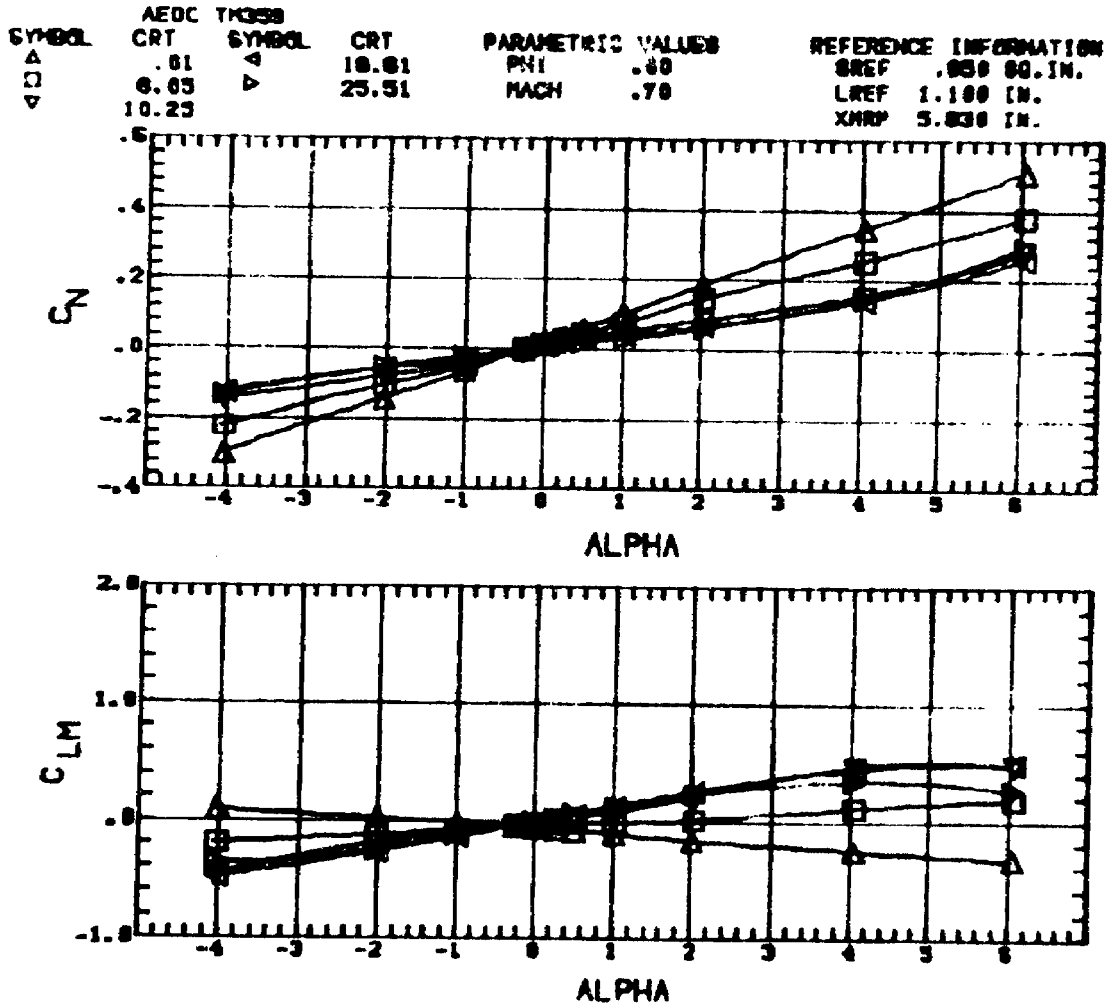

Figure 4. Continued. F12D1

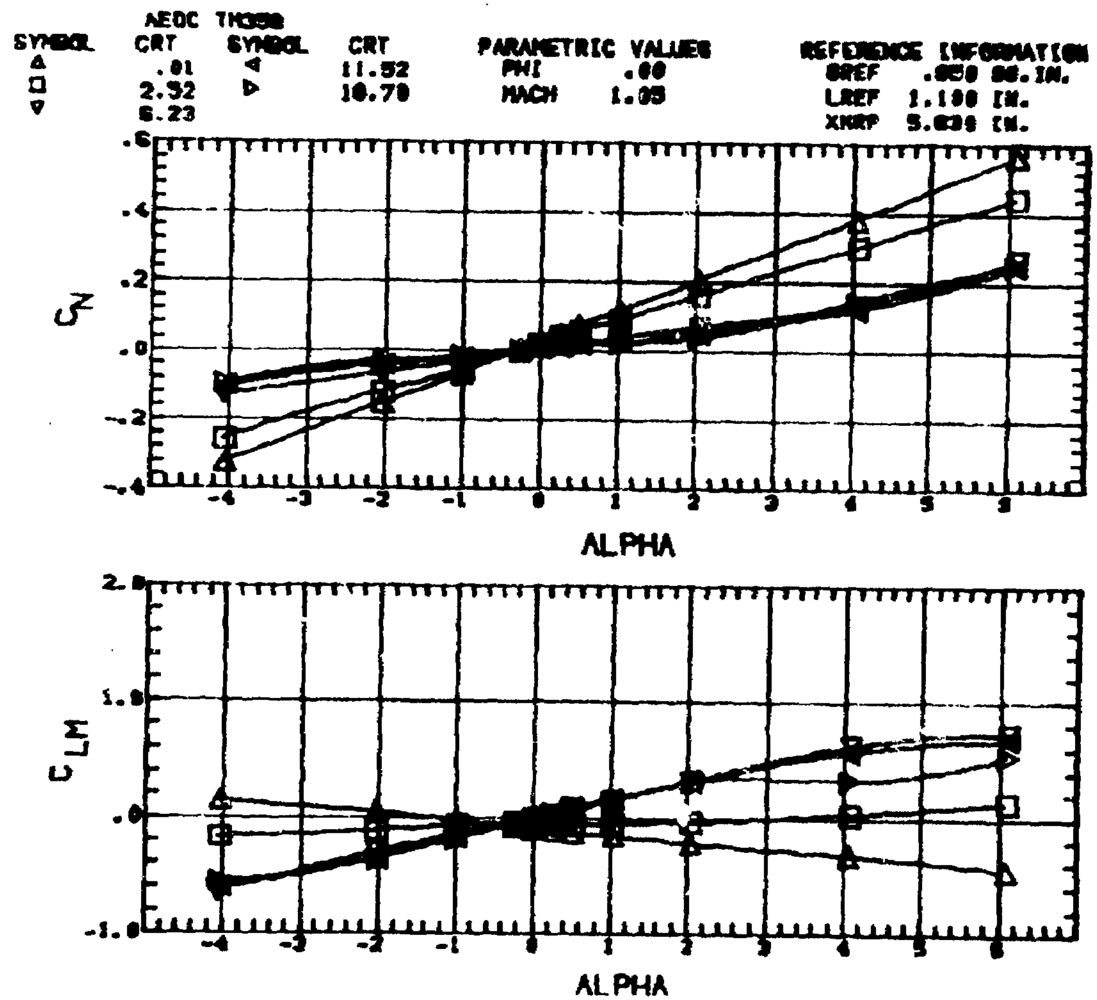

Figure 4. Continued. F12D1

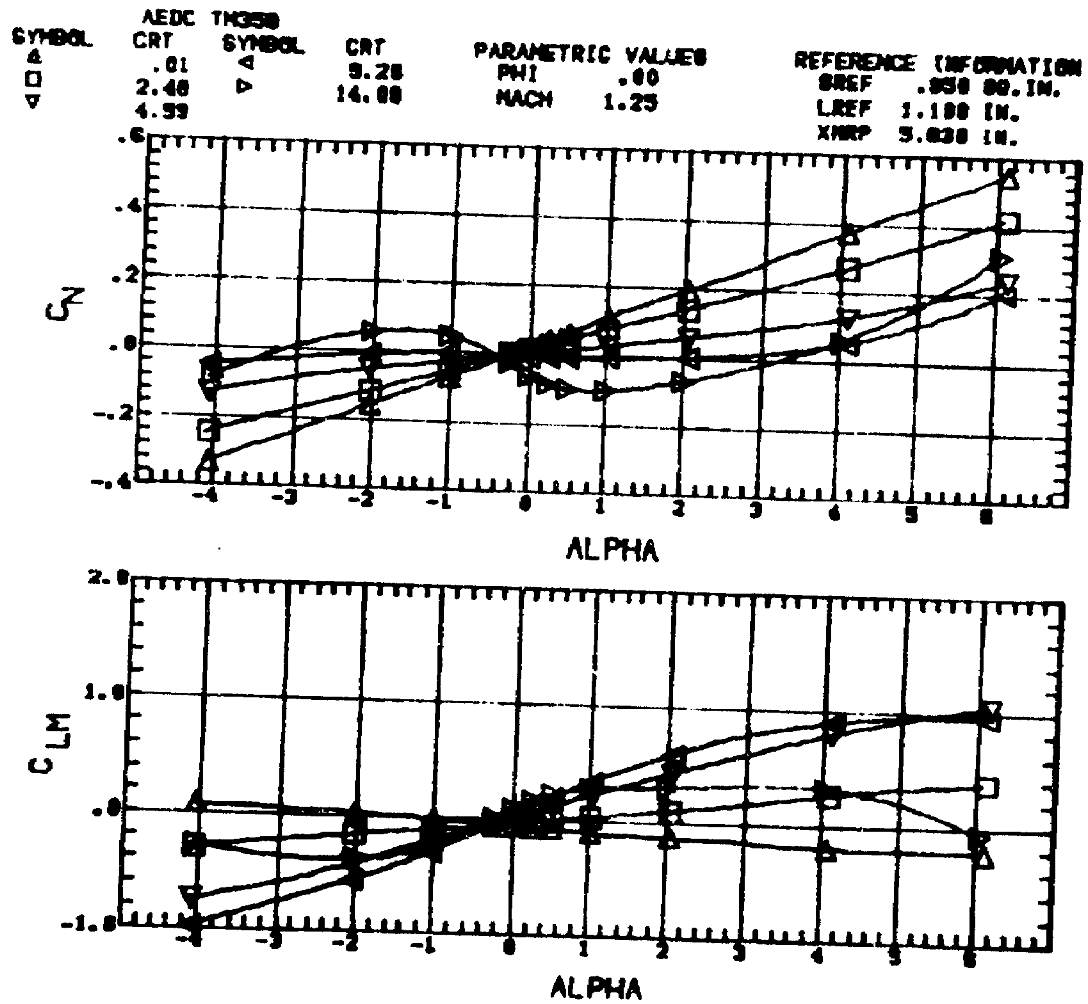

Figure 4. Continued. F12D1

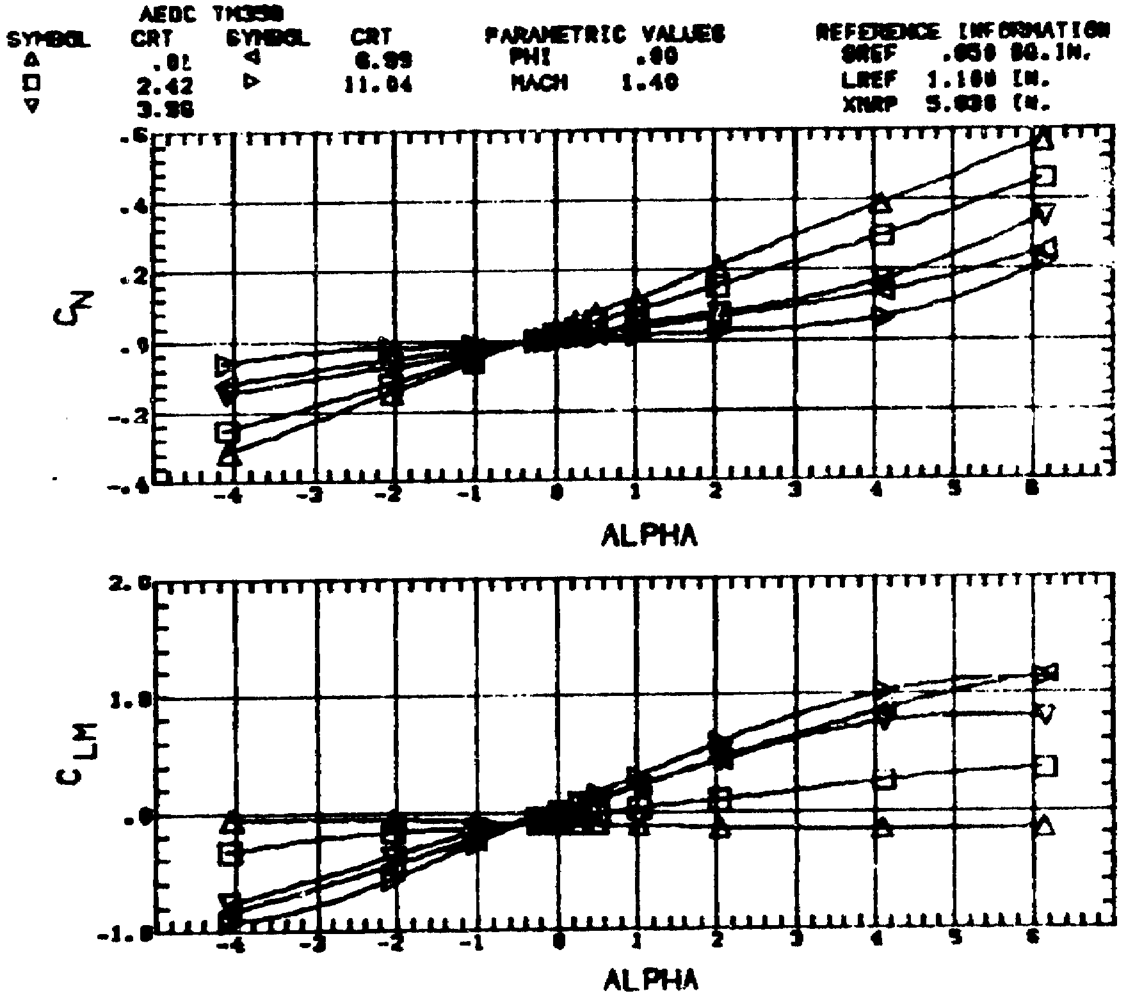

Figure 4. Continued. F12D1

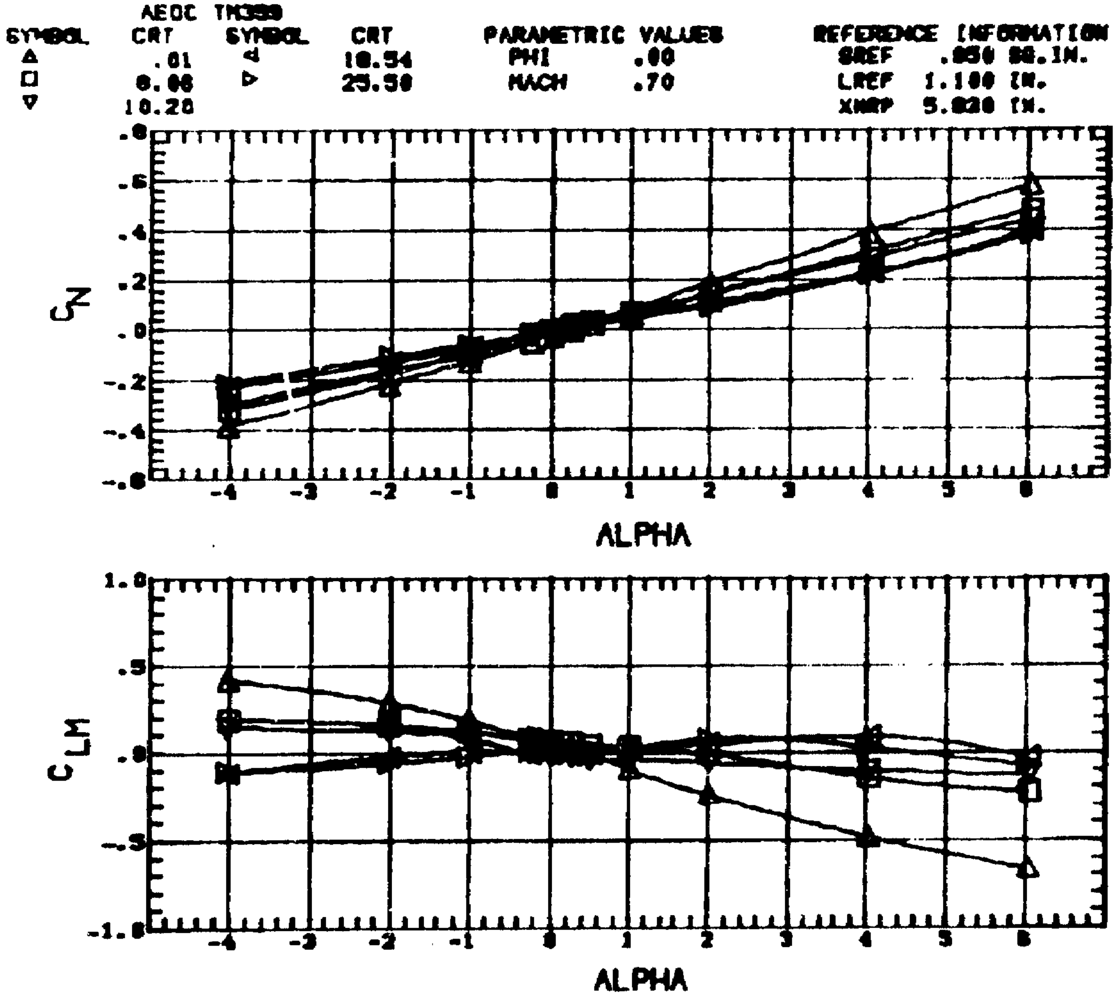

Figure 4. Continued. F12D2

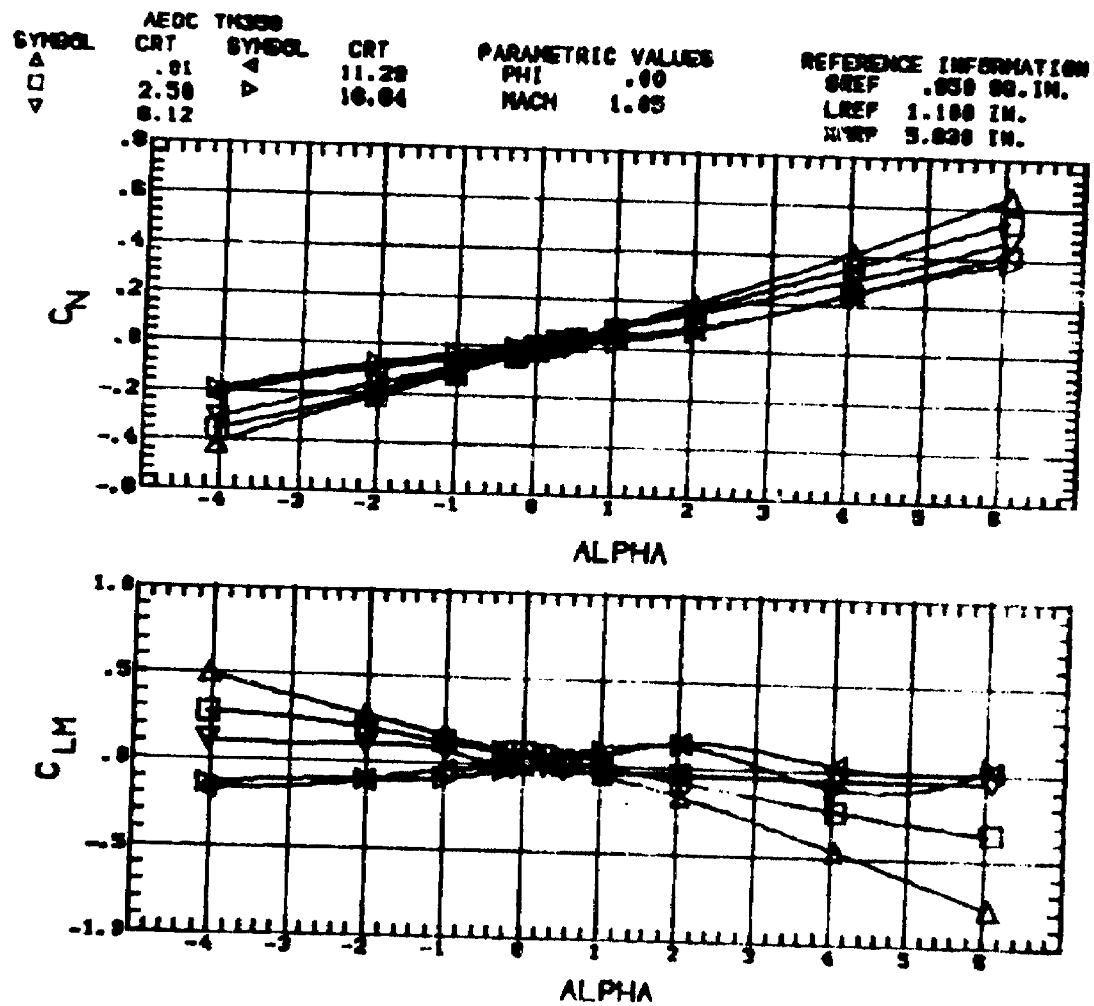

Figure 4. Continued. F12D2

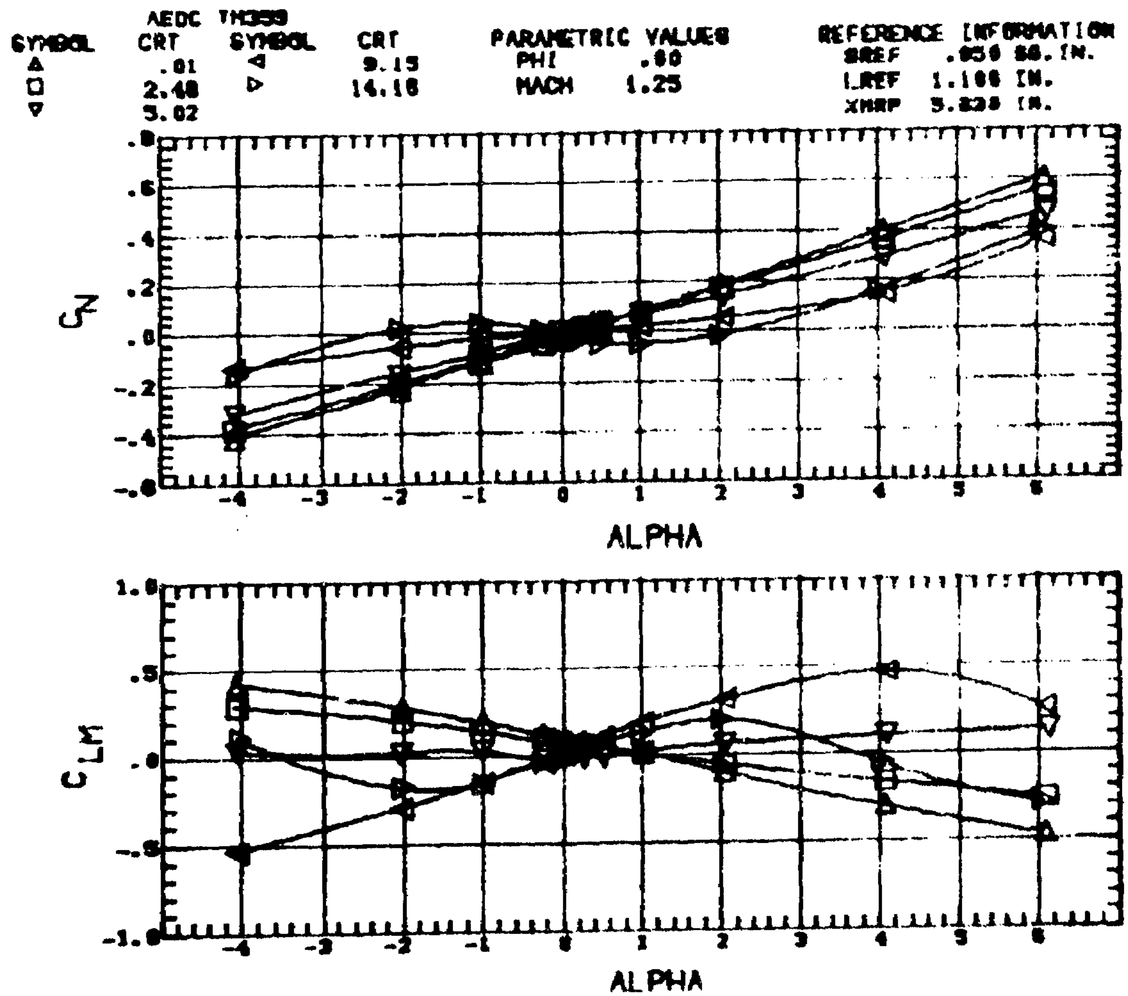

Figure 4. Continued. F12D2

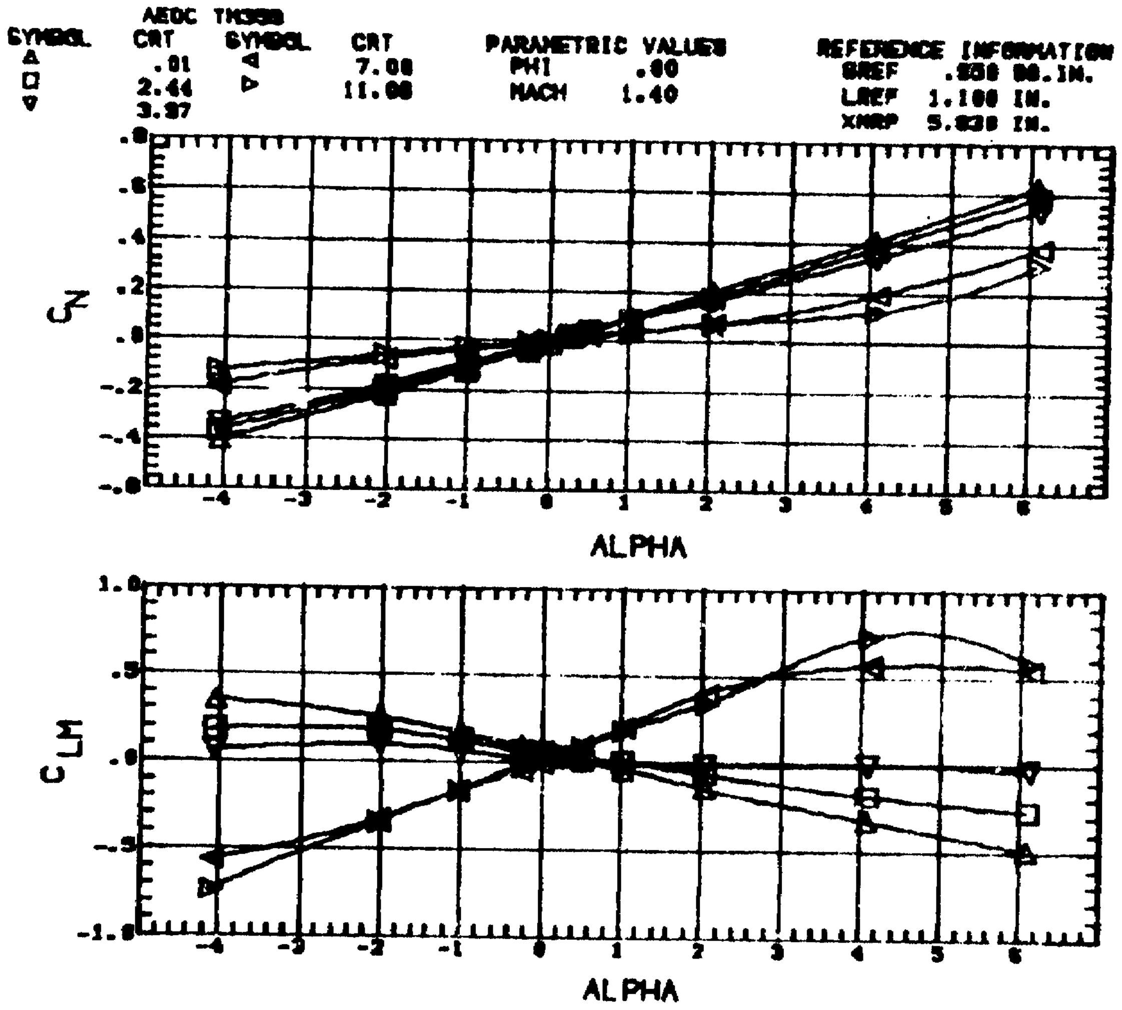

Figure 4. Continued. F12D2

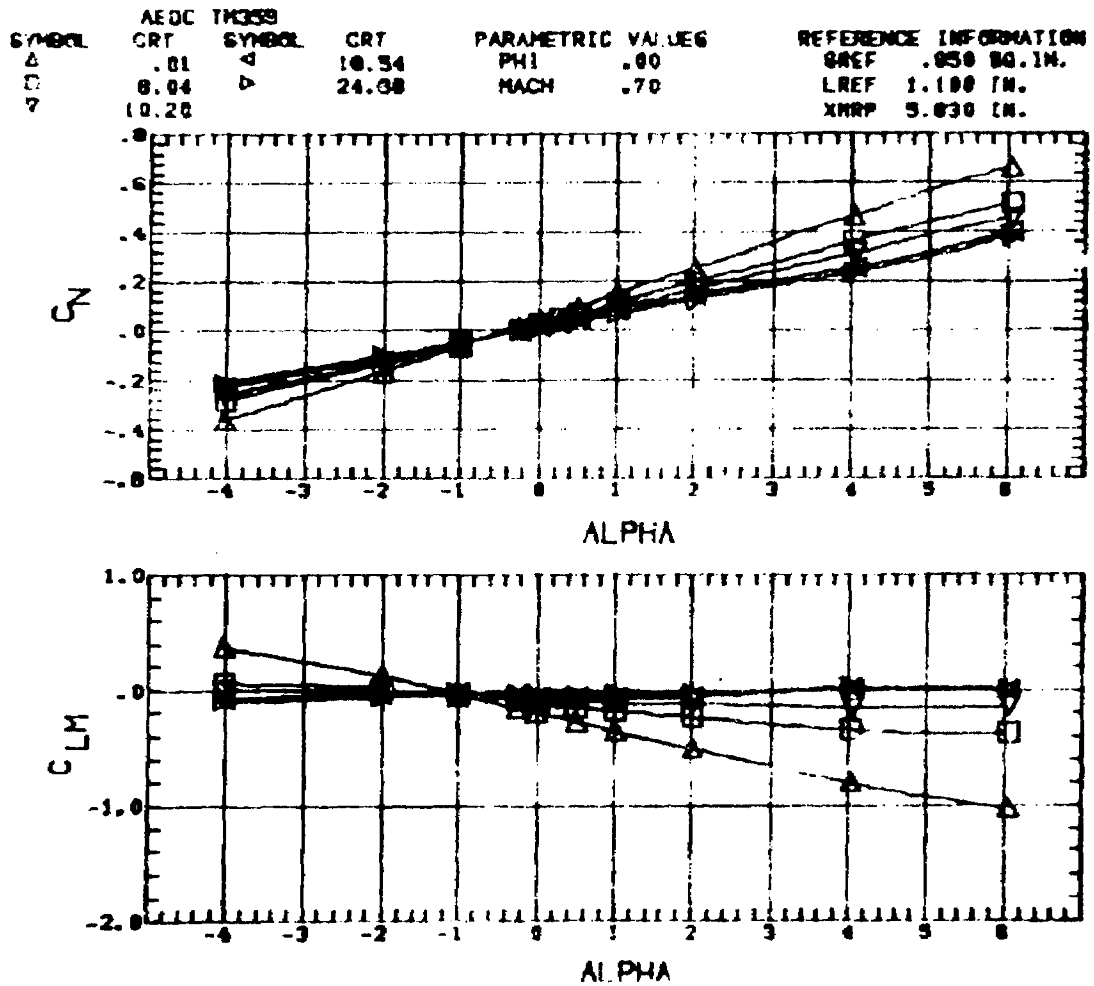

Figure 4. Continued. F6D2

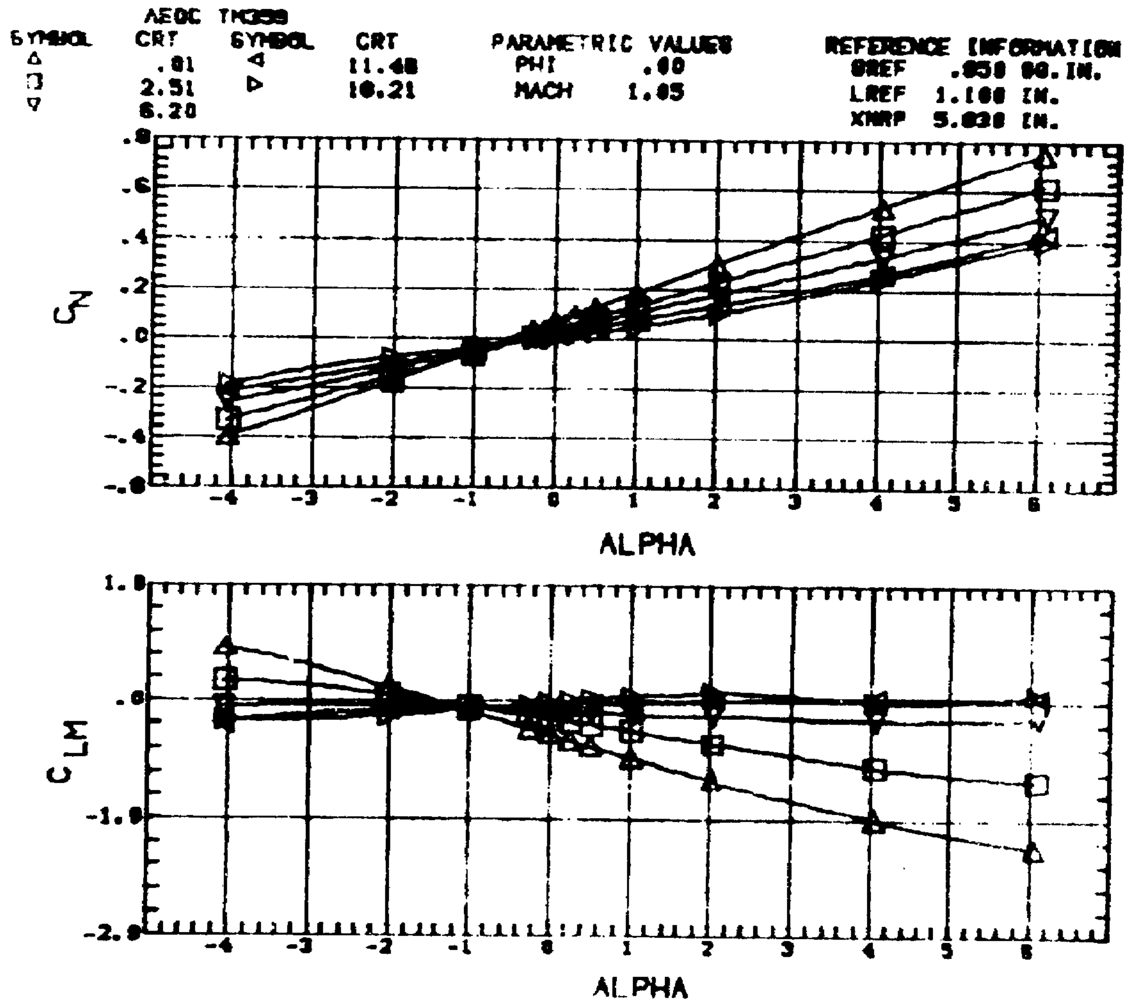

Figure 4. Continued. F6D2

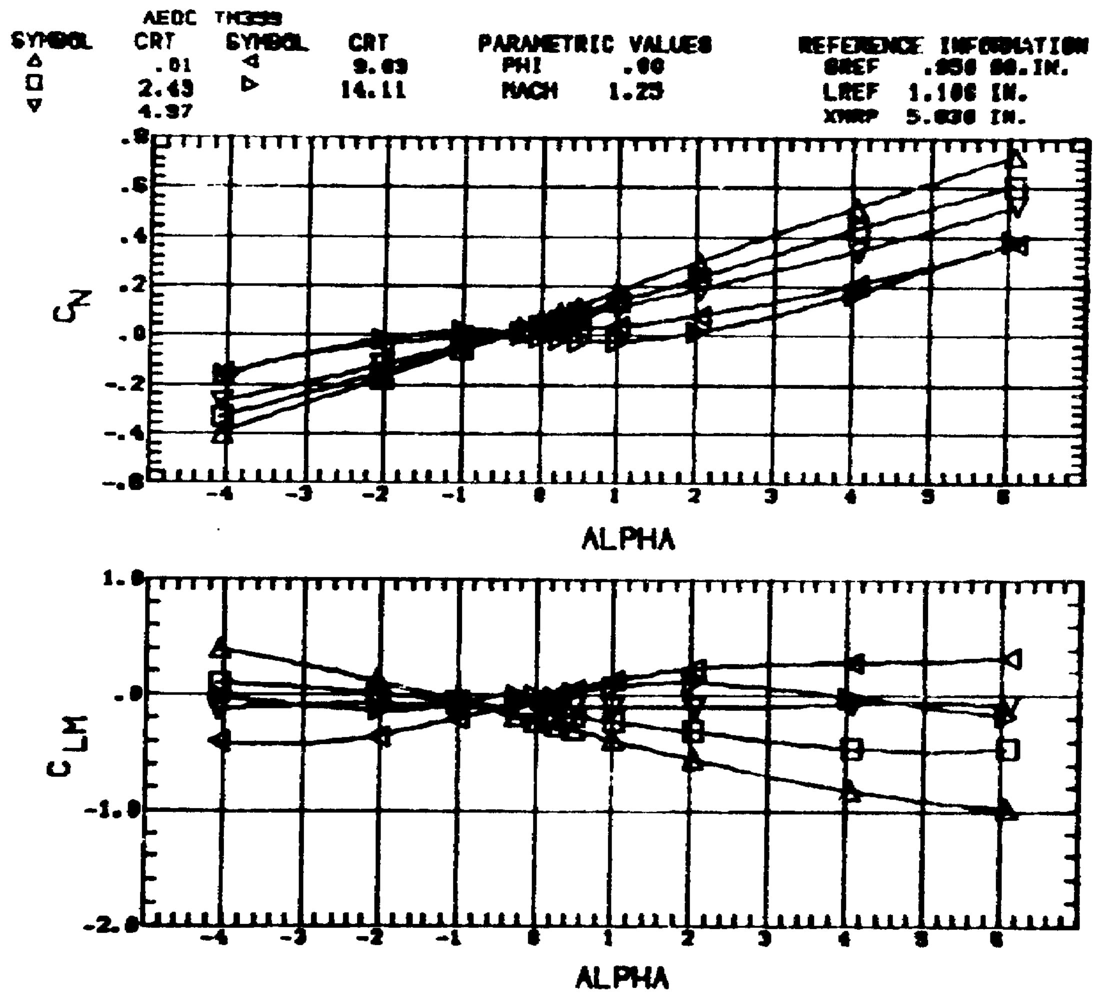

Figure 4. Continued. F6D2

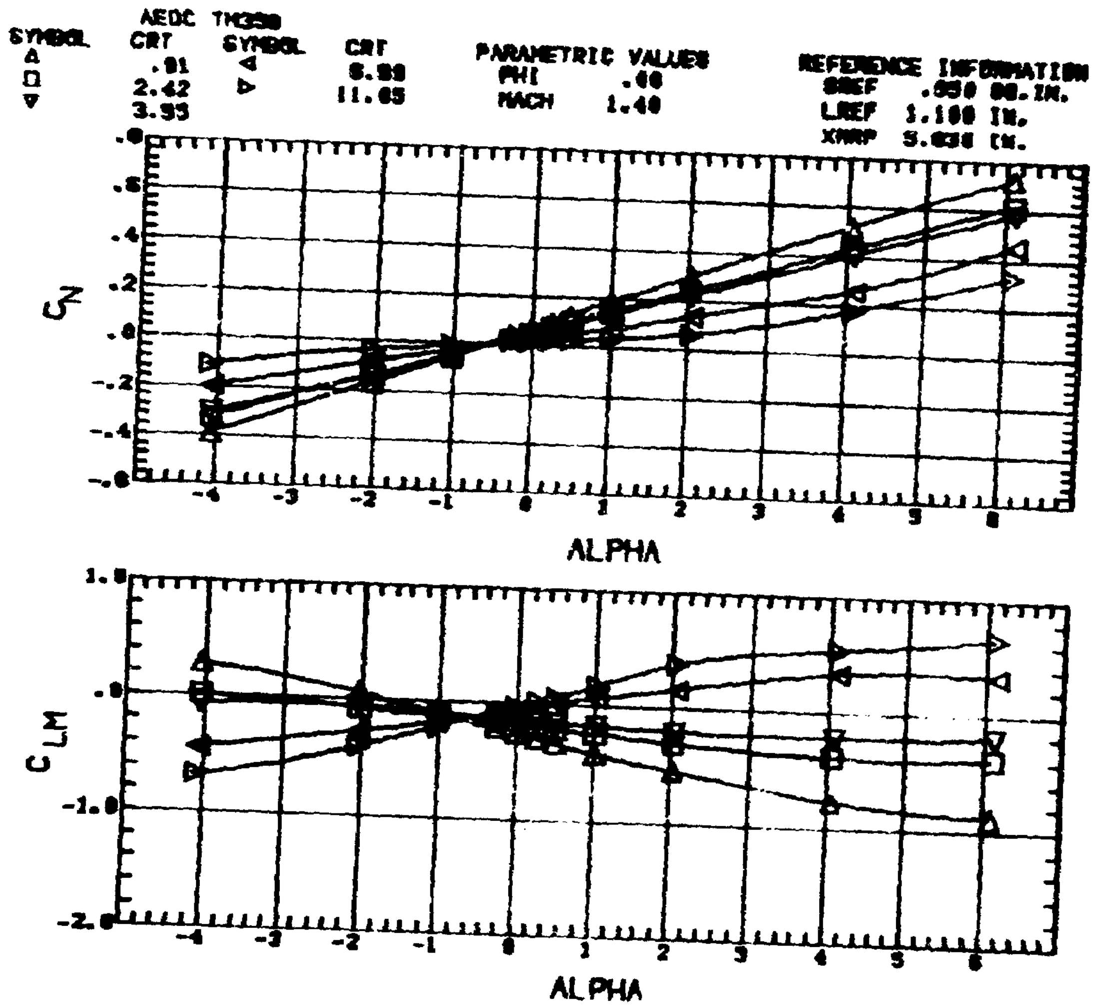

Figure 4. Continued. F6D2

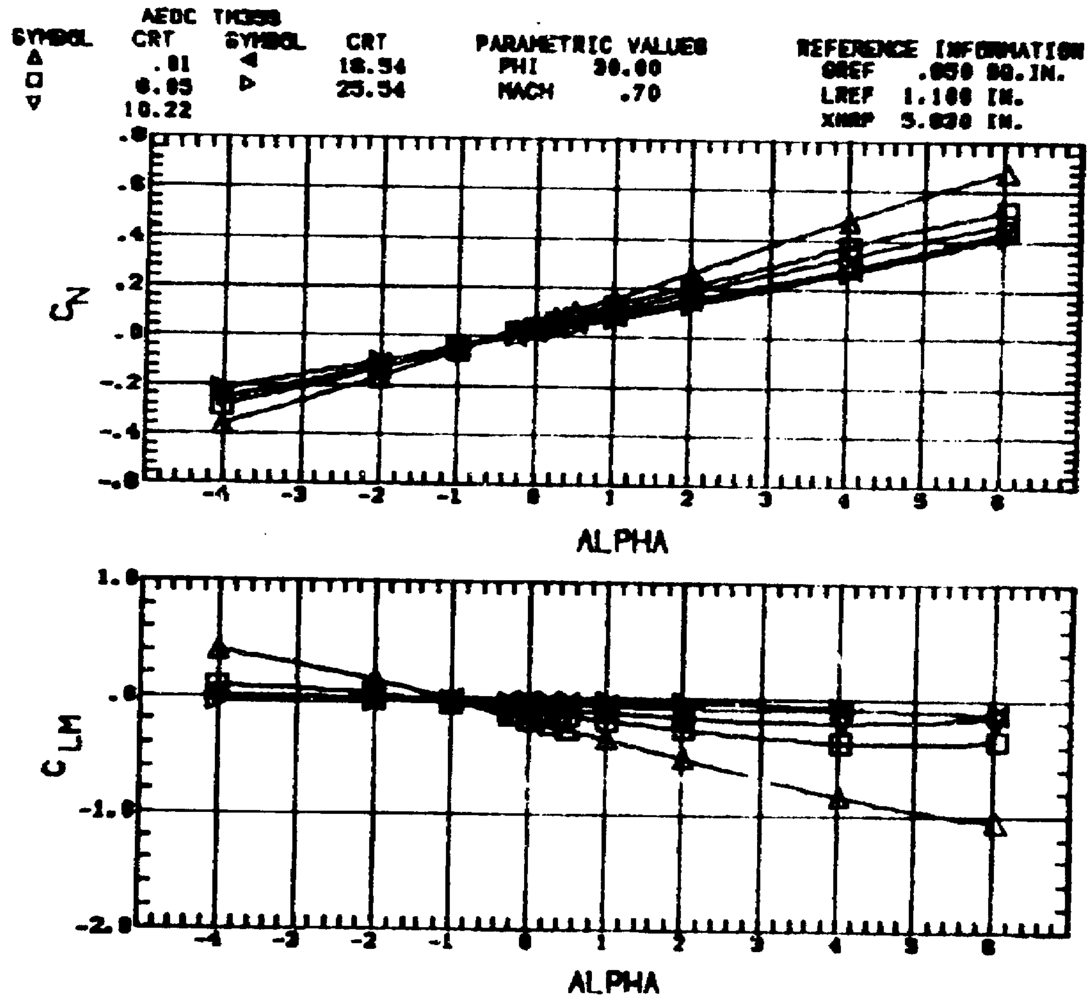

Figure 4. Continued. F6D2, PHI=30 DEG

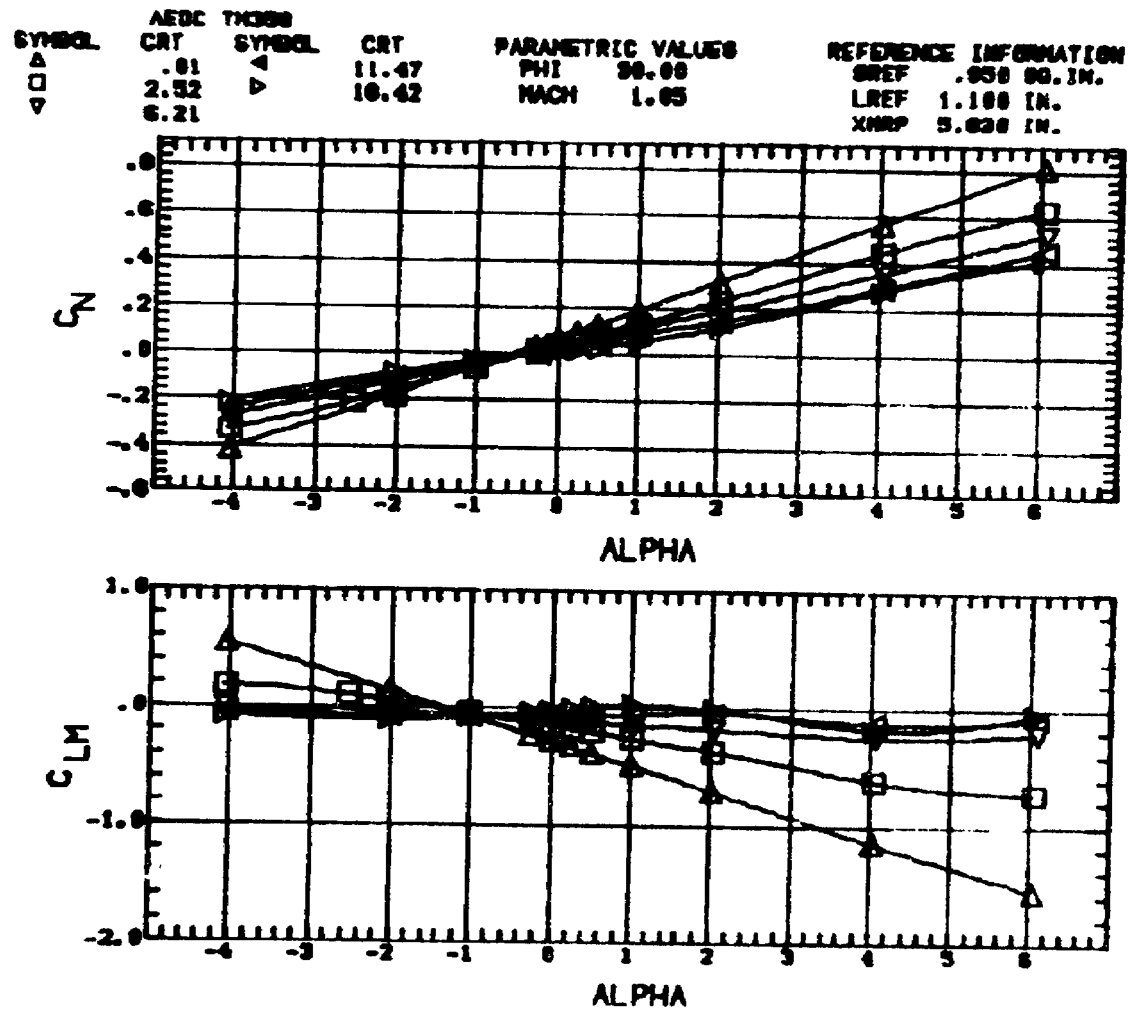

Figure 4. Continued. F6D2, PHI=30 DEG

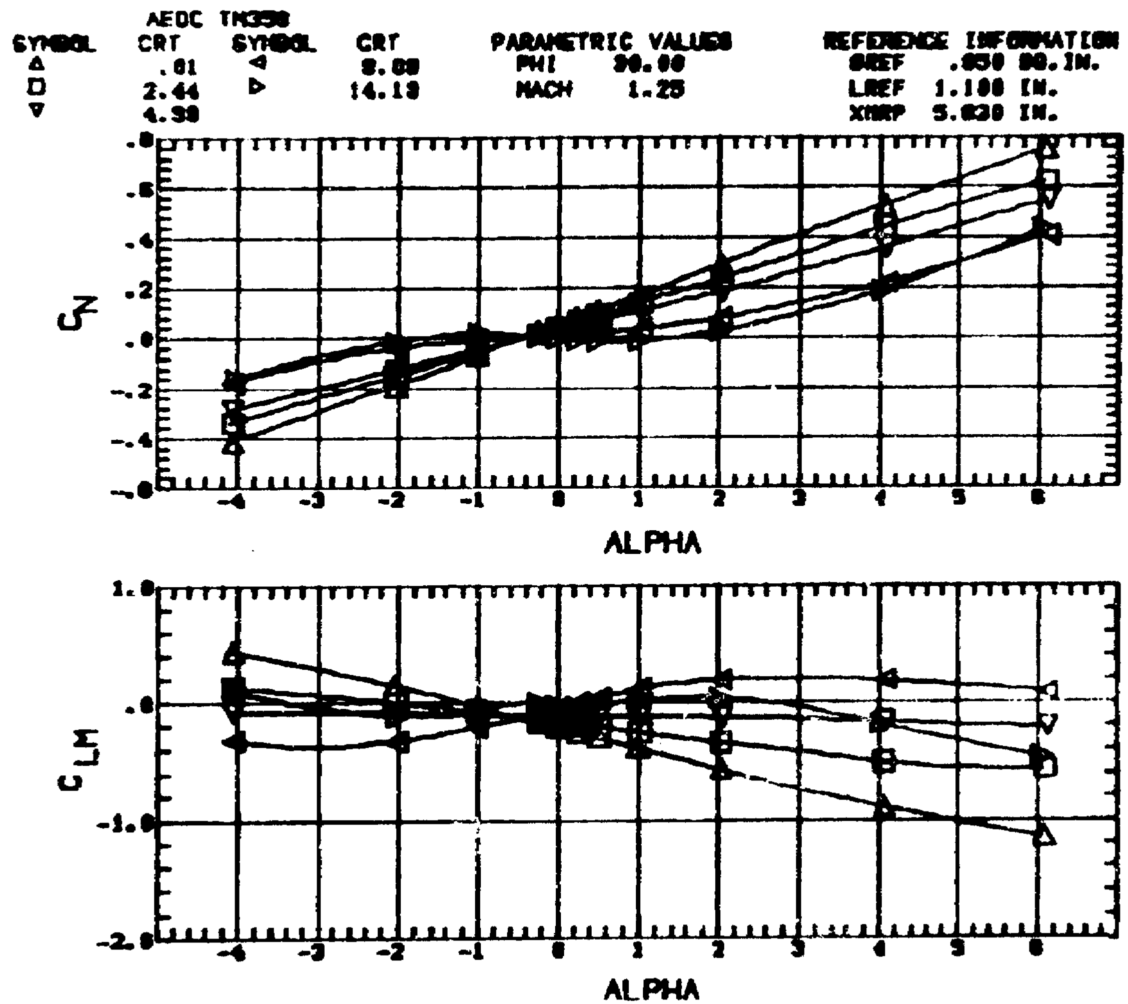

Figure 4. Continued. F6D2, PHI=30 DEG

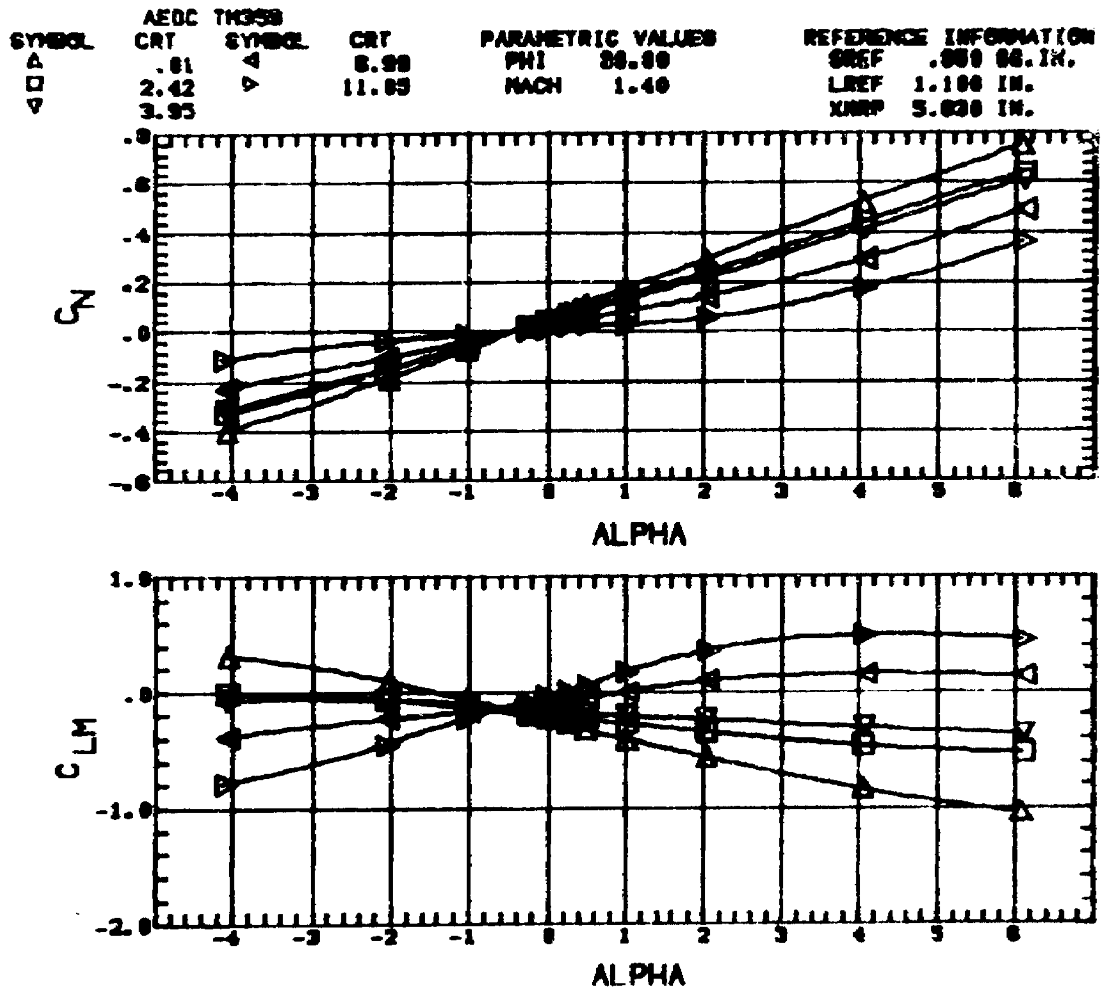

Figure 4. Continued. F6D2, PHI=30 DEG

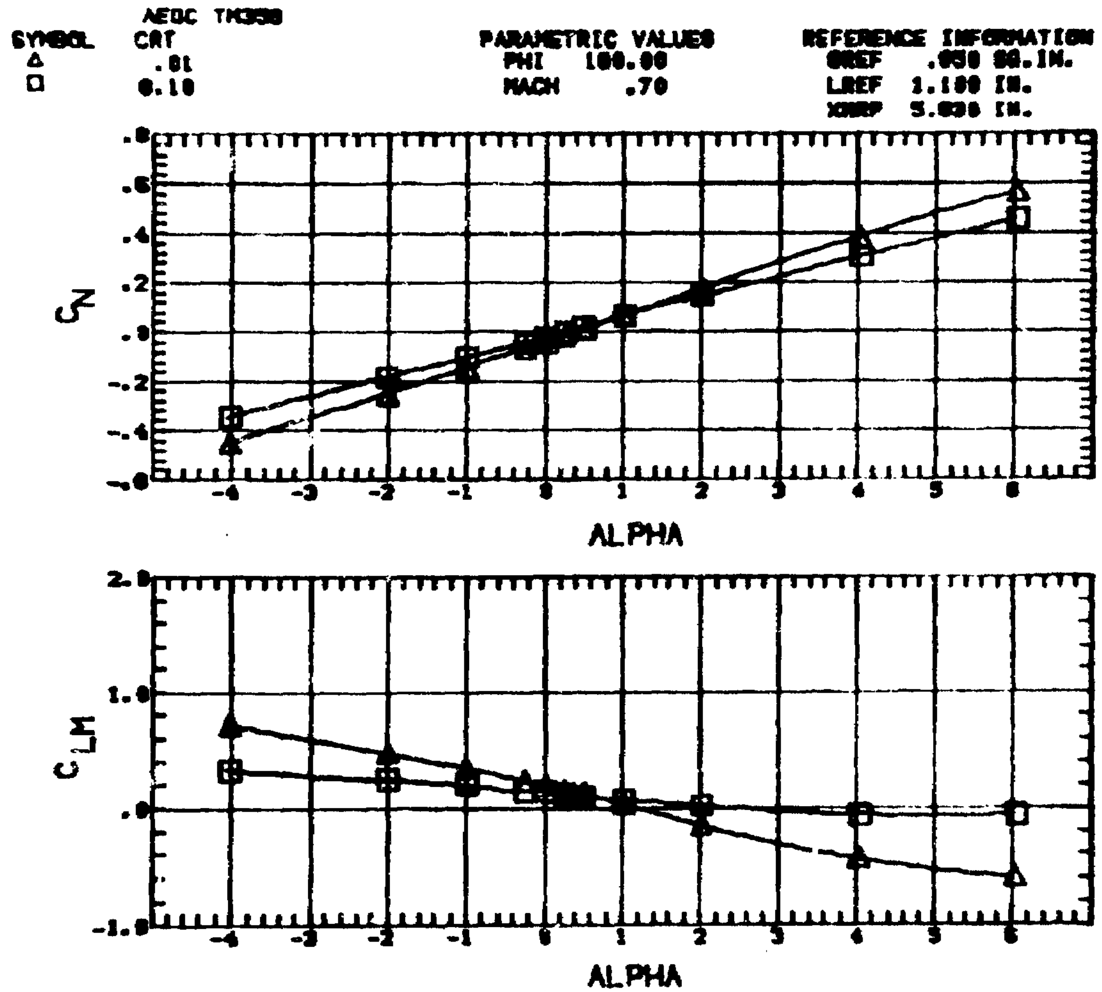

Figure 4. Continued. F6D2, PHI=180 DEG

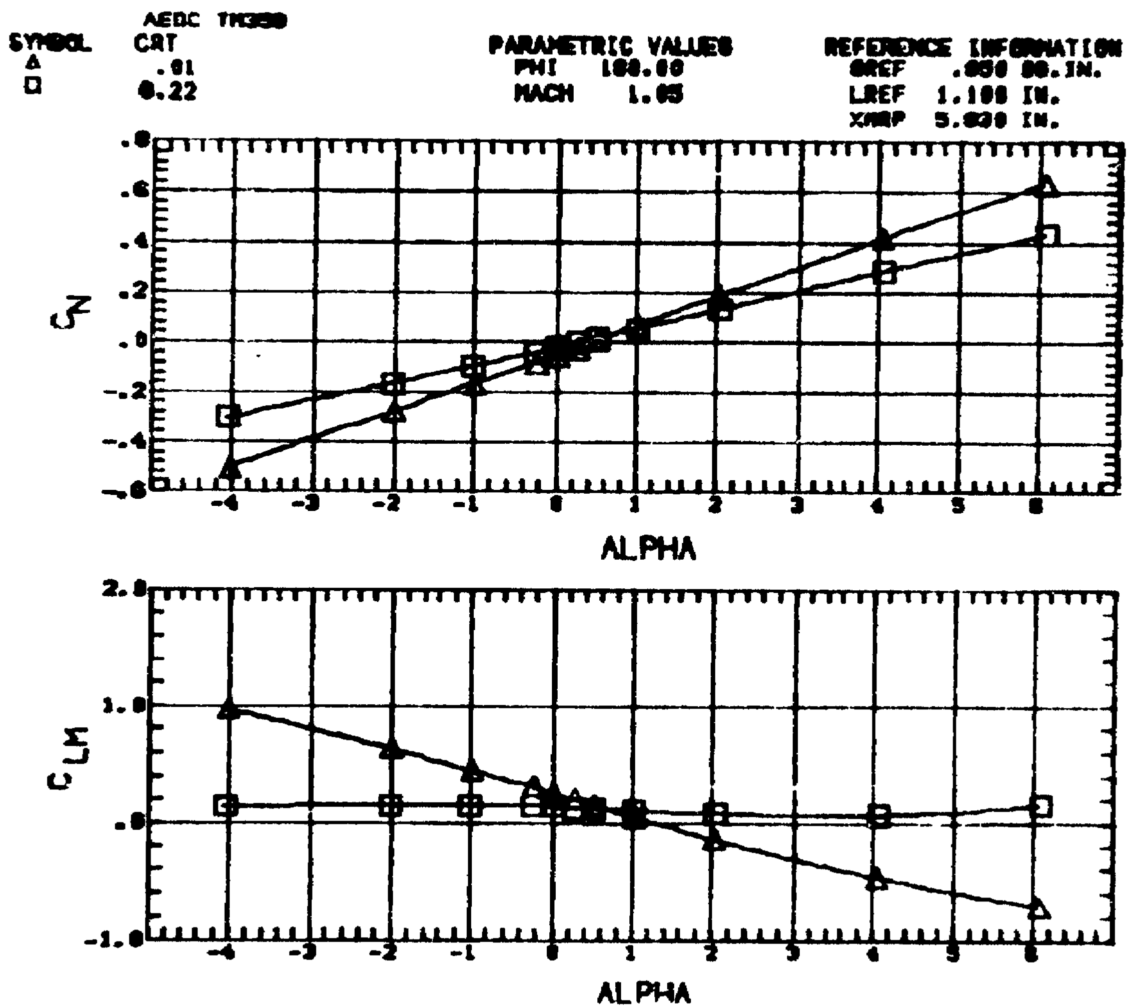

Figure 4. Concluded. F6D2, PHI=180 DEG

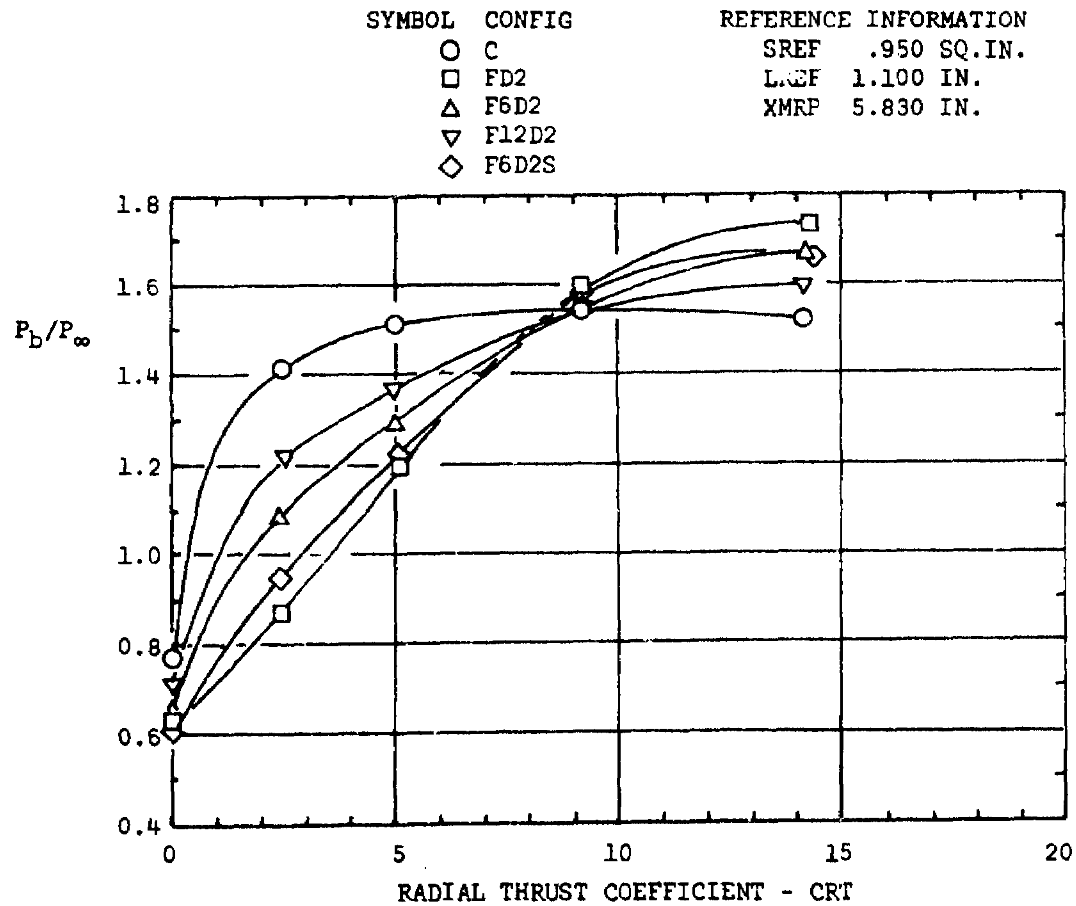

Figure 5. Typical thrust effect on base pressure ratio $-M_\infty = 1.25$, $\alpha = 0^\circ$.

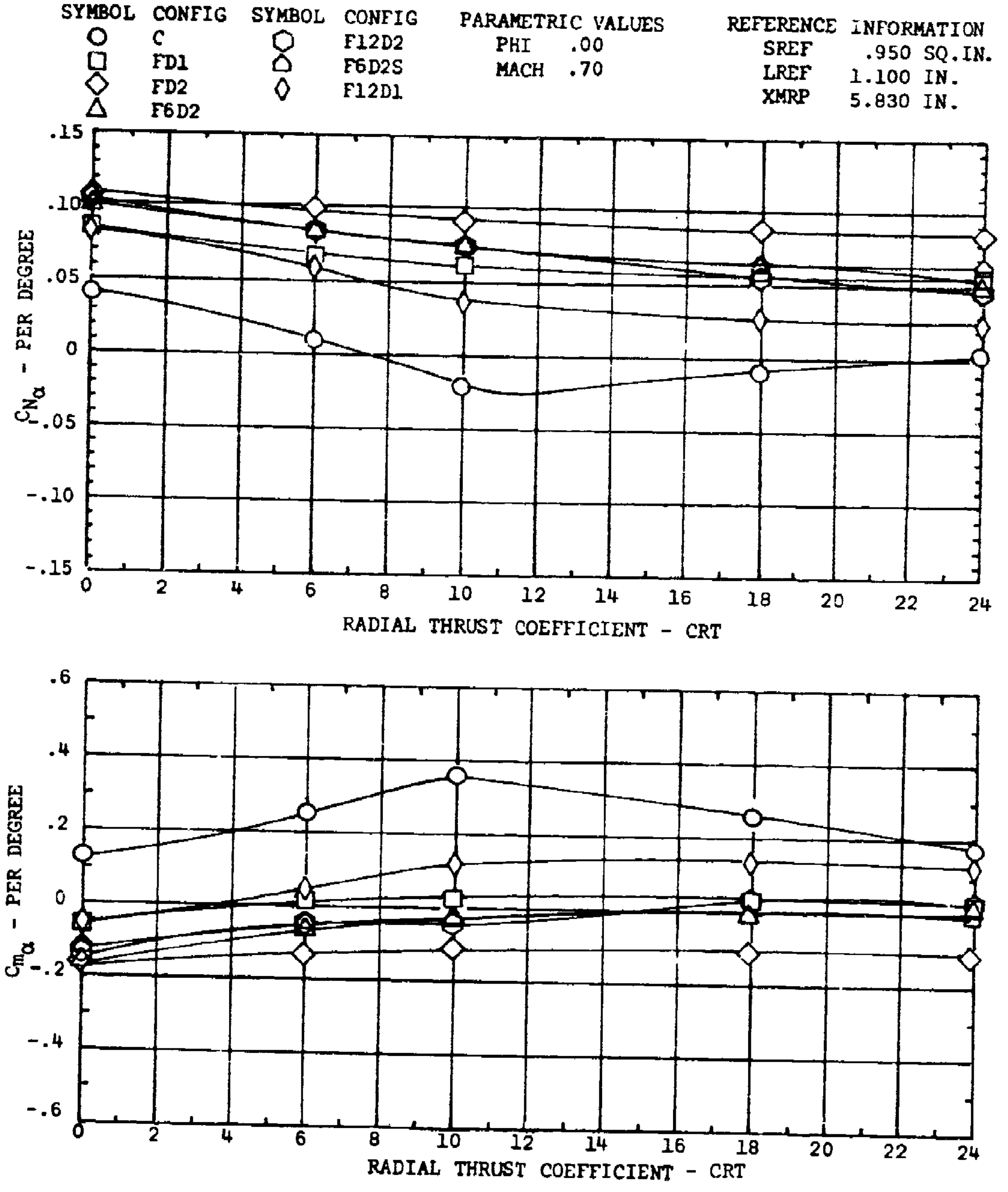

Figure 6. Thrust effects on initial normal force and pitching moment coefficient slopes.

SYMBOL	CONFIG	SYMBOL	CONFIG	PARAMETRIC VALUES	REFERENCE INFORMATION
○	C	⬡	F12D2	PHI .00	SREF .950 SQ. IN.
□	FD1	⌂	F6D2S	MACH 1.05	LREF 1.100 IN.
◇	FD2	◊	F12D1		XMRP 5.830 IN.
△	F6D2				

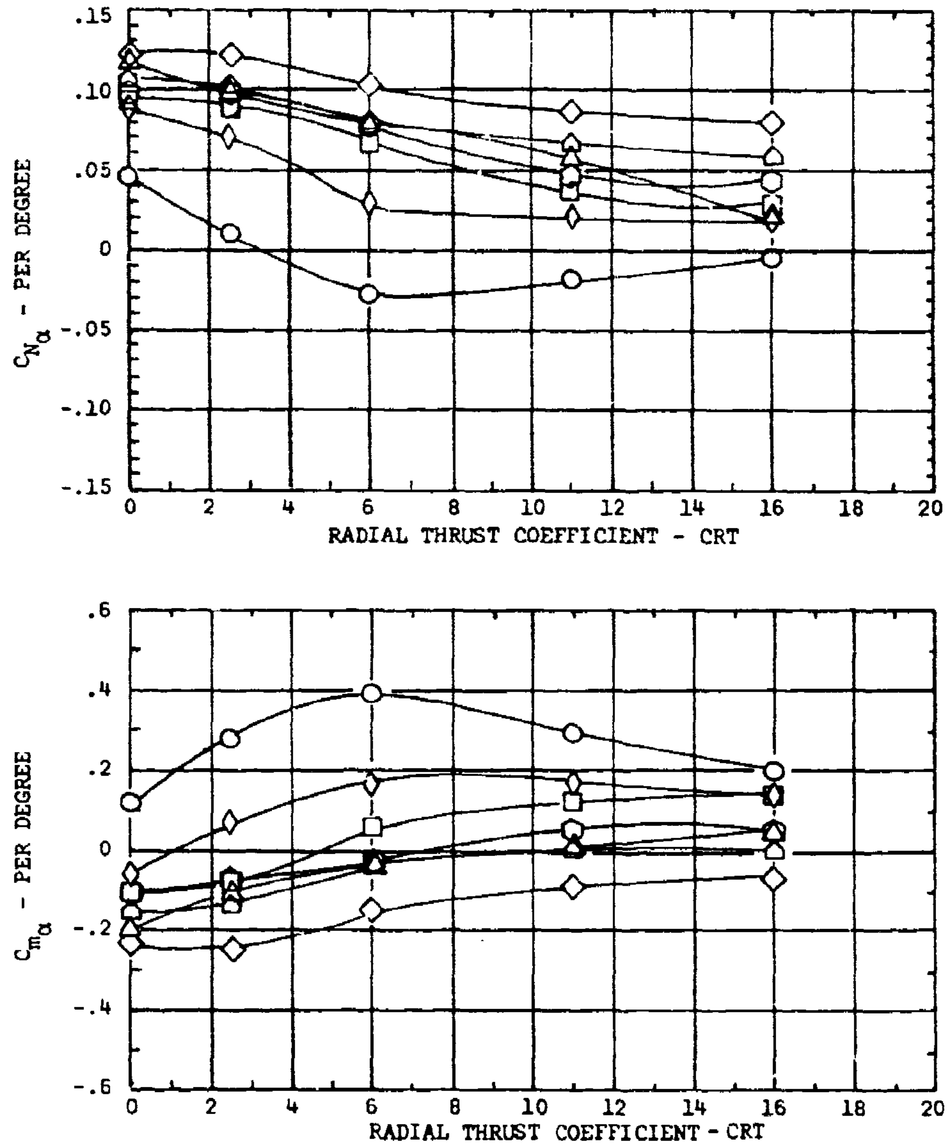

Figure 6. Continued.

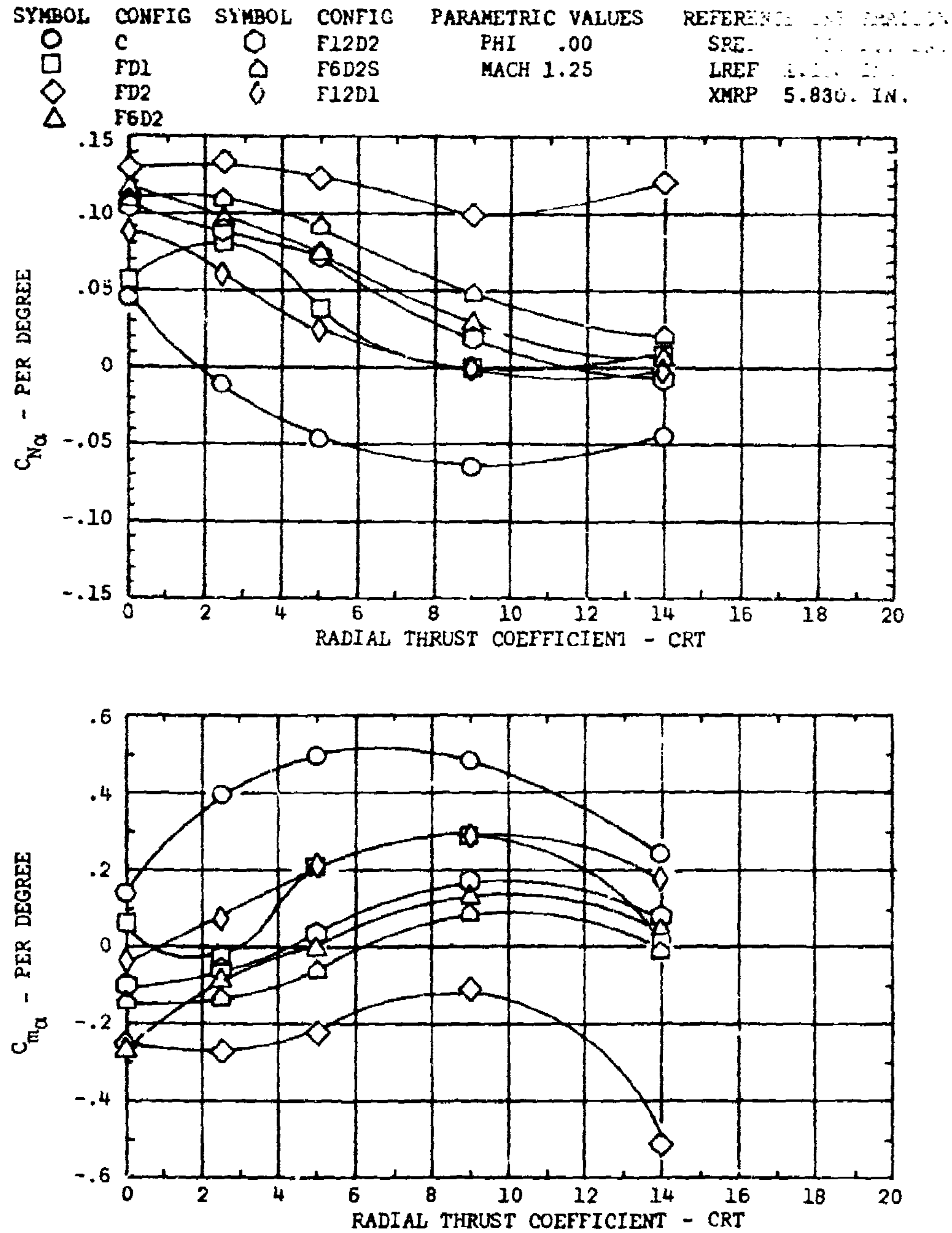

Figure 6. Continued.

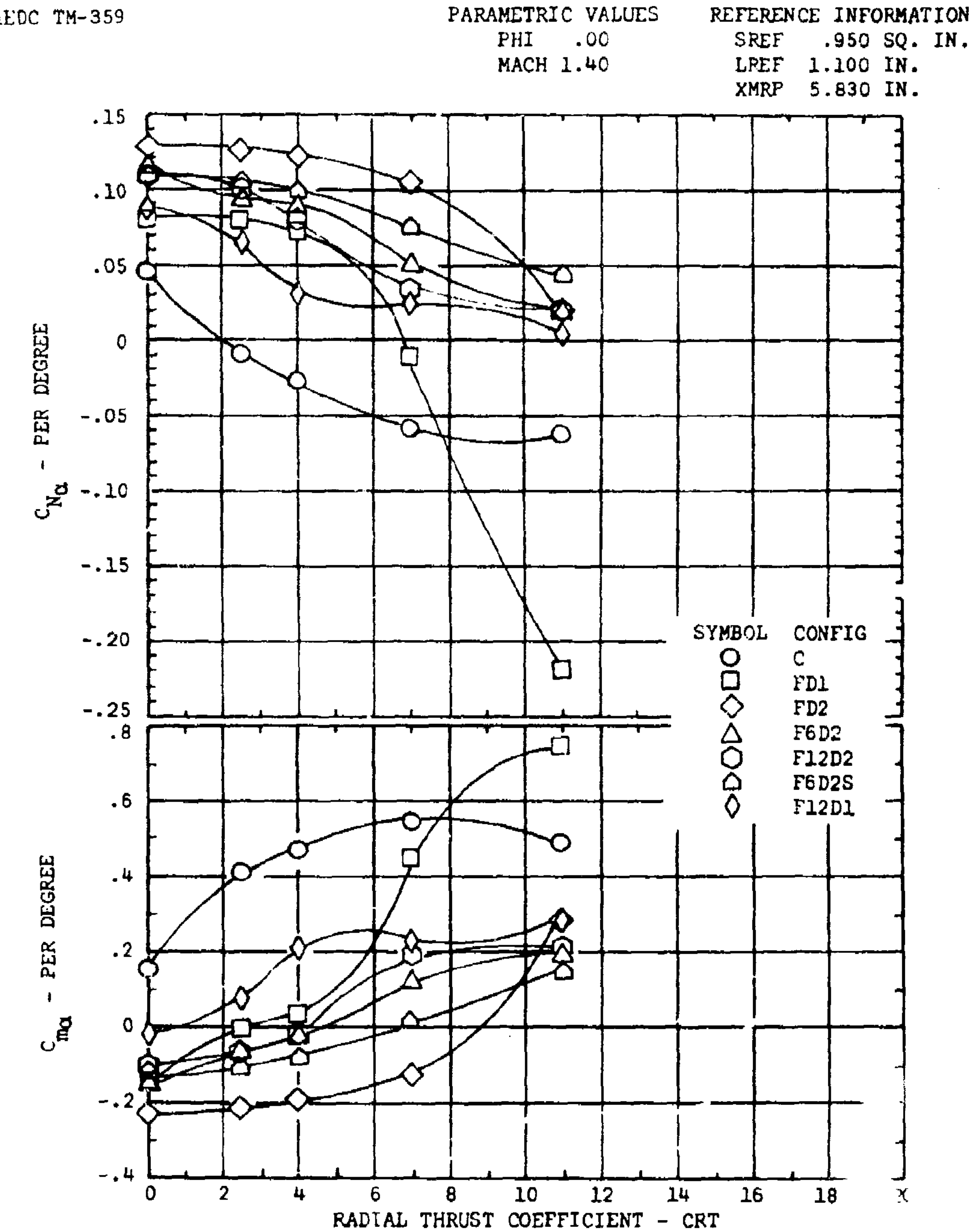

Figure 6. Concluded.

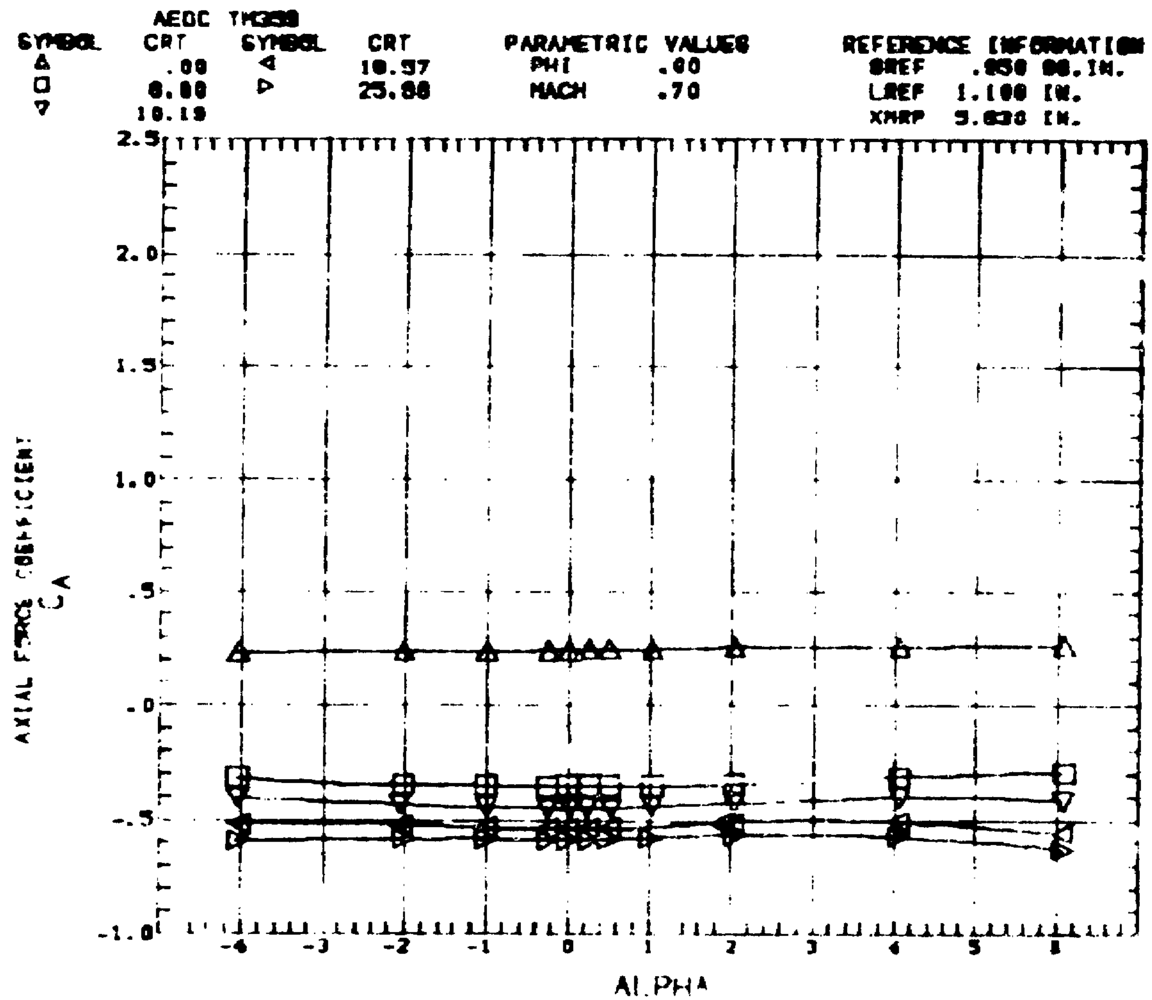

Figure 7. Thrust effects on axial force coefficient. C

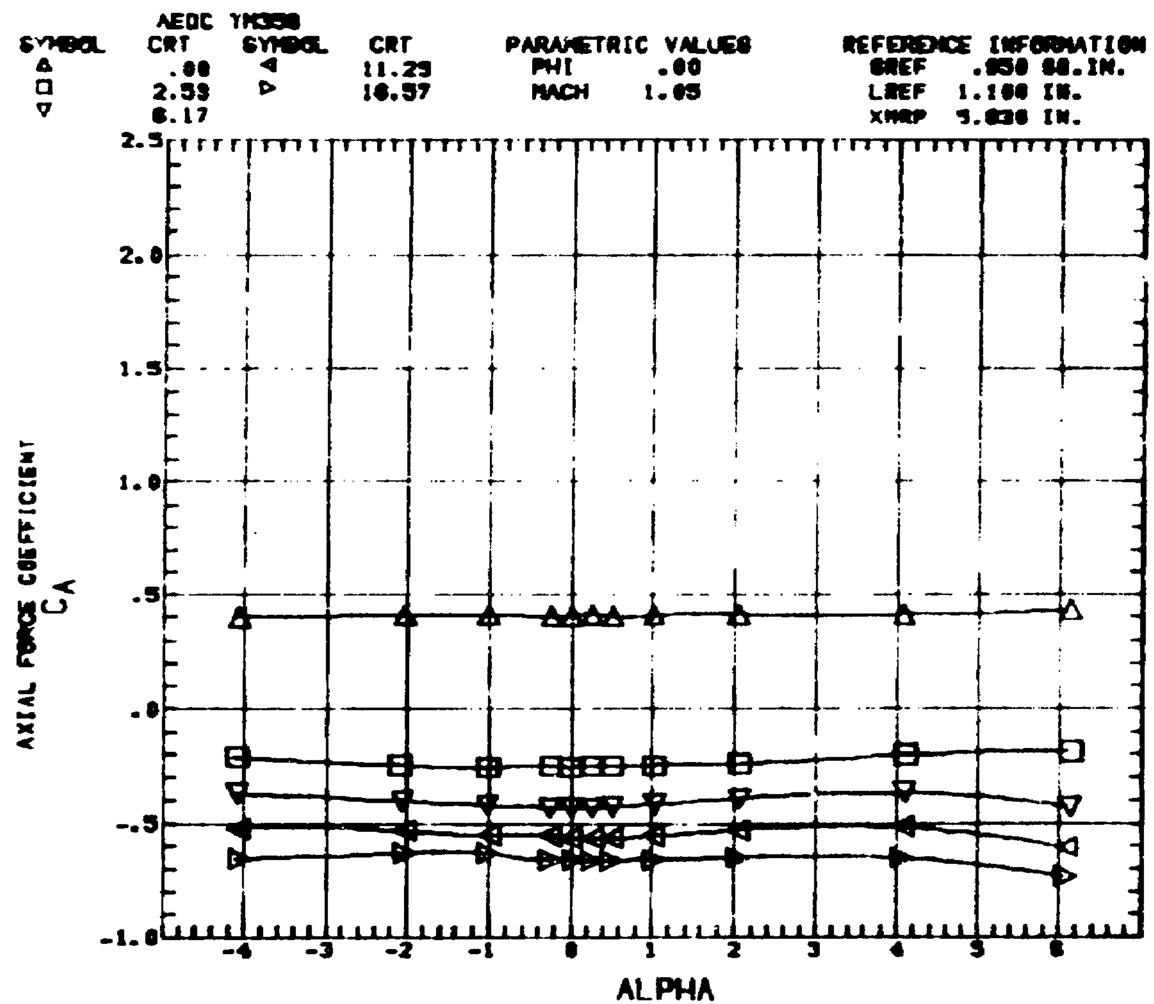

Figure 7. Continued. C

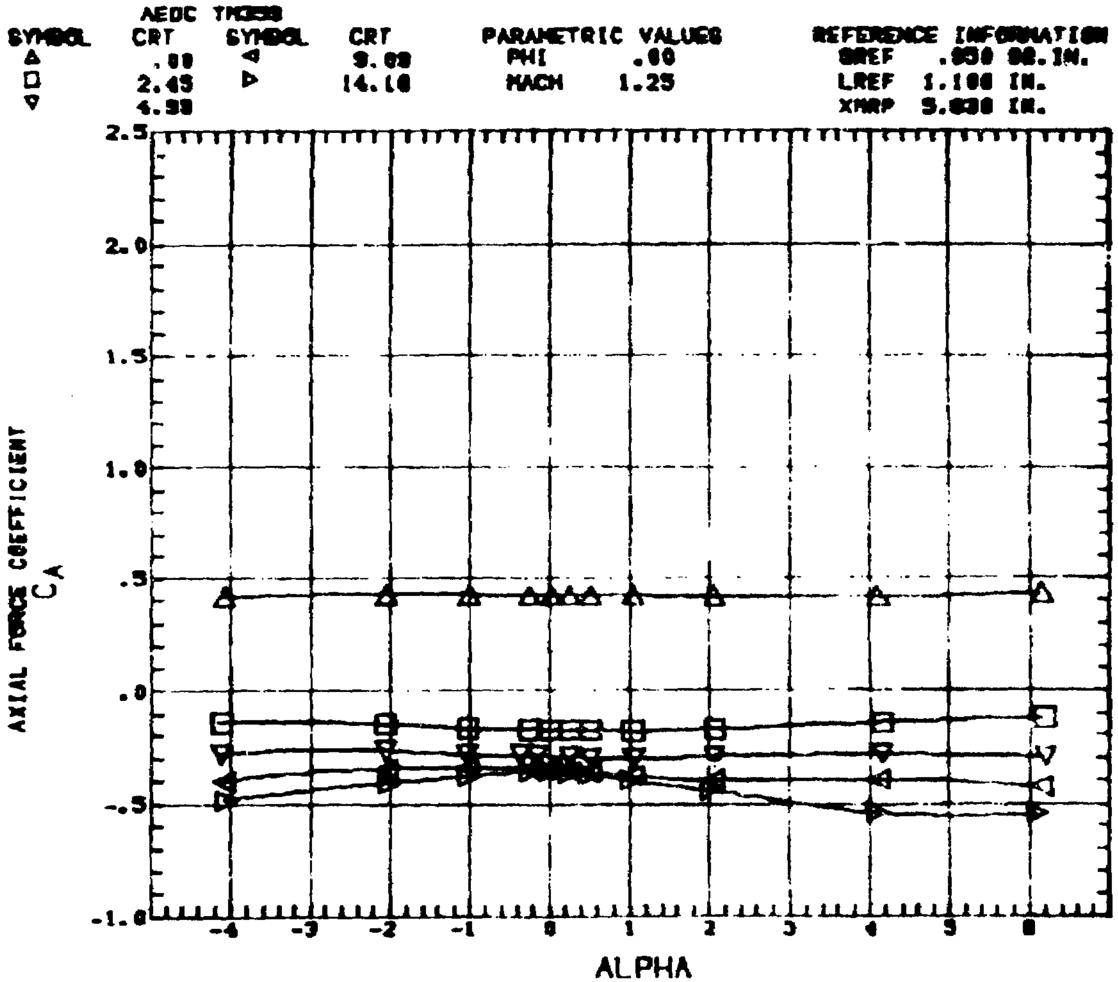

Figure 7. Continued. C

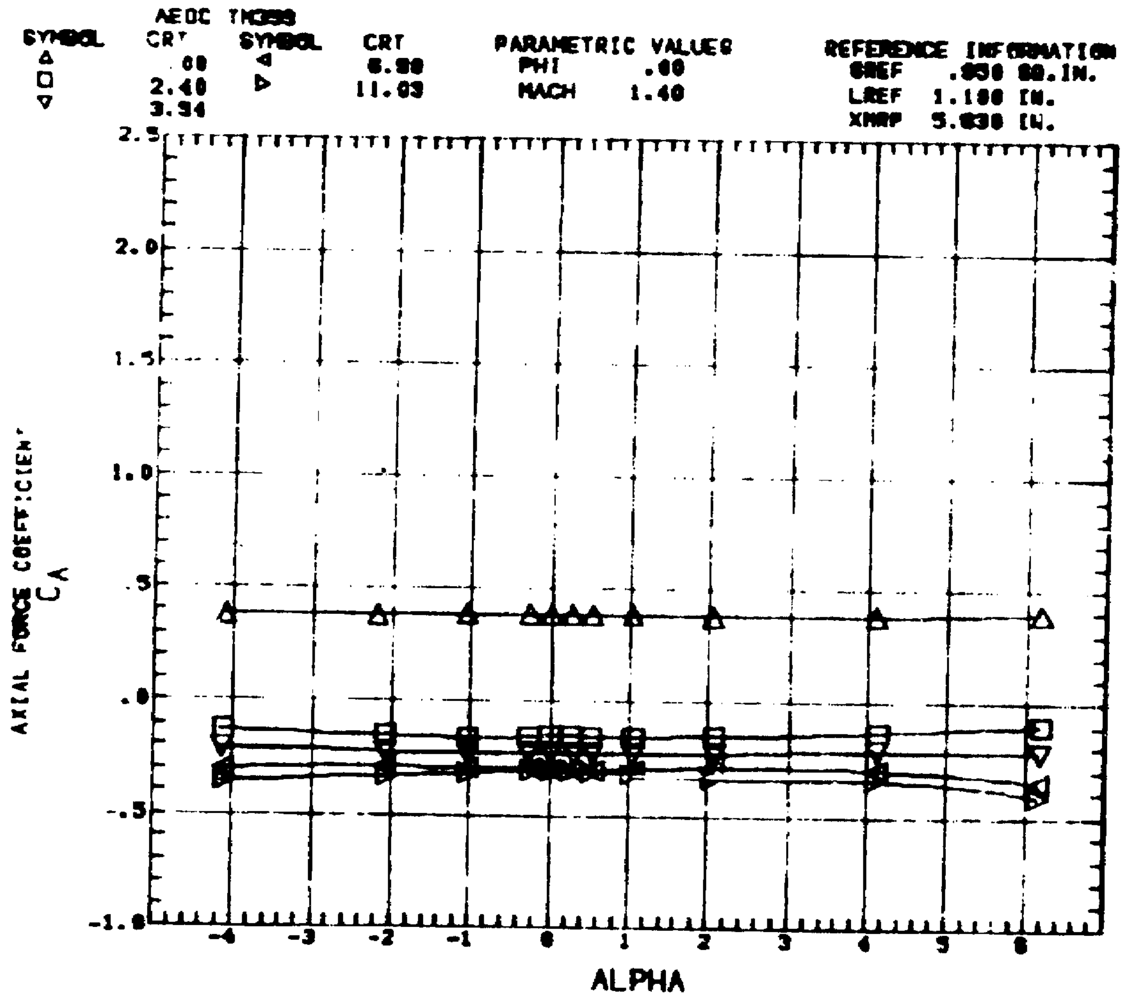

Figure 7. Continued. C

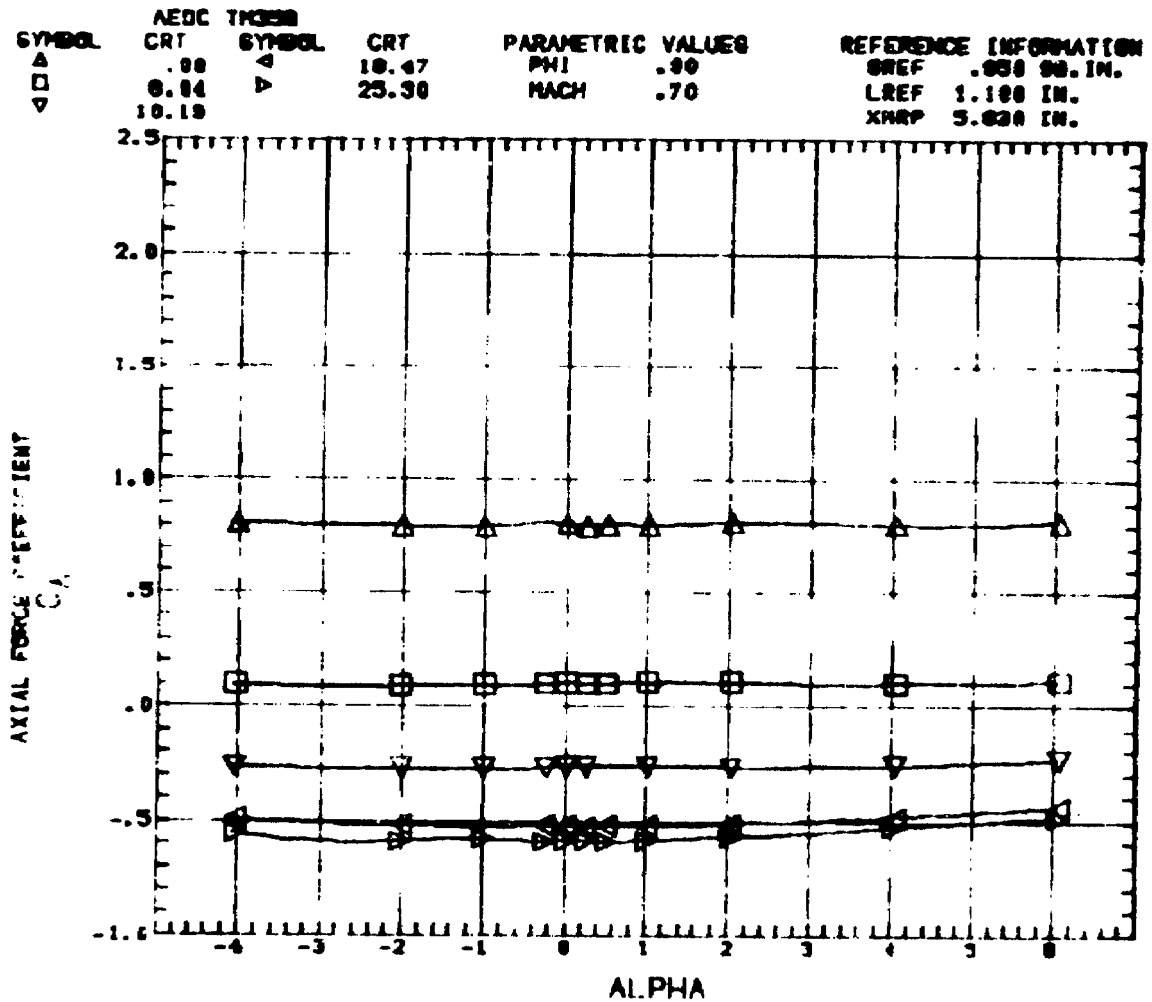

Figure 7. Continued. FD1

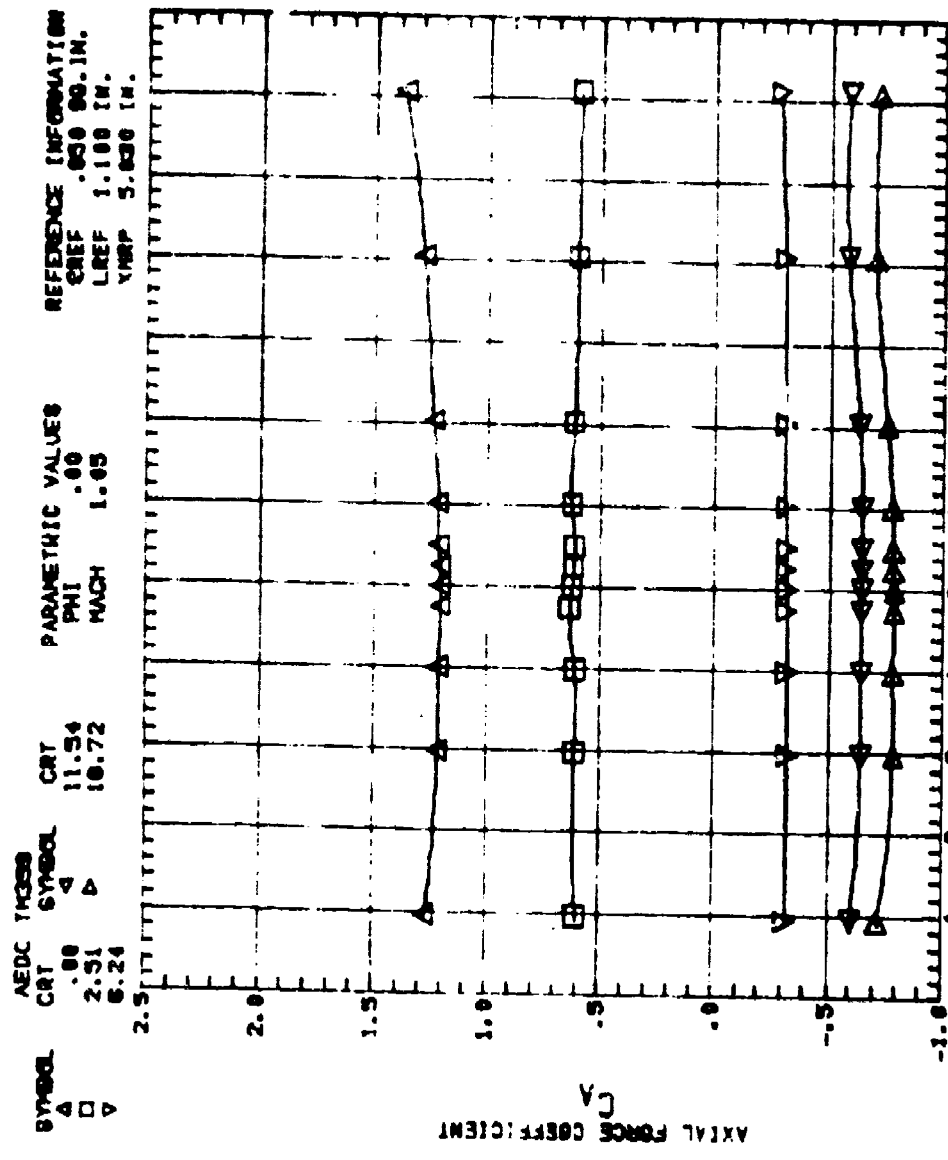

Figure 7. Continued. FD1

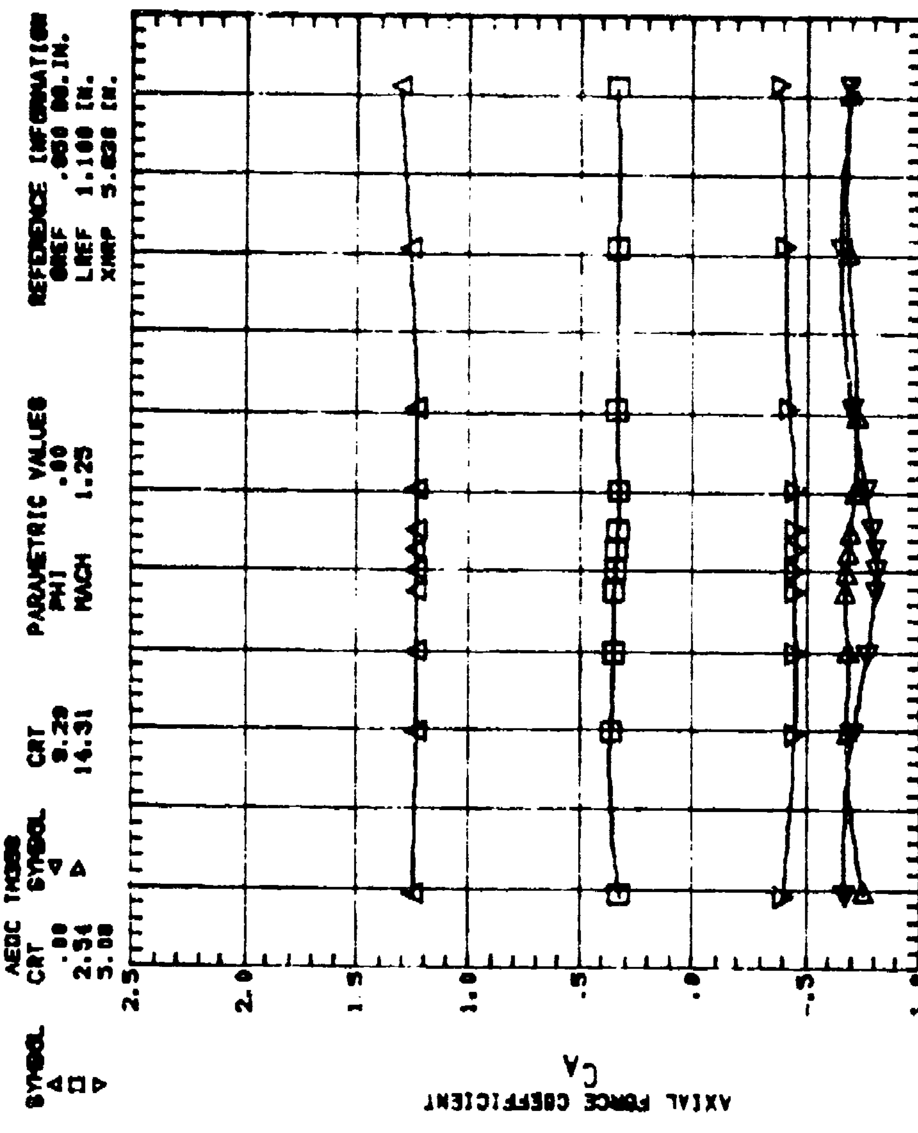

Figure 7. Continued. FD1

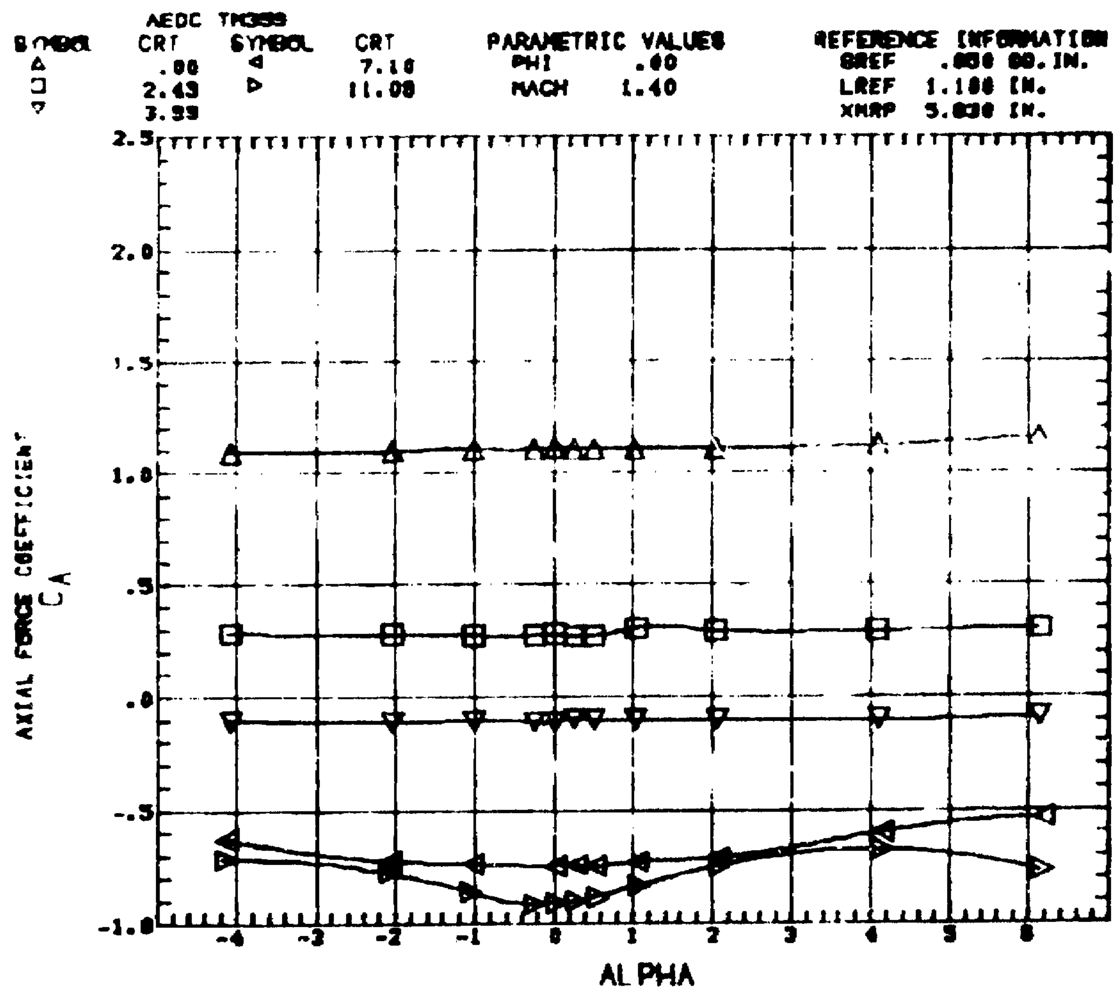

Figure 7. Continued. FD1

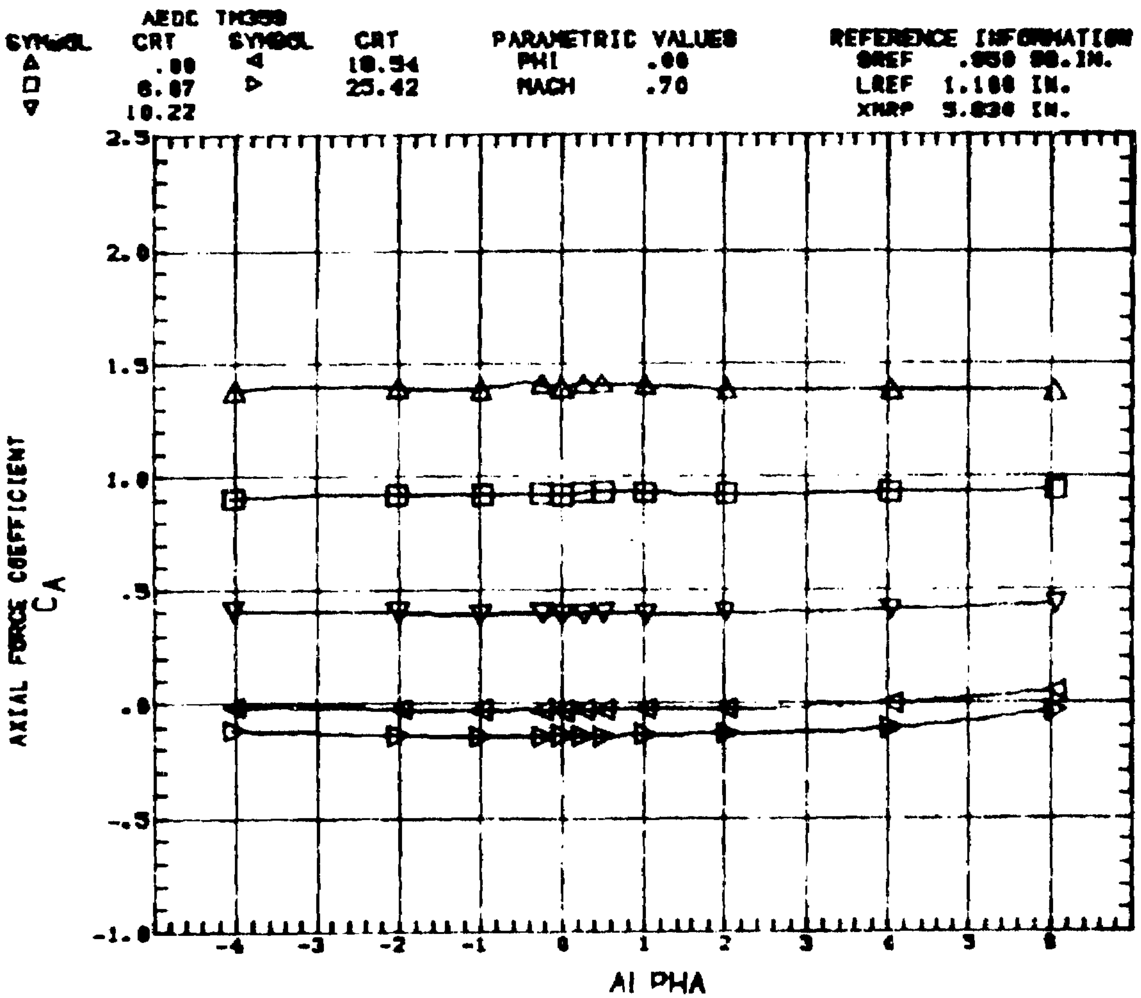

Figure 7. Continued. FD2

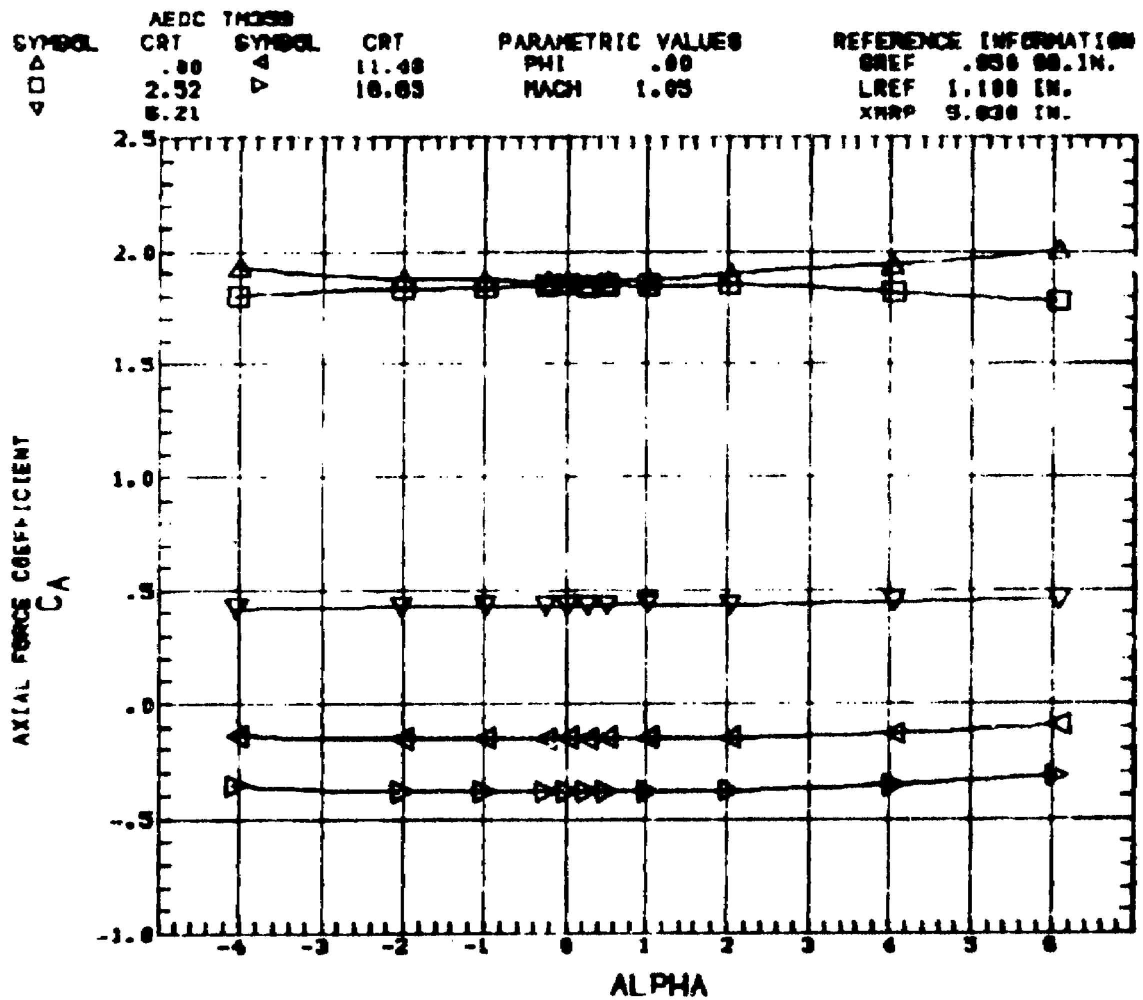

Figure 7. Continued. FD2

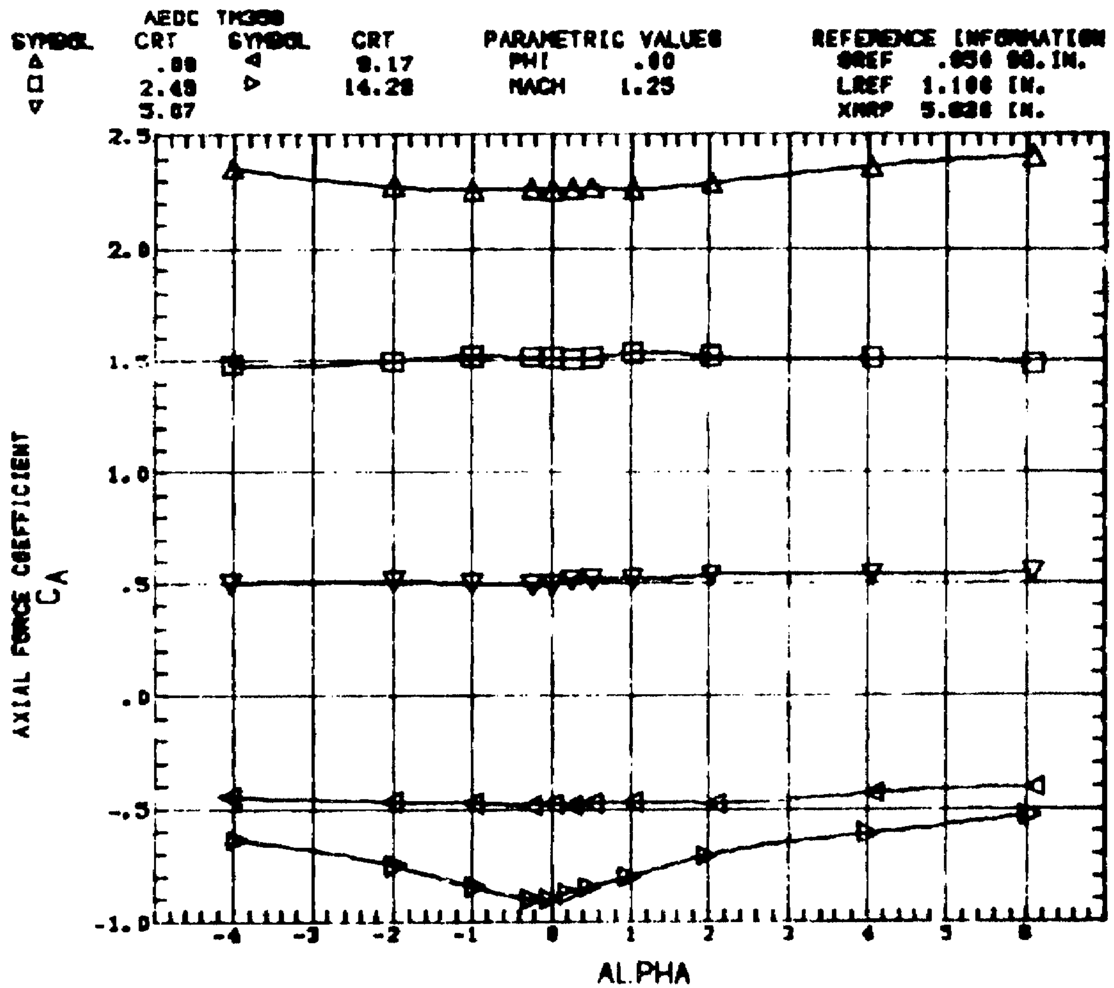

Figure 7. Continued. FD2

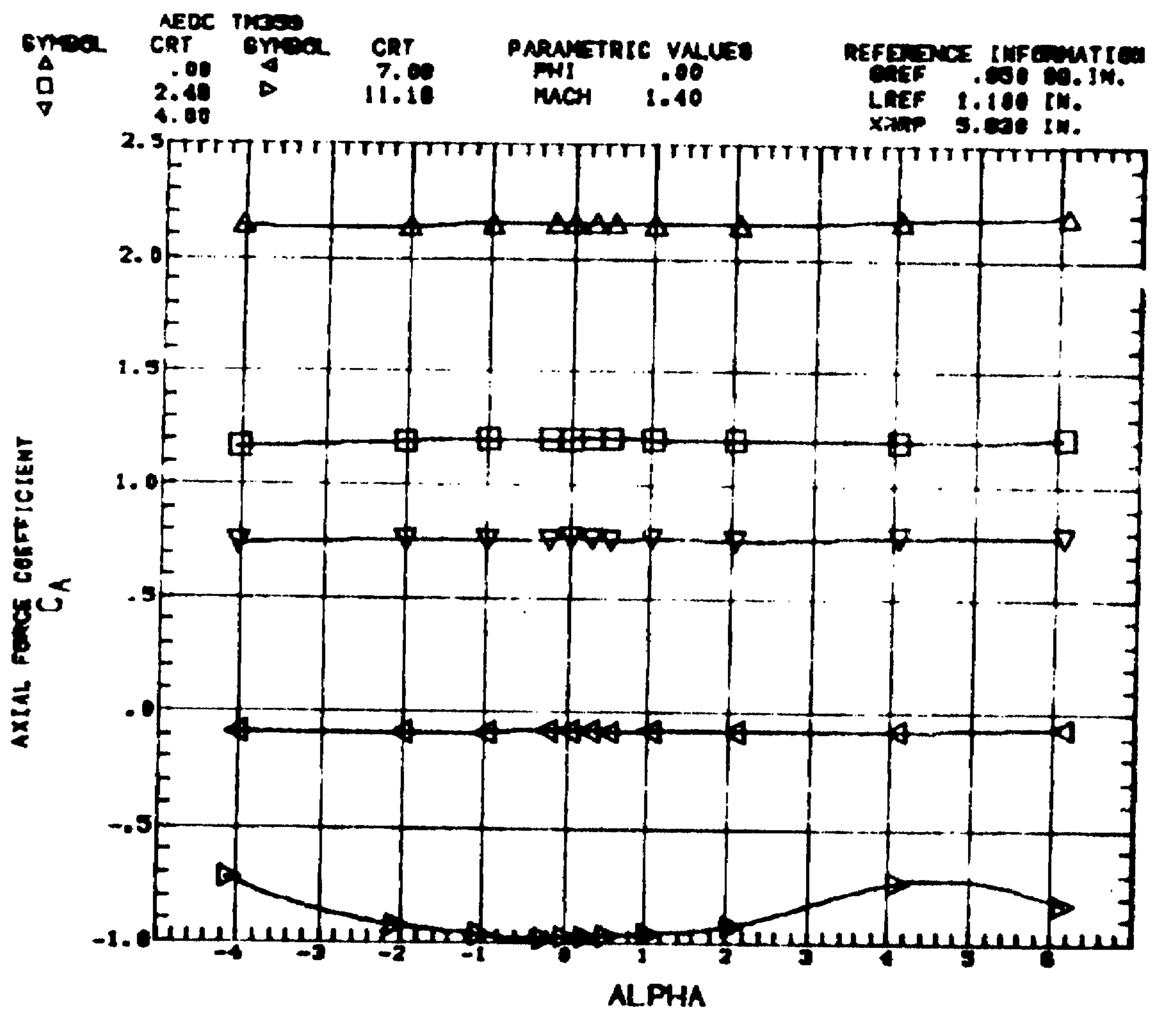

Figure 7. Continued. FD2

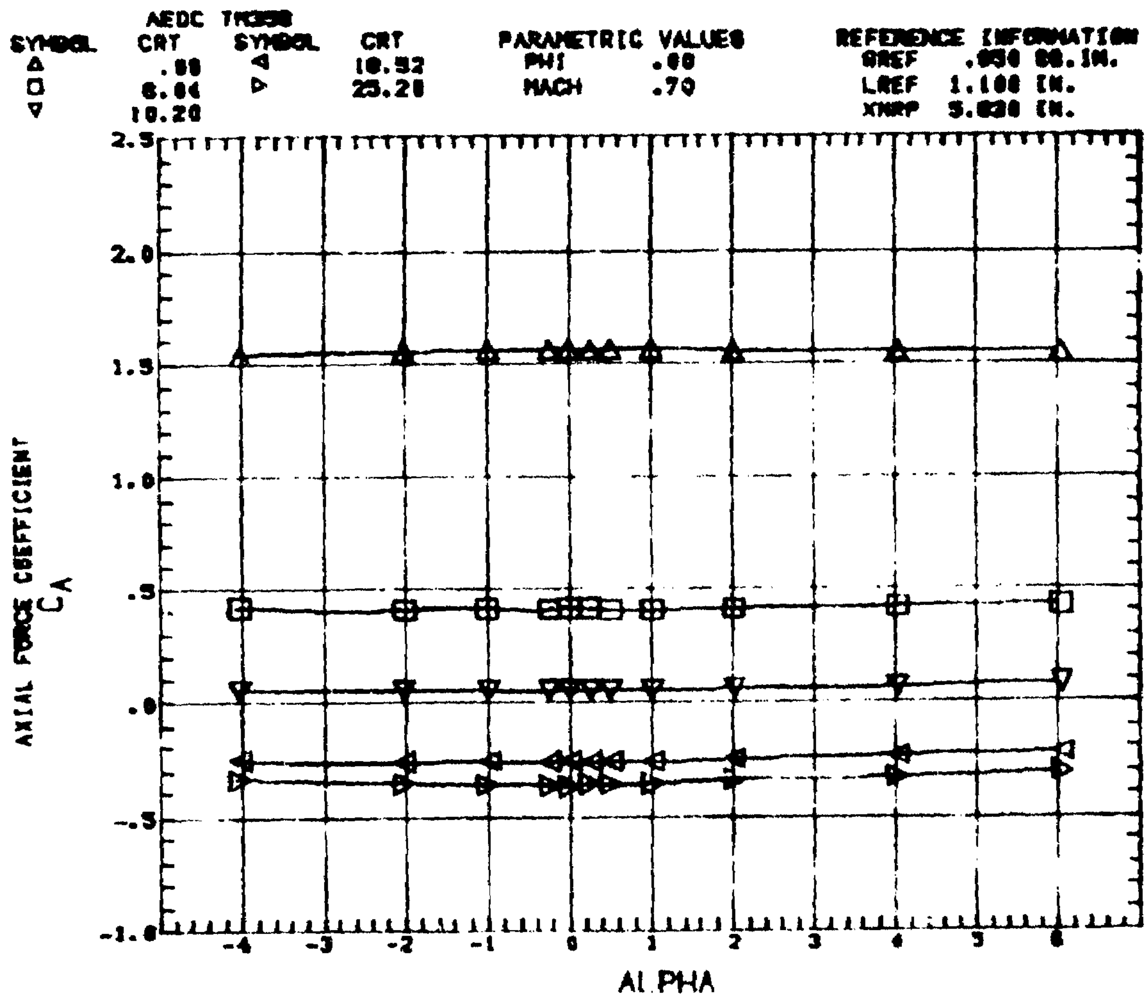

Figure 7. Continued. F6D2S

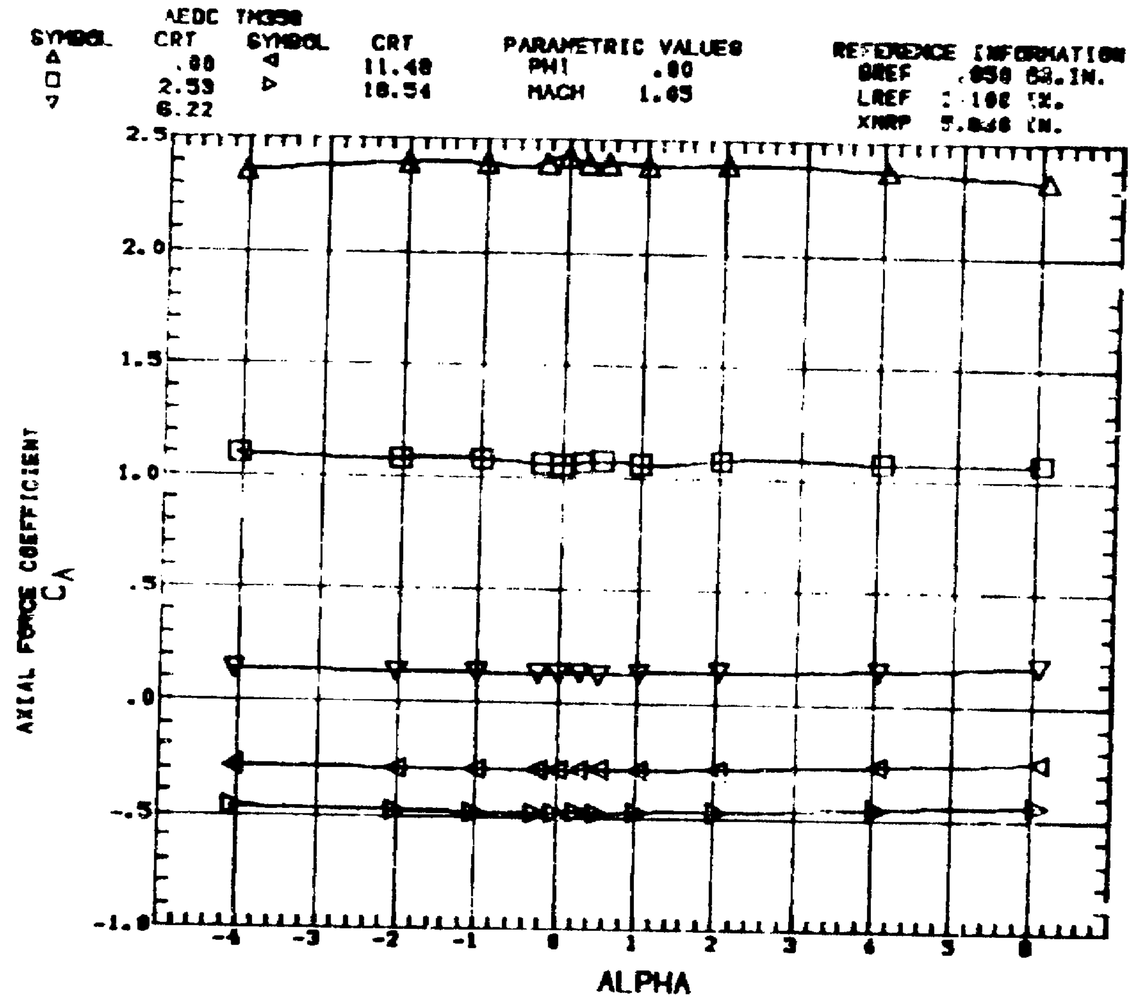

Figure 7. Continued. F6D2S

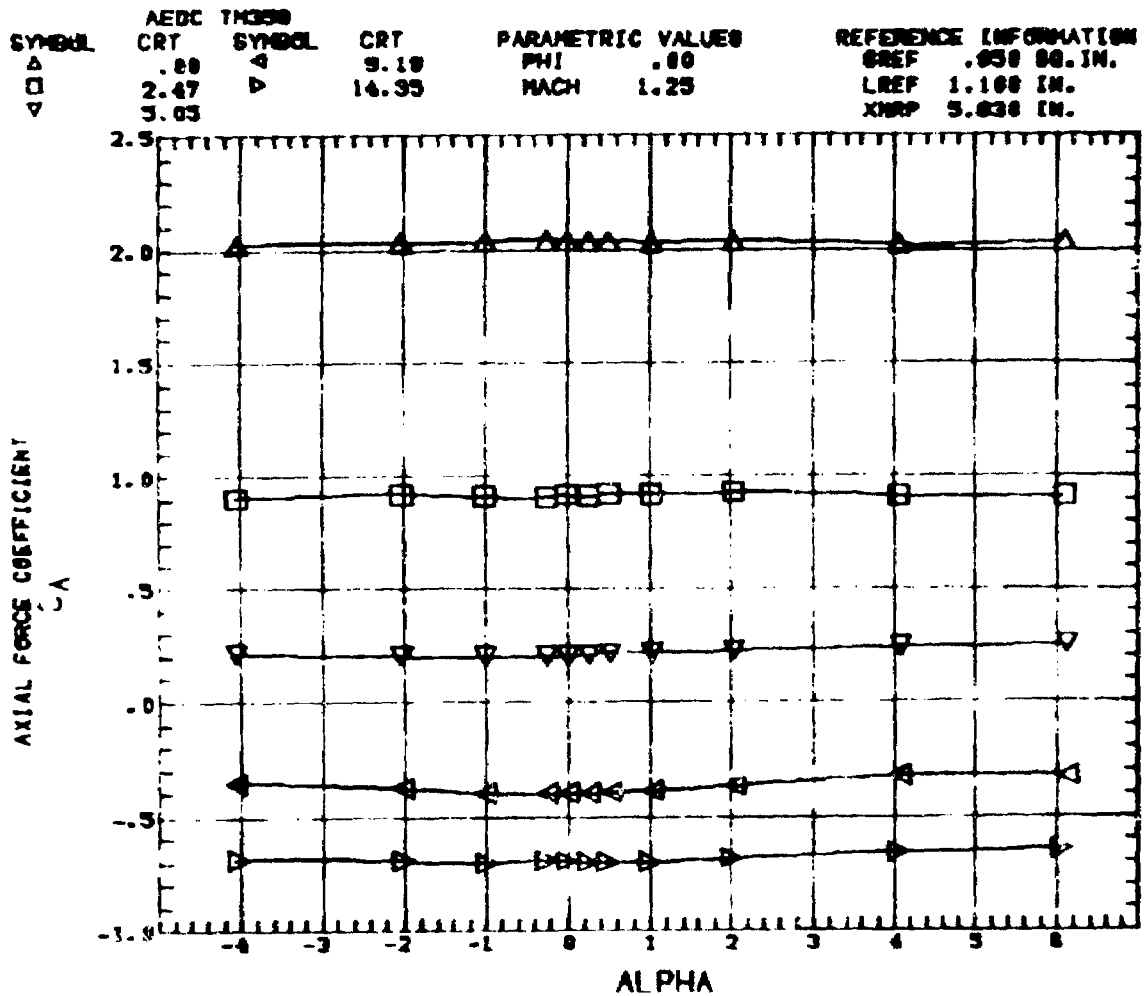

Figure 7. Continued. F6D2S

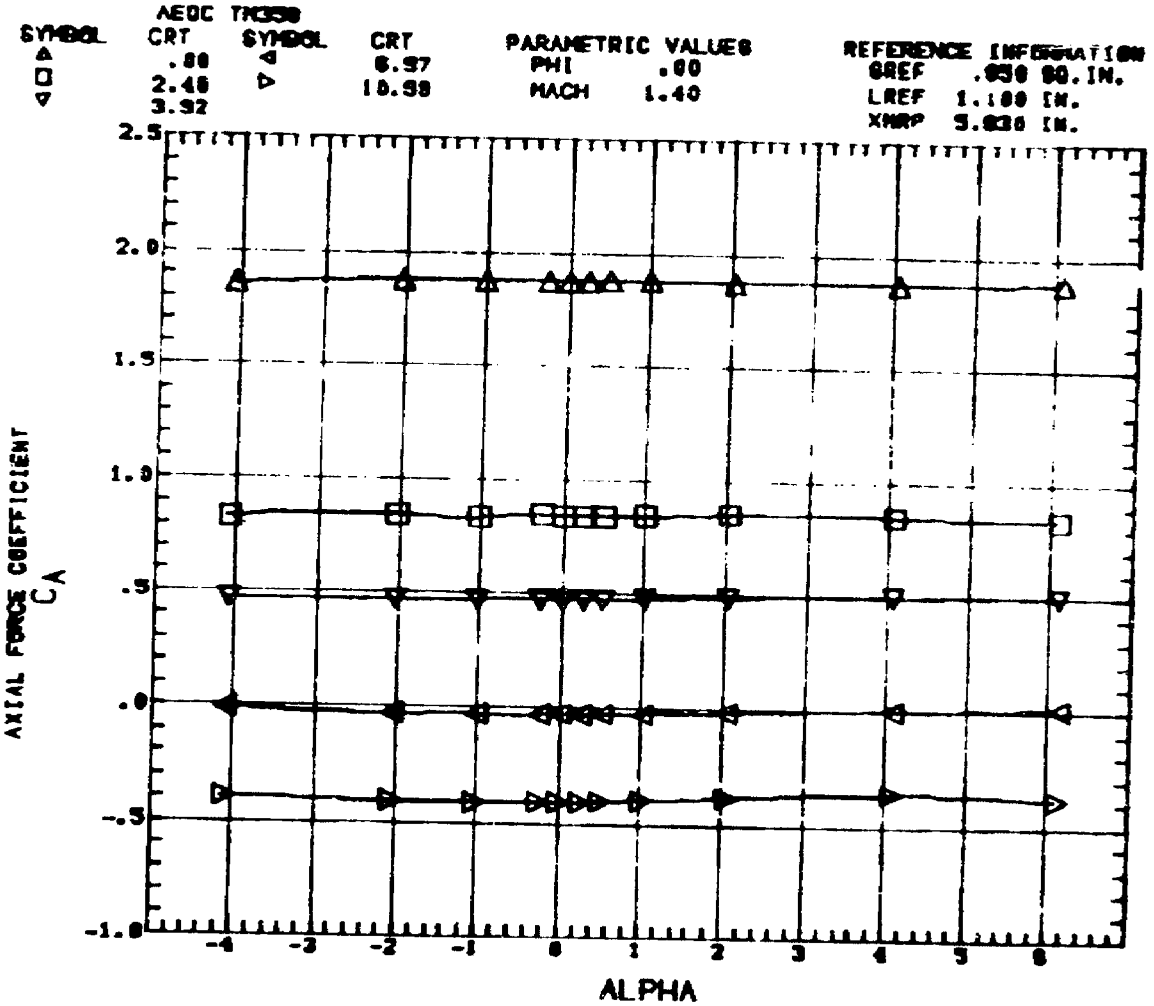

Figure 7. Continued. F6D2S

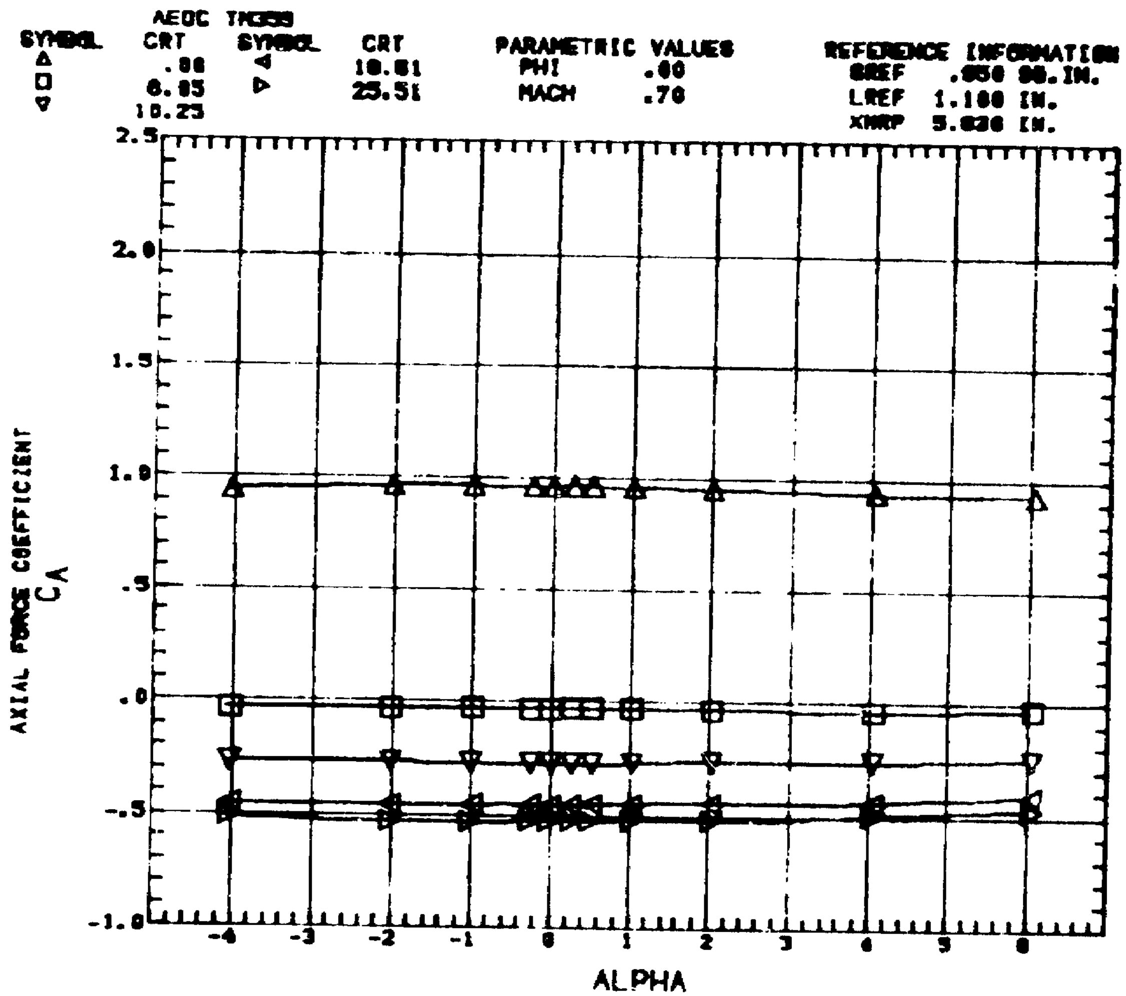

Figure 7. Continued.

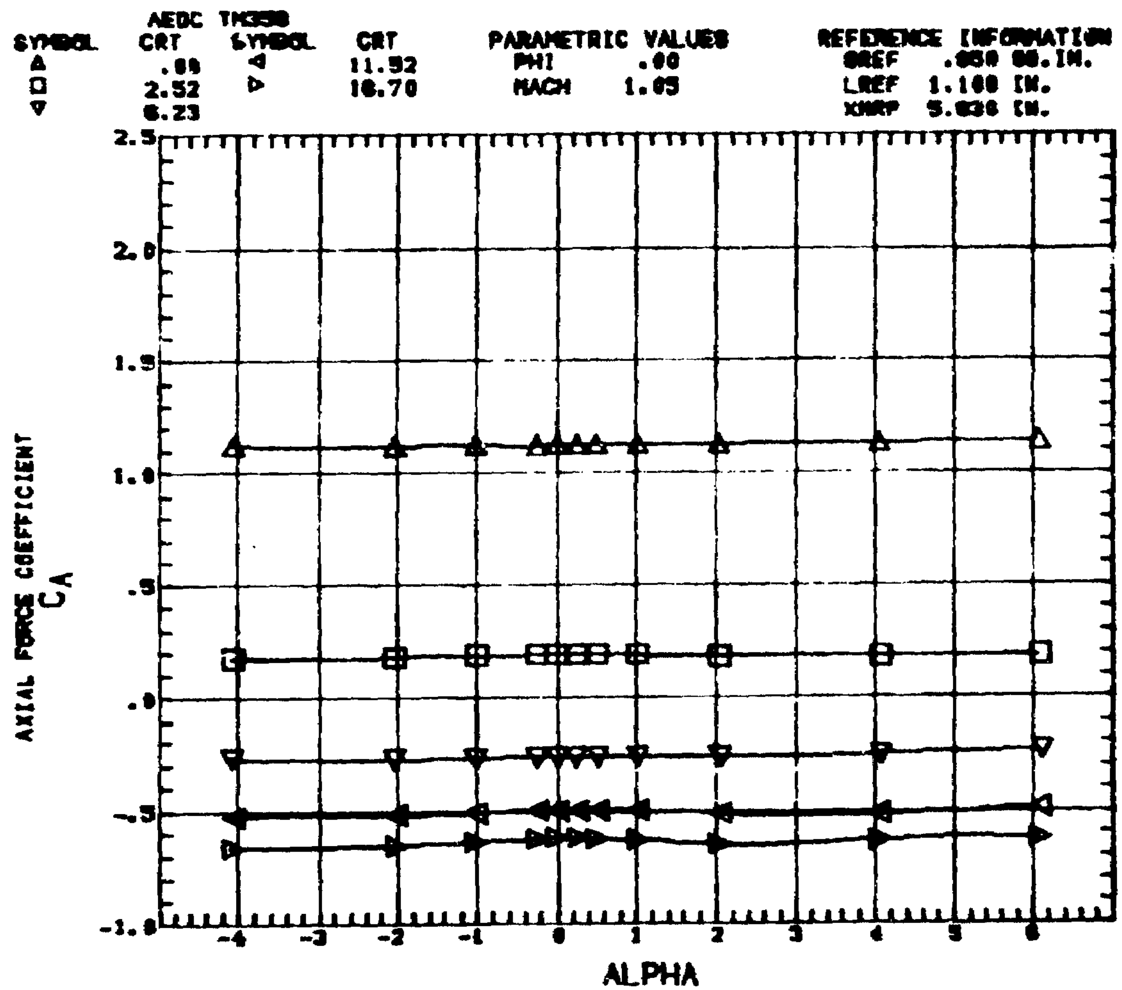

Figure 7. Continued. F12D1

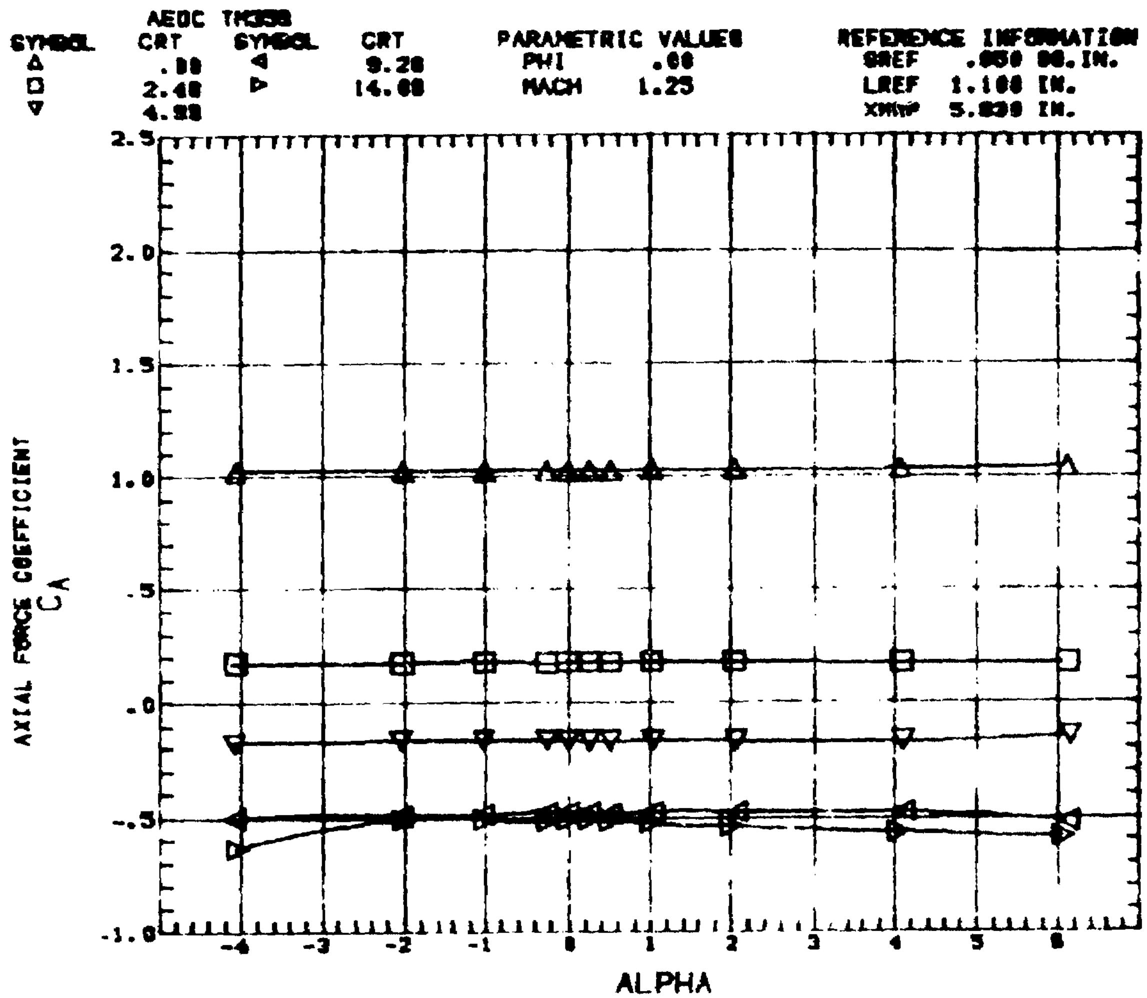

Figure 7. Continued. F12D1

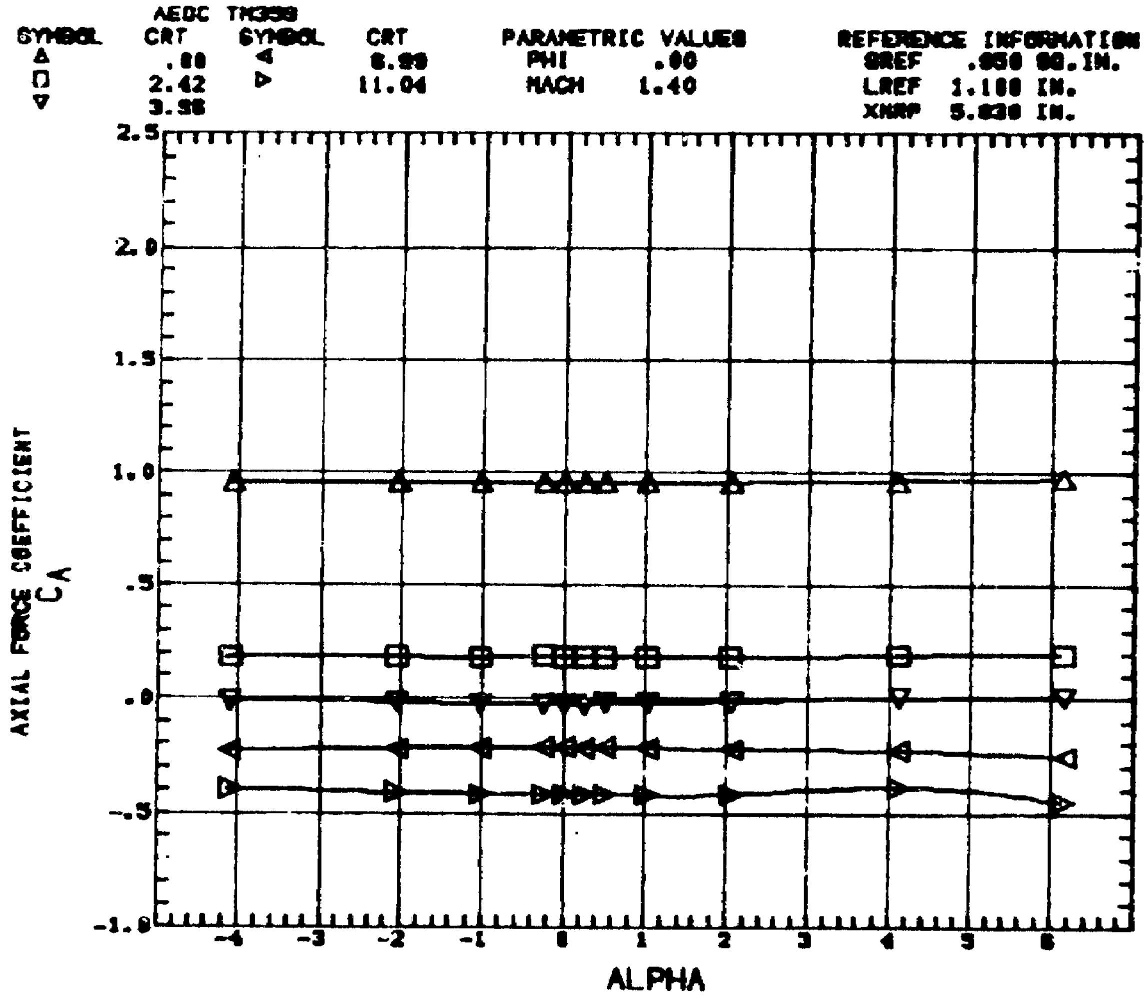

Figure 7. Continued. F12D1

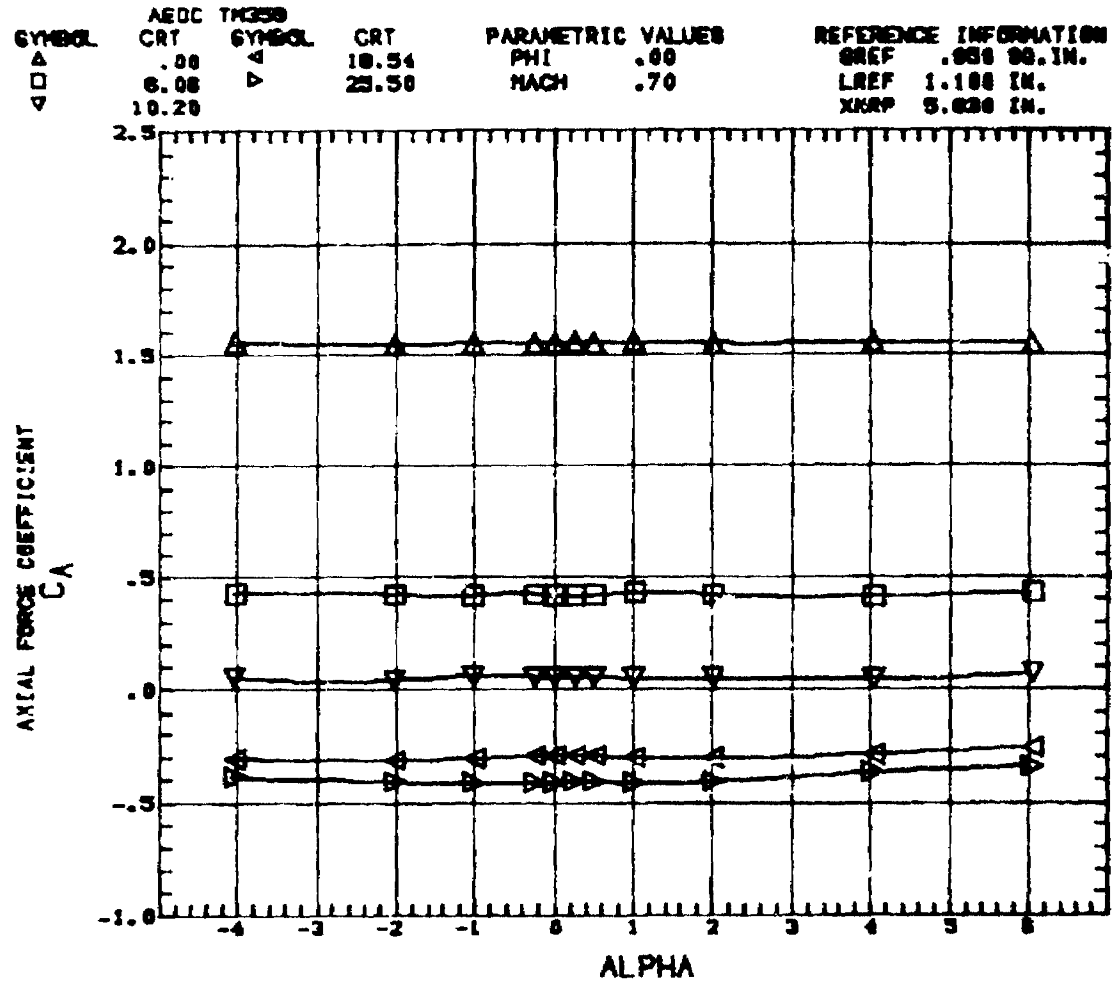

Figure 7. Continued. F12D2

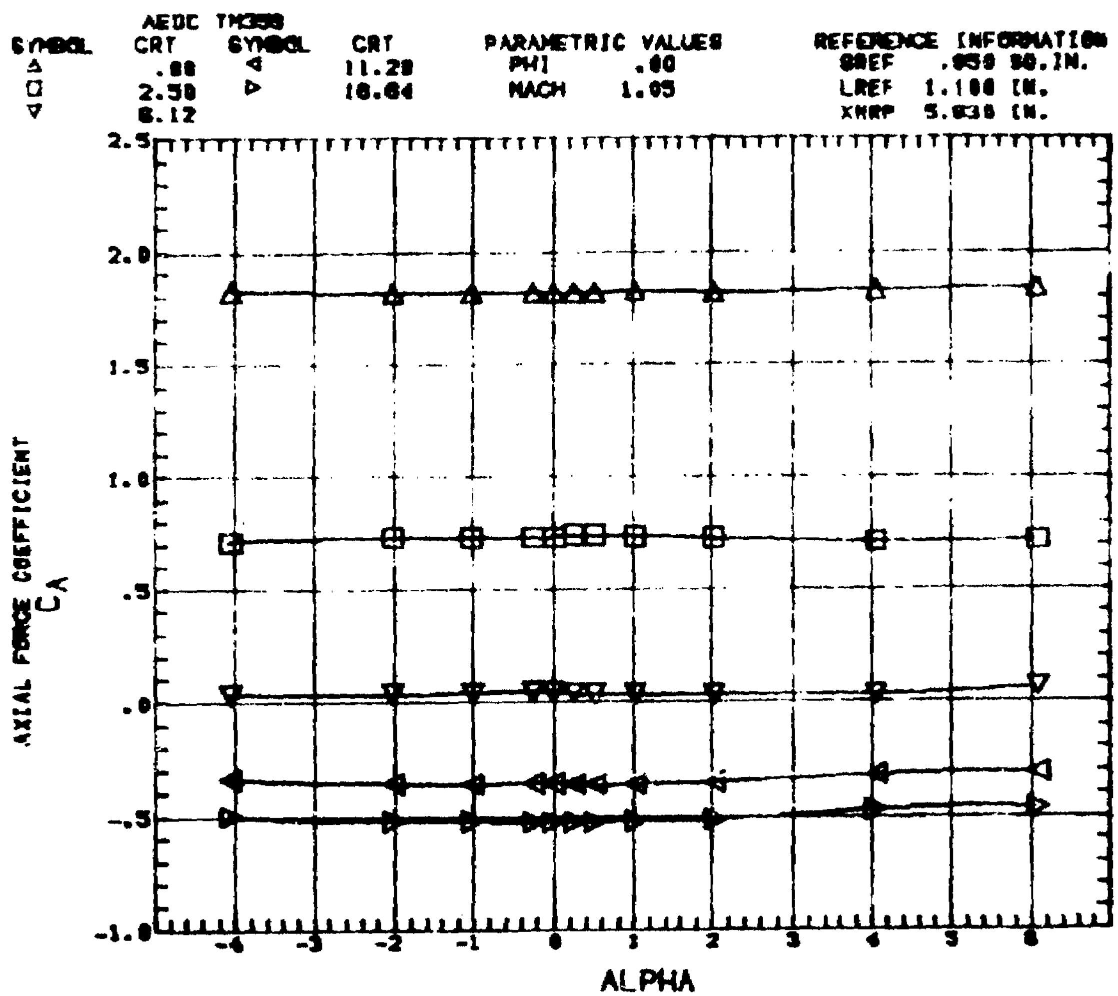

Figure 7. Continued. F12D2

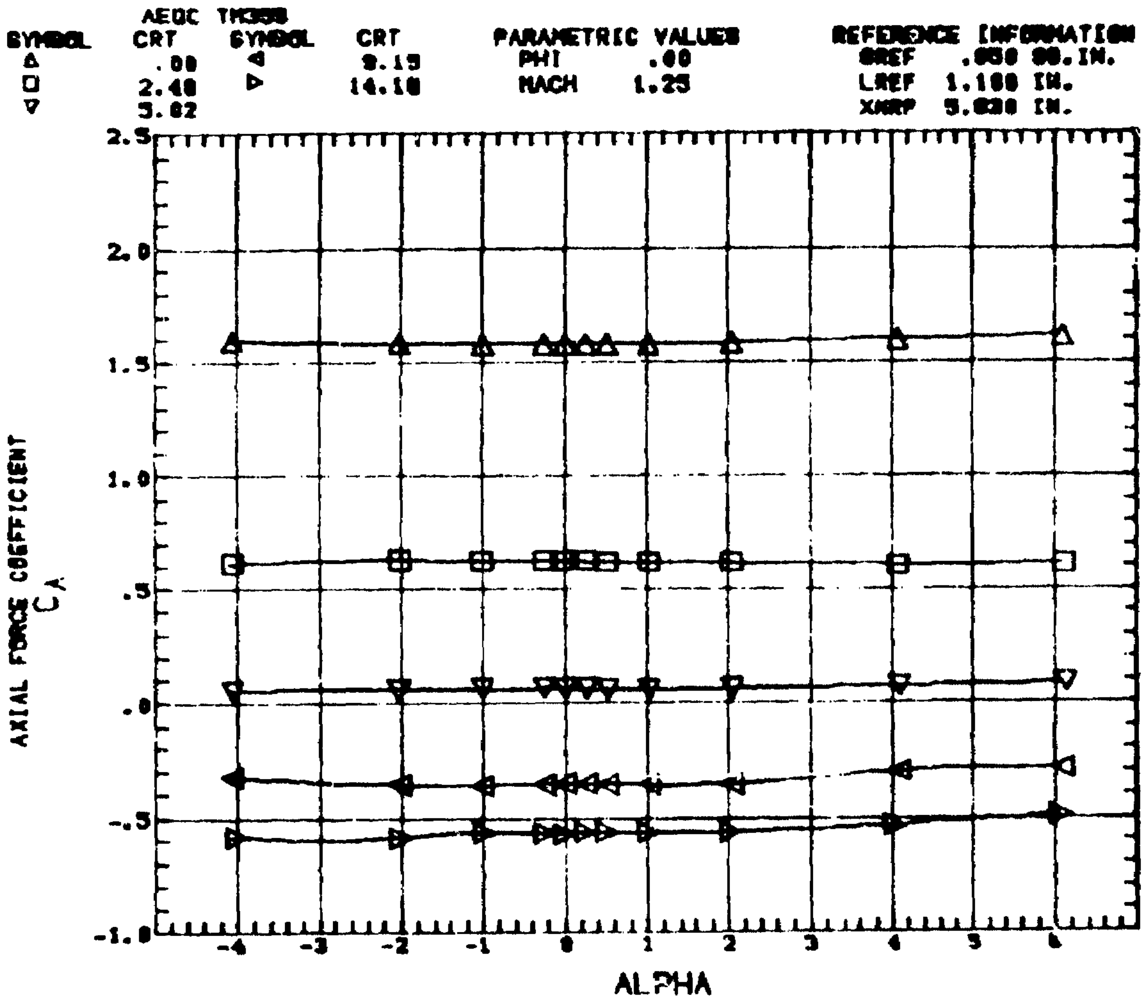

Figure 7. Continued. F12D2

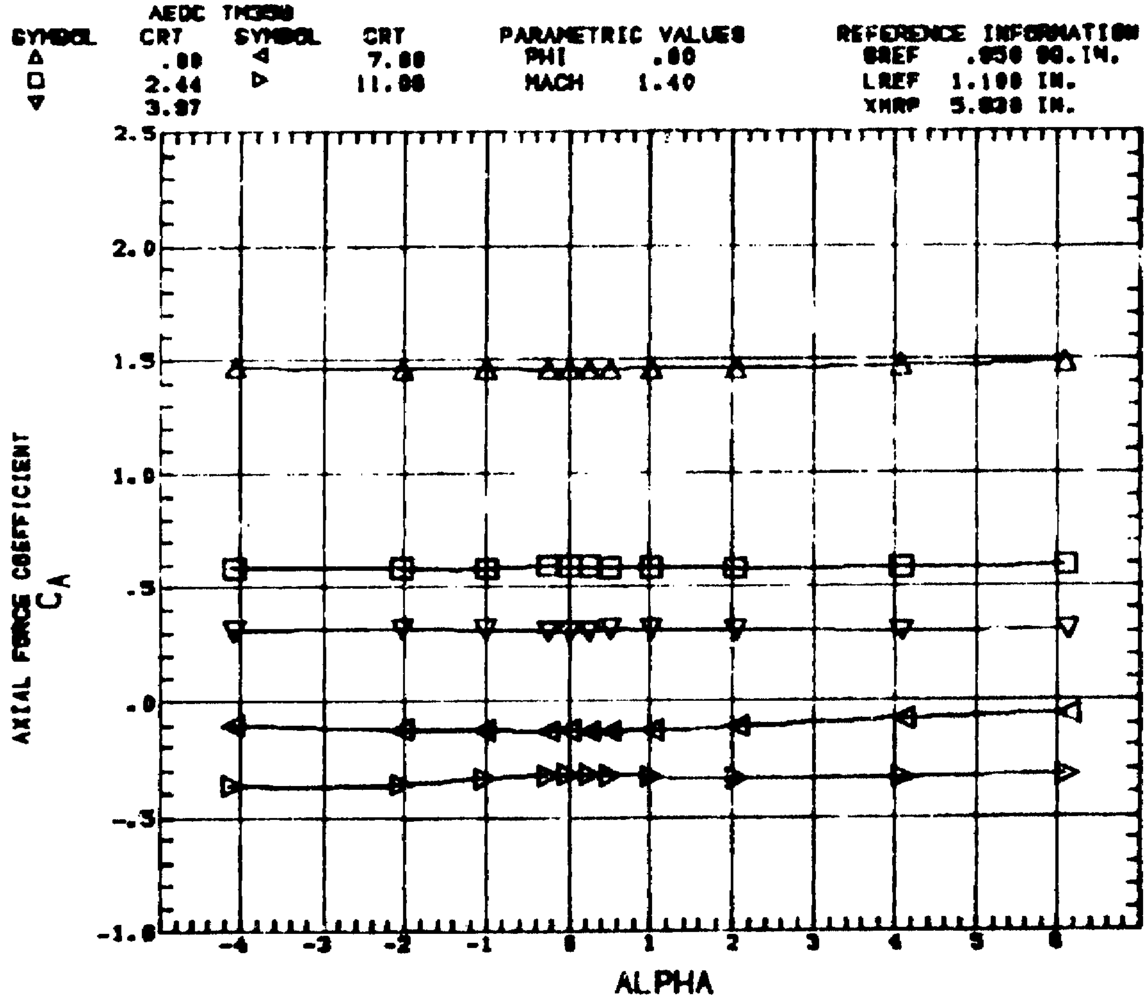

Figure 7. Continued. F12D2

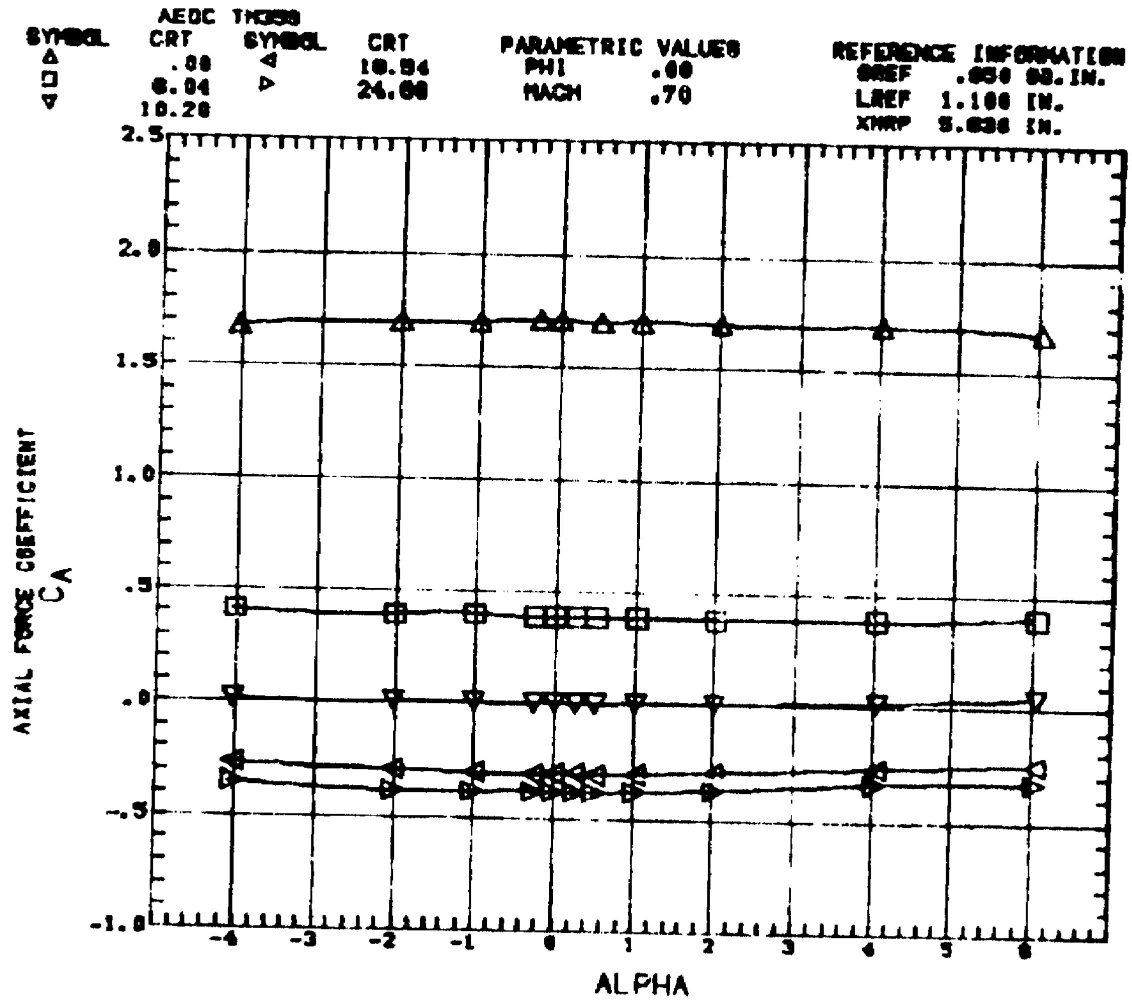

Figure 7. Continued. F6D2

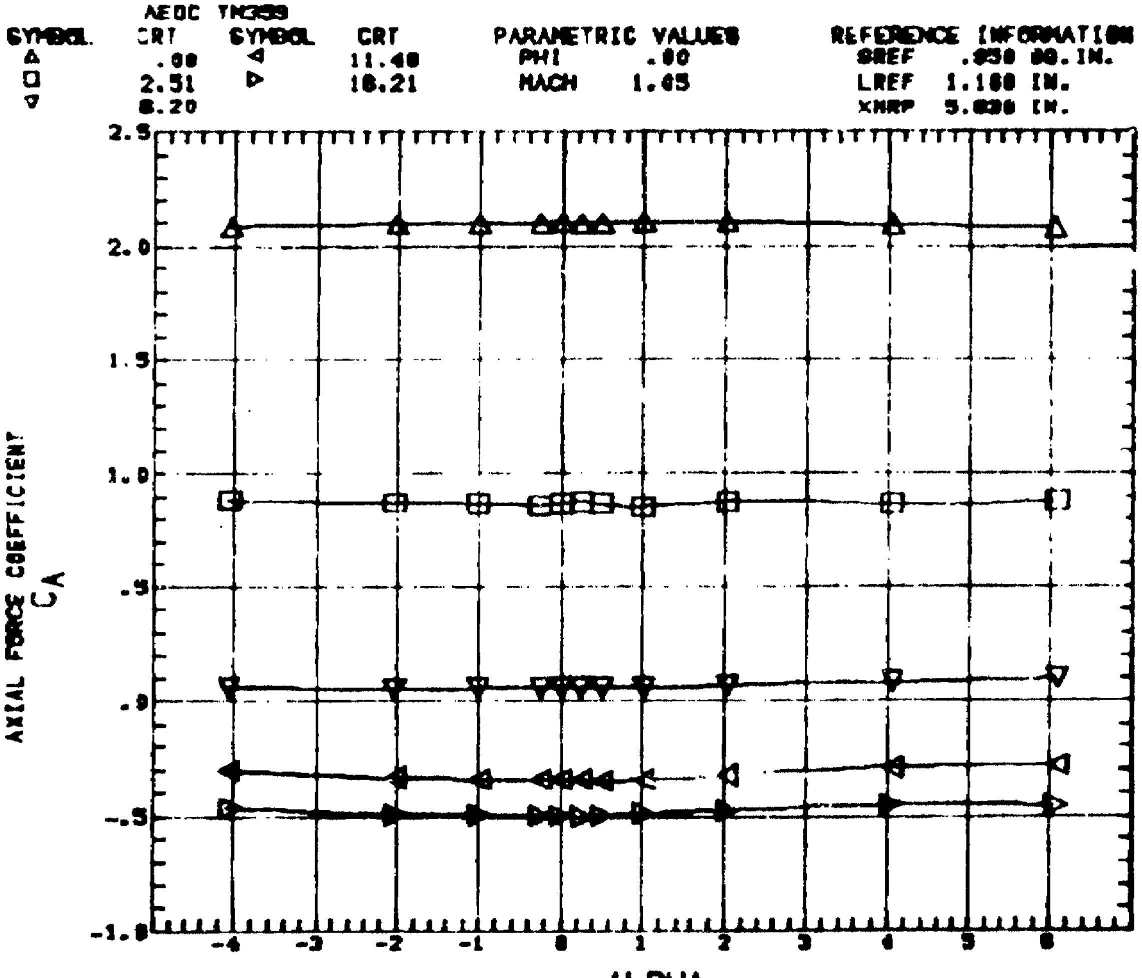

Figure 7. Continued. F6D2

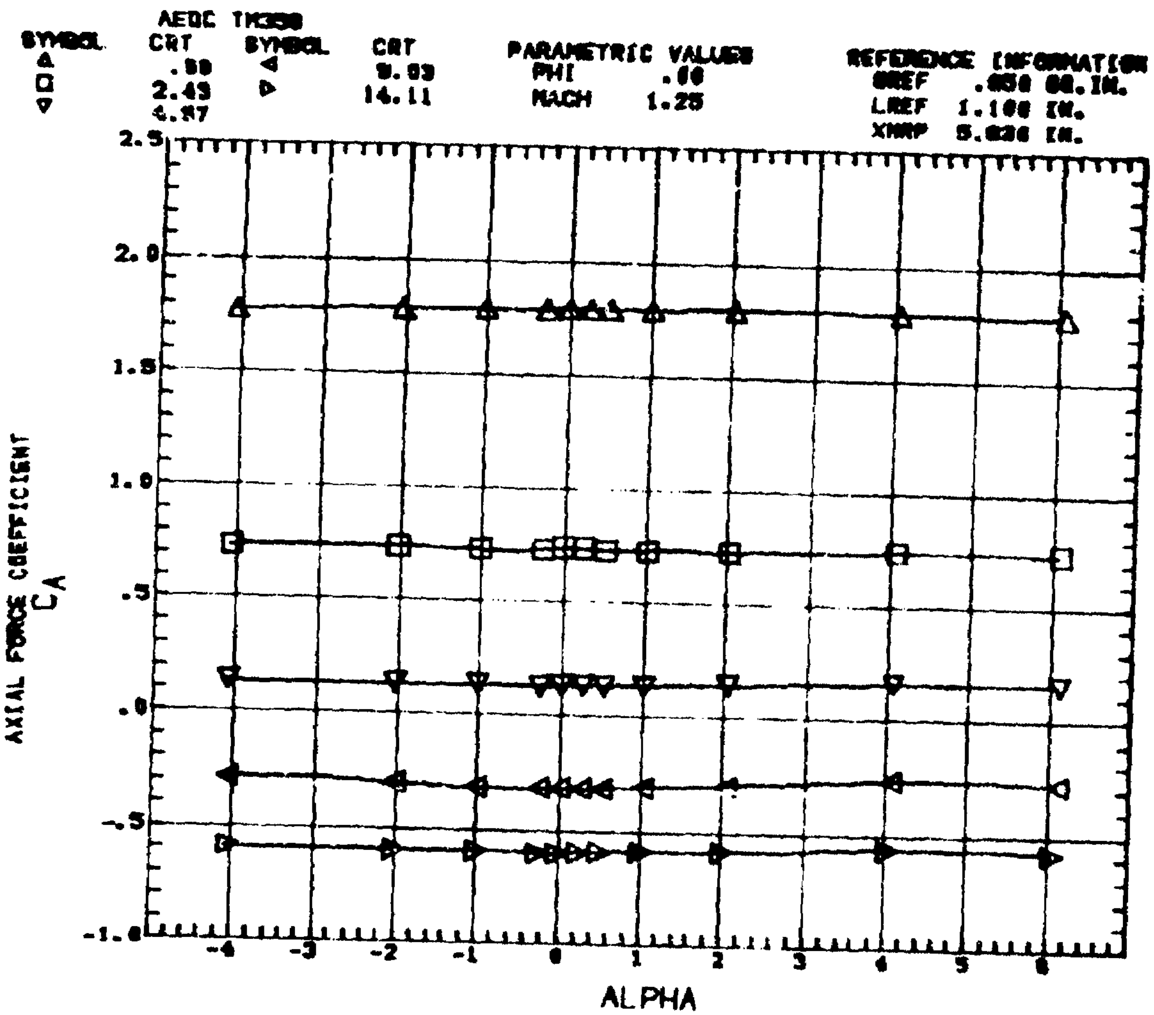

Figure 7. Continued. F6D2

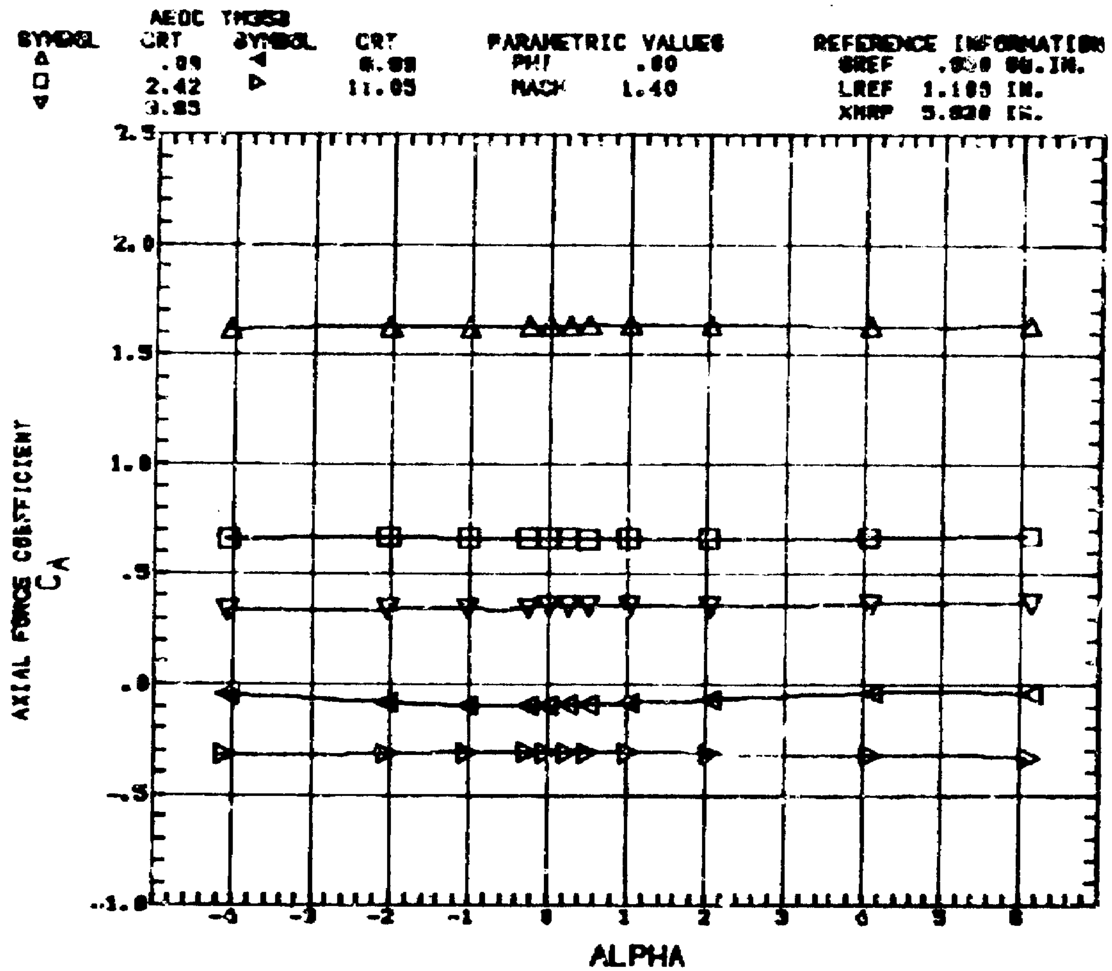

Figure 7. Continued. F6D2

DISTRIBUTION

	Number of Copies
Defense Documentation Center Cameron Station Alexandria, Virginia 22314	12
Commanding General US Army Materiel Command Research & Development Directorate ATTN: DRCRD Washington, D. C. 20315	1
Commanding Officer US Army Picatinny Arsenal ATTN: SMUPA-VC3, Mr. A. Loeb Dover, New Jersey 07801	1
Director US Army Mobility Research and Development Laboratory ATTN: SAVDL-AS Ames Research Center Moffett Field, California 94035	1
Commanding Officer Research Laboratories ATTN: SMUEA-RA, Mr. Abraham Flatau Edgewood Arsenal, Maryland 21010	1
Commanding Officer Air Force Armament Laboratory ATTN: Mr. C. Butler Mr. F. Howard Dr. F. Findley Eglin Air Force Base, Florida 32542	 1 1 1
Arnold Engineering and Development Center ATTN: Dr. McKay Library Arnold Air Force Station, Tennessee 37389	 1 1
Air Force Flight Dynamics Laboratory ATTN: FDMM, Mr. Gene Fleeman Wright-Patterson Air Force Base, Ohio 45433	1

	Number of Copies
Commanding Officer Ballistic Research Laboratories ATTN: AMXRD-BEL, Mr. R. Krieger Aberdeen Proving Ground, Maryland 21005	1
Commanding Officer US Naval Ordnance Laboratories ATTN: Mr. S. Hastings Mr. R. T. Hall Library White Oak Silver Spring, Maryland 20910	 1 1 1
NASA-Langley Research Center ATTN: Mr. Leroy Spearman Mr. Charles Jackson Technical Library Hampton, Virginia 23665	 1 1 1
Commanding Officer & Director Naval Ship Research and Development Center ATTN: Aerodynamic Laboratory Carderock, Maryland 20007	1
NASA-Ames Research Center ATTN: Technical Library Moffett Field, California 94035	1
NASA-Lewis Research Center ATTN: Technical Library Cleveland, Ohio 44135	1
NASA-Marshall Space Flight Center ATTN: Mr. K. Blackwell, ED32 Mr. J. Sims, ED32 Mr. H. Struck, ED31 Technical Library Marshall Space Flight Center, Alabama 35812	 1 1 1 1
US Air Force Academy ATTN: Lt. Col. W. A. Edgington DFAN UASF Academy, Colorado 80840	1

	Number of Copies
Philco Corporation	
Aeronutronic Division	
ATTN: Technical Information	
Services-Acquisitions	
Mr. Lee Horowitz	
Ford Road	
Newport Beach, California 92663	1
Rockwell International	
Columbus Aircraft Division	
ATTN: Mr. Fred Hessman	
4300 East Fifth Avenue	
Columbus, Ohio 43216	1
Sandia Corporation	
Sandia Base Division 9322	
ATTN: Mr. W. Curry	
Box 5800	
Albuquerque, New Mexico 87115	1
Purdue University	
ATTN: Dr. J. Hoffman,	
Propulsion Center	
Lafayette, Indiana 47907	1
University of Tennessee	
Space Institute	
ATTN: Dr. J. M. Wu	
Tullahoma, Tennessee 37388	1
University of Alabama	
Department of Aerospace Engineering	
ATTN: Dr. Zien	1
Dr. J. O. Doughty	1
University, Alabama 35486	
Jet Propulsion Laboratory	
California Institute of Technology	
ATTN: Mr. R. Martin, Mr. P. Jaffe	
4800 Oak Grove Drive	
Pasadena, California 91109	1

	Number of Copies
Commander	
US Naval Ordnance Station	
Code 563	
ATTN: Mr. N. Seiden	
Indian Head, Maryland	1
Naval Weapons Center	
ATTN: Mr. R. Meeker	
China Lake, California 93555	1
University of Missouri at Columbia	
Dept. of Mechanical Engineering	
ATTN: Dr. D. E. Wollersheim	
Columbia, Missouri 65201	1
University of Illinois	
College of Engineering	
ATTN: Dr. A. L. Addy	1
Dr. H. H. Korst	1
Dr. R. A. White	1
Engineering Library	1
Urbana, Illinois 61801	
John Hopkins University	
Applied Physics Laboratory	
ATTN: Dr. L. Cronvich	1
Mr. Gordon Dugger	1
Mr. R. Walker	1
Silver Spring, Maryland 20910	
University of Notre Dame	
Dept. of Aerospace Engineering	
ATTN: Dr. T. J. Mueller	
Notre Dame, Indiana 46556	1
Naval Air Systems Command	
ATTN: Mr. William Volz	
Air 320-C, Room 778, JP-1	
Washington, D. C. 20361	6
For Transmittal to:	
TTCP	

	Number of Copies
Boeing Company ATTN: Library Unit Chief	1
Mr. R. J. Dixon	1
Mr. H. L. Giles	1
P. O. Box 3707 Seattle, Washington 98124	
Convair, A Division of General Dynamics Corporation ATTN: Division Library Pomona, California 91776	1
Nielson Engineering & Research, Inc. ATTN: Dr. Jack N. Nielson 850 Maude Avenue Mountain View, California 94040	1
Hughes Aircraft Company ATTN: Documents Group Technical Library Florence Avenue at Teale Street Culver City, California 90230	1
Ling-Temco-Vought Aerospace Corp. ATTN: Mr. Dick Ellison P. O. Box 404 Warren, Michigan 48090	1
Ling-Temco-Vought Aerospace Corp. Vought Aeronautics Division ATTN: C. R. James, Unit 2-53330 Box 5907 Dallas, Texas 75222	1
Lockheed Missiles & Space Company Huntsville R&E Center ATTN: Mr. M. M. Penny 4800 Bradford Boulevard, N.W. Huntsville, Alabama 35805	1
Lockheed Missiles & Space Company ATTN: Technical Information Center P. O. Box 504 Sunnyvale, California	1

	Number of Copies
The Martin-Marietta Corporation Orlando Division ATTN: D. Tipping	1
L. Gilbert	1
Orlando, Florida 32804	
McDonnell Douglas Astronautics Co.-West ATTN: Library A3-328 5301 Bolsa Avenue Huntington Beach, California 92646	1
McDonnell Douglas Corporation P. O. Box 516 St. Louis, Missouri 63166	1
Northrop Corporation Electro-Mechanical Division ATTN: Mr. E. Clark 500 East Orangethorpe Y20 Anaheim California 92801	1
Emerson Electric Company ATTN: Mr. Robert Bauman 8100 Florissant Rd. St. Louis, Missouri 63136	1
REMTECH, Inc. ATTN: Mr. L. M. Hair 2603 Artie Street Huntsville, Alabama 35805	6
DRDMI-X	1
-TX, Dr. Kobler	1
-PD	3
-TDK, Mr. Deep	1
Mr. Henderson	2
Mr. Burt	10
DRDMI-TI, (Record Set)	1
(Reference Set)	1